Department of Applied Physics

# Convergent Close-Coupling Approach to Positron-Helium Collisions

Ravshanbek Utamuratov

This thesis is presented for the Degree of
Doctor of Philosophy
of
Curtin University

October, 2010

# Declaration

*To the best of my knowledge and belief this thesis contains no material previously published by any other person except where due acknowledgment has been made.*

*This thesis contains no material which has been accepted for the award of any other degree or diploma in any university.*

Signature

date

# Contents

# Summary

This thesis presents the theoretical studies of positron scattering on the helium atom using two-center Convergent Close-Coupling (CCC) theory.

The thesis organized in the following way:

In the Introduction (Chapter I) the motivation for the study and the current status of the positron-helium scattering problem are presented. Other theoretical methods that previously have been applied to this problem are reviewed and their limitations are indicated. The application of the two-centre CCC to positron-helium is presented in Chapter 2. The derivations of the scattering equations and transition matrix elements are given in detail. The results of the two-centre CCC calculations for positron scattering from the helium ground state are compared with available experimental data and the results of other calculations in Chapter 3. Chapter 4 presents CCC results of positron scattering from the metastable $2^3S$ excited state of helium. Finally, in Chapter 5, we draw conclusions arising from this work and indicate future directions for the research.

**Main results of this work**

- The two-centre Convergent Close-Coupling method is generalized to positron scattering on the helium atom.

- Cross sections, free from pseudo-resonances, are obtained for all major channels of interest and over a wide range of scattering energy. The importance of the inclusion of pseudo-states from both centers is demonstrated.

- The elastic cross section below the Ps-formation threshold is obtained, for the first time, by using a two-centre close-coupling approach.

- A consistent agreement of the CCC calculations with the available integrated cross section measurements of Ps-formation has been achieved at energies from the threshold of 17.8 eV up to 150 eV.

- The CCC calculations exhibit a qualitative agreement with the measurements of the total cross section for ionization of the ground state of helium by positron impact.

- The separation of the spin part of the total wave function is demonstrated and possible ortho- to para- Ps formation ratios are derived from first principles without assumptions.

- Calculations of positron scattering from the $2^3$S metastable state of helium are done for the first time. Converged results for the total scattering, Ps-formation, helium and Ps excitation as well as breakup cross sections are obtained.

- Both considered cases (scattering from the ground and the $2^3$S metastable states) confirm the equal atomic and Ps contributions to near-threshold breakup cross section, a behavior previously observed in positron scattering from hydrogen.

# Publications resulting from the Project

- R. Utamuratov, A. S. Kadyrov, D. V. Fursa, I. Bray and A. T. Stelbovics, *Convergent close-coupling calculations of positron scattering on metastable helium*, Phys. Rev. A **82**, 042705 (2010).

- R. Utamuratov, A. S. Kadyrov, D. V. Fursa, I. Bray and A. T. Stelbovics, *Multiconfigurational two-centre convergent close-coupling approach to positron scattering on helium*, Journal of Physics B: Atomic, Molecular and Optical Physics **43**, 125203 (2010).

- R. Utamuratov, A. S. Kadyrov, D. V. Fursa, and I. Bray, *A two-centre convergent close-coupling approach to positron-helium collisions*, Journal of Physics B: Atomic, Molecular and Optical Physics **43**, 031001 (2010).

- R. Utamuratov, A. S. Kadyrov, D. V. Fursa, and I. Bray, *Convergence study of the close-coupling approach to positron-helium collisions*, Journal of Physics: Conference Series **199**, 012021 (2010).

# Acknowledgments

It is a great pleasure to thank those who made this thesis possible by giving me their support in a number of ways.

I owe my deepest gratitude to my supervisor, Dr Alisher Kadyrov, for his constant guidance, help and encouragement throughout the period of this project.

I am also deeply grateful to my co-supervisor Professor Igor Bray, whose expertise and continuous support in every aspect of my research were invaluable.

I am indebted to Associate Professor Dmitry Fursa and Professor Andris Stelbovics for their assistance and constructive comments during the project.

For financial and technical support I acknowledge Curtin University International Postgraduate Research Scholarship, the Centre of Excellence for Matter-antimatter Studies and Australian National Computing Infrastructure Facility.

Finally, I wish to thank my friends and my family who have always been for me an indispensable source of spiritual and emotional support.

# Chapter 1

# Introduction

## 1.1 Motivation

Scattering experiments are the main tool of modern physics to learn about the foundation of matter and antimatter. Even in our daily life we get much of the information through collisional processes. We can see objects because the scattered photons are being detected by our eyes. However, if we would like to learn about very small objects then we use modern sophisticated technologies that use collisions of particles. By analyzing collision products we can extract useful information about the objects being studied.

Until recently, mostly electrons were used as scattering particles in experimental atomic and molecular physics. Recent developments in positron beams allowed for the use of positrons as alternative scattering particles. Differences and similarities between interactions of positrons and electrons with atoms give opportunity to test existing theories under various conditions.

Moreover, recent developments in the positron beams lead to new technologies, which found broad practical applications. One of the main areas that benefit from these technologies are medicine and material science. In medicine,

the use of the Positron Emission Tomography Scanners (PETS) help to make diagnoses of brain function disorders and certain types of cancers. Material science uses positron annihilation lifetime spectroscopy (PALS), to analyze and design specific materials. Such important applications of positron beams motivate theoretical investigations together with experimental studies.

The positron is the simplest antimatter particle. Studies of positron interactions with other particles have fundamental importance in learning about antimatter-matter interactions. Deeper knowledge about such interactions may help studies in astrophysics, such as the search for antimatter in the universe.

When a positron collides with an atom it can capture an electron from the atom and form a new exotic atom called positronium (Ps), which has similar structure as hydrogen but with different mass. Mainly because of this process the positron scattering problem has been a focus of both experimental and theoretical investigations. A proper formulation of Ps-formation processes makes the theoretical studies very challenging. The first theoretical studies of positron scattering from atoms date back to the 1950s, when Massey and Mohr [1] used the Born approximation to describe $e^+$-H collision and then later Massey and Moussa [2] extended it to the $e^+$-He system. Despite the fact that such studies have been continuously conducted since then, there are still some unresolved problems even in the simplest cases such as $e^+$-H collisions. Considerable progress in the description of $e^+$-H has been made by Mitroy [3] by using a close-coupling approach and then by Kadyrov and Bray [4] using the convergent close-coupling method. Theoretical studies of positron scattering from the next simplest target – He has an additional challenge, as obtaining the He structure is not analytically possible. Many approaches have been applied to this problem so far. However, until the present work none has been able to give the complete description of the available experimental data over a wide energy range. Previous approaches have

limitations regarding the scattering energy range and processes at which they can be applied. It is our aim to develop a positron-He scattering theory that can produce accurate results over a wide range of collision energies for all major scattering processes. Considering the successful application of the two-centre CCC method to the $e^+ - H$ system, presented by Kadyrov and Bray [4], one may expect that this method can also be successfully extended to the helium target.

## 1.2 Overview of existing positron-helium scattering theories

During the past few decades many different approaches have been developed for solving the $e^+$-He scattering problem. Each method has certain advantages and disadvantages over others in describing different processes and in different collisional energy regimes. Before we start reviewing existing theoretical models, we list below the possible processes that may take place during $e^+$-He collisions.

1) The elastic scattering, $e^+$-He$\rightarrow e^+$-He, may occur at any given collision energy. Apart from annihilation, it is the only process possible below 17.8 eV, which is the Ps-formation threshold for $e^+$-He($1^1$S).

2) Ps formation, $e^+$-He$\rightarrow$Ps-$He^+$, is possible at energies above the Ps-formation threshold.

3) The excitation $e^+$-He$\rightarrow e^+$-He* channels are open above the first excitation threshold of 20.6 eV in the case of scattering from He($1^1$S).

4) He single ionization, $e^+$-He$\rightarrow e^+$-$e^-$-$He^+$, may happen if the collision energy is above the ionization threshold, which is 24.6 eV for He in its ground

state.

5) Positron-electron direct annihilation $e^+$-He$\rightarrow n\gamma$-$He^+$ can happen at any scattering energy. In this process the positron collides with one of the target's electrons and annihilates into 2 or 3 gamma rays.

The first four channels are most important in atomic physics. Theoretical (Reeth and Humberston [5] and Laricchia and Wilkin [6]) and experimental studies (Kurz et al. [7]) of the annihilation process have shown that its cross section is up to $10^5$ times smaller than the elastic scattering cross section. Therefore the annihilation channel can be safely omitted from scattering calculations.

We also exclude from our consideration two-electron excitation (or ionization with excitation) channels. The contribution of these channels is typically two orders of magnitude smaller than the corresponding one-electron excitation processes in the energy range of our interest (see Ref. [8]).

In the next sections we briefly discuss theoretical methods previously applied to positron-helium collisions. Comprehensive reviews of positron physics has been given by Charlton and Humberston [9] and Surko et al. [10].

### 1.2.1 The Born and distorted-wave approximations

The Born method is based on the assumption that the wavefunction for the scattering system can be expanded in a rapidly convergent series. This approximation consists in using planewaves to describe the projectile and product particles. The Born approximation is a good approach when the scattering potential is relatively small compared to the incident energy, and thus is applicable only at high energies.

First Born-type calculations of $e^+$-He scattering have been performed by Massey and Moussa [2]. They used only the ground states of He and Ps and obtained cross sections for the elastic scattering and Ps-formation in its ground state. Their study highlighted the importance of Ps-channel coupling with the elastic channel and motivated further studies. Another extensive study based on the Born-approximation was presented by Mandal et al. [11], to estimate Ps-formation cross sections into arbitrary S-states.

From the first Born-approximation (BA) studies it became clear that more sophisticated approaches to the problem were required. The distorted-wave Born approximation (DWBA), for example, is based on the fact that the projectile wavefunction is distorted in the Coulomb field of the target. The DWBA results are obtained by using the distorted wave functions in first-order calculations. At low energies this method can give more accurate results than the BA.

Studies utilizing the DWBA by Parcell et al. [12, 13] were applied to the helium $2^1S$ and $2^1P$ excitations by positrons in the energy range from near the threshold up to 150 eV. Although the agreement with experimental data was not very satisfactory, the method indicated the importance of the inclusion of the polarization potential in the excitation channels at low energies.

The most systematic study of the ionization process within the framework of DWBA was carried out by Campeanu et al. [14, 15]. They used Coulomb and plane waves and also included exchange effects. They obtained very satisfactory results for ionization, agreeing well with the experimental results of Fromme et al. [16], Knudsen et al. [17] and Moxom et al. [18] over the energy range from near-threshold to 500 eV. However, the most important and difficult channel, Ps formation, was not included in the early DWBA studies.

Srivastava et al. [19] calculated the differential and total cross sections for

the excitation of the helium $2^1S$ state using the second-order DWBA method. Another DWBA method including Ps channels has recently been reported by Sen and Mandal [20] for intermediate to high scattering energies. They have calculated Ps-formation cross sections and achieved good agreement with available experimental data above 60 eV. However their results were not accurate for Ps-formation below 60 eV. Considering the fact that Ps formation starts at 17.8 eV and reaches its maximum around 40 eV, the applicability of this method is quite limited.

### 1.2.2 Many-body perturbation theory

The many-body theory of Fetter and Walecka [21] utilizes techniques that originated from quantum field theory. Using the diagrammatic technique the terms of the perturbation series in the interaction between particles can be written in an intuitive and comprehensive way. When it is applied to positron-atom scattering, however, difficulties arise from the need to take into account (virtual) Ps formation. Being a bound state, Ps cannot be described by a finite number of perturbation-theory terms.

Amusia et al. [22] have applied the random phase approximation (RPA), based on many-body theory [21], to the positron-helium scattering at low energies. By using a simple approximation to account for virtual Ps-formation they have obtained a good agreement with the experimental data by Jaduszliwer and Paul [23] and Canter et al. [24] at the lowest elastic scattering energies.

A similar RPA method was used by Varracchio [25] to calculate positron impact excitation of He into $2^1$S and $2^1$P states. A good agreement with available theory of Parcell et al. [12, 13] suggested a possible error in the experimental

data by Sueoka [26] and Coleman and Hutton [27].

Gribakin and King [28] devised a more sophisticated method based on the many-body perturbation theory. They used an approximation by considering virtual Ps-formation only in the ground state. The calculations with this method showed that for the elastic scattering of positrons by hydrogen and helium atoms, the virtual Ps-formation contribution is about 30% and 20% of the total correlation potential, respectively. Applications of the method to various atomic targets, including noble gases, were reported in Ref. [29, 30]. Gribakin and Ludlow [31] have further improved the method by introducing the techniques for the exact summation of the electron-positron ladder diagram series. The method has been applied to $e^+ - H$ scattering in the elastic scattering region and the obtained results were in good agreement with accurate variational calculations.

### 1.2.3 The Kohn variational method

One of the most successful methods applied to the low-energy $e^+$-He elastic scattering problem is the Kohn variational method. The method was initially developed for scattering phase shifts in nuclear reactions by Kohn [32]. Later this method was extended to positron-hydrogen scattering by Schwartz [33]. For positron-helium collisions, this method was first applied by Humberston et al. [34–37]. A detailed description of the method has been given by Armour and Humberston [38].

The method is based on guessing the form of the functional (called Kohn functional) for the scattering phaseshift as a parametric function of target wave functions. The required condition, that the Kohn functional be stationary with respect to the variations of the parameters, generates linear equations for the given parameters. The phaseshifts can be accurately obtained by performing

iterative calculations and finding the actual values of the required parameters.

A more recent and comprehensive study of positron-helium scattering with the Kohn variational method was given by Reeth and Humberston [39]. By using very flexible trial wave functions and helium wave functions below Ps-formation threshold they obtained the elastic cross section with very high accuracy. The elastic scattering and positronium formation cross sections converged to within 5% and 10%, respectively. The calculated positronium formation cross section displayed a similar energy dependence as the experimental results of Mizogawa et al. [40] and Stein et al. [41] but with a 25% difference in magnitude that was not quite satisfactory. However, the theoretical total cross section, both above and below the positronium formation threshold, agreed with the experimental measurements within 10%.

The limitation of the variational methods is that their application is problematic when there are many open transition channels. The problem arises because of the complexity of guessing the initial form of the Kohn functional and the increasing number of parameters in order to account for a large number of channels. Therefore its application is restricted to the low-energy elastic region.

### 1.2.4 Optical potential methods

The momentum space coupled channel optical (CCO) potential method was first developed for electron-atom scattering in the 1980s by McCarthy and Stelbovics [42, 43]. The method is based on solving momentum-space coupled-channel optical equations and relies on constructing a complex equivalent local potential to account for the ionization and the Ps-formation channels.

The CCO method gave excellent ionization (Ratnavelu [44]), total and Ps formation (Zhou et al. [45]) cross sections for positron scattering on hydrogen. Very recently this method was applied to positron-helium scattering by Cheng and Zhou [46]. The Ps formation cross sections in the energy range from the threshold to 400 eV and the total scattering cross sections at the energies from 17 to 500 eV were reported and compared with available experimental measurements and other theoretical calculations. The calculated results agreed well with the corresponding experimental data except for the data by Griffith and Heyland [47] for the total cross section in the energy range from 50 to 100 eV.

McEachran et al. [48] applied a polarized-orbital approximation method to low energy elastic positron-helium scattering and obtained a good agreement with the experimental results.

Other calculations using optical potentials were presented by Tancić et al. [49] and independently by Gianturco and Melissa [50] for slow positron scattering from helium. The elastic scattering cross sections of both reports were in good agreement with experimental data.

In general, the optical potential methods proved to be useful for calculations of total cross sections. It is problematic, however, when applied to more detailed cross sections like target excitation and Ps-formation in excited states.

### 1.2.5 Classical-trajectory Monte-Carlo technique

Schultz and Olson [51] utilized the classical trajectory Monte-Carlo (CTMC) technique to model positron scattering on helium. The method is described fully for ion-atom collisions by Abrines and Percival [52] and by Olson and Salop [53]. The CTMC technique is a method in which a large ensemble of projectile-

target configurations is sampled in order to simulate the collision. This method generally consists of three steps: (1) initialization of the projectile-target configuration, (2) calculation of the classical trajectories, and (3) a final-state test for reaction. In the first step the active electron is randomly initialized in its orbit according to a micro-canonical distribution, so that its position and momentum on average initiate the quantum mechanical position and momentum distributions. The impact parameter is randomly distributed between 0 and some $b_{\max}$. In the second step, 6N coupled differential equations, representing the Hamiltonian equations of motion for the N bodies in the collision, are integrated numerically from some large initial projectile-target separation, through the collision, and continuing to some large final separation. After integration, the relative energies between the particles are found and what reactions, if any, have occurred is established. The main advantage of this method is that it can describe dynamic effects occurring in collisions.

Using this technique, Schultz and Olson [51] calculated the ionization differential scattering cross-section for the positron-helium and positron-krypton collisions. They found that the cross section for the scattering of positrons to large angles in ionizing collisions was of the same order, or much greater than, the total cross section for positronium formation. From their analysis of the experimental data, they demonstrated that by accounting for the flux in the experiments measuring positronium formation due to positrons scattered to angles that allow them to escape confinement, the disagreement between theory and experiment at above 60 eV might be resolved.

Recently, Tökési et al. [54] have also applied the CTMC method to helium ionization by positron impact. They obtained good agreement with experimental data by Fromme et al. [16].

Results of CTMC reported by Schultz and Olson [51] overestimate the recent experimental data by Caradonna et al. [55] for the Ps-formation cross section below 60 eV. The reason for this overestimation probably indicates the inapplicability of the classical trajectory approach at positron scattering at low and intermediate energies.

### 1.2.6 Close-coupling approximation

The most sophisticated and commonly used method is the close-coupling (CC) formalism, which is based on the expansion of the total wave function using the target state wave-functions. Substitution of this expansion into the Schrödinger equation yields coupled integro-differential equations in coordinate space, or Lippmann-Schwinger integral equations for the T-matrix in momentum space. By solving these equations the transition amplitudes are obtained for all open channels. Many CC approaches (e.g. Mitroy [3] and Campbell et al. [56]) use a Slater basis to generate target wave functions, which are then used to expand the total wavefunction. The Slater basis is not orthogonal. Therefore one would need larger basis than required with an orthogonal basis to respresent the same physics. This, in turn, may cause linear dependence problems.

The most comprehensive study of positron-helium scattering using the close-coupling method was carried out by Campbell et al. [56]. They used two kinds of expansions, the first one consisting of 24 helium pseudo-states and the lowest three Ps eigenstates and the second one with only 30 helium pseudo-states. The helium target structure was modeled using a frozen core approximation, which can produce good excited states but less accurate ground state. The atomic pseudo-states were constructed using a Slater basis. For the 27-state approximation, only results in the energy range above the positronium formation

threshold were given. Results for lower energies were unsatisfactory, and it was suggested that this might be due to the lack of convergence from the use of an inaccurate helium ground state wave-function. The total cross sections from both the 27- and 30-state approaches agreed well with the experimental results of Stein et al. [41], Kauppila et al. [57] and Mizogawa et al. [40] for the energy range above the threshold of positronium formation. For lower energies, qualitative agreement was obtained in terms of the shape and the reproduction of the Ramsauer-Townsend minimum near 2 eV, while the theoretical results were significantly, by factor of 2, larger than the experimental data. The Ps formation cross sections from the 27-state approximation were in good agreement with the experimental data of Moxom et al. [18] up to about 60 eV and with the data of Fornari et al. [58] and Diana et al. [59] up to 90 eV. Above 100 eV, however, the theoretical results were much lower than the experimental data of Diana et al. [59] and Fromme et al. [16] while being closer to the data of Overton et al. [60].

Another close-coupling calculation by Hewitt et al. [61, 62], using a few helium and positronium states with a simple one-electron model for the helium atom, showed less satisfactory agreement with the experimental data. Chaudhuri and Adhikari [63–65] performed calculations using only 5 helium and 3 positronium states in the expansion. Their results for Ps-formation agreed well with the experimental results by Moxom et al. [18] at energies near the Ps-threshold and displayed a better agreement with the data of Overton et al. [60] at the higher energies. However, the theoretical results were much lower than the experimental data at energies near the maximum of the cross section.

Igarashi et al. [66] applied the hyper-spherical CC approach to the problem. However, they considered helium atom as a single-electron target, and thus the excitation and Ps-formation cross sections were multiplied by factor of 2. Satisfactory results were obtained for the total Ps-formation and He(2s) and

He(2p) excitation cross sections. The method was not able to describe low-energy scattering mainly because the single-electron approach to helium is not realistic at low energies.

Despite the obvious advantages of the above-mentioned close-coupling calculations in handling many scattering channels simultaneously, none was able to describe low-energy elastic scattering. In addition, the presence of pseudo-resonances in cross sections below the ionization threshold [56, 62] indicates that there is a room for improvement. The use of the frozen-core He states also needs some attention as it cannot describe accurately the ground state of He.

### 1.2.7 Single-center convergent close-coupling method

The convergent close-coupling (CCC) method is also based on the close-coupling scheme. The main difference of CCC from other close-coupling approaches is the use of a basis of orthogonal square-integrable ($L^2$) functions to form target wave functions. The use of such a basis allow to avoids the linear dependence problem and allows to include as many states as required to get sufficiently converged results. The method was initially developed for the electron-hydrogen system by Bray and Stelbovics [67] and then extended to the electron-helium case by Fursa and Bray [68]. These are single-centre approaches that can also be applied to positron scattering but without Ps-formation. The first application of the single-centre CCC method to positron scattering was made by Bray and Stelbovics [69] for hydrogen and more recently by Wu et al. [70–72] for helium targets. Wu et al. [70–72] used, for the first time, very accurate helium wave functions obtained within the multi-core approximation. Very accurate elastic cross sections were obtained below the Ps formation threshold by using orbitals with very high angular momenta. It was suggested that the necessity for inclusion of very high

angular momentum orbitals was to mimic the virtual Ps-formation processes. The method also gave accurate results for medium to high energy scattering processes except for the Ps formation. Interestingly, the method was not able to produce a converged result at the Ore-gap region (where only the elastic and Ps-formation channels are open). Comparison of the frozen-core and the multi-core results has shown that the frozen-core wave functions result in overall about 10% higher cross sections.

Studies of Wu et al. [70–72] have shown that single-centre the expansions may yield correct results in certain restricted kinematic regimes, but generally are inadequate and inclusion of the Ps centre into expansions is important. The CCC method has been generalized to incorporate Ps formation by Kadyrov and Bray [4] and convergence of the (non-orthogonal) two-centre expansions has been explicitly demonstrated in the positron-hydrogen case. The CCC calculations with such a combined basis have shown very good agreement with the experimental data of Zhou et al. [73] and Jones et al. [74].

Extension of two-centre CCC to positron scattering on helium was attempted by Wu [70]. However, the formulation of the method was not completed and equations for transition matrix elements were not obtained in practical form for further calculations.

# Chapter 2

# Theory

In general, the two-centre CCC method is based on expanding the total wavefunction of the scattering system using the bases of target and Ps states. Then using the two-centre expansion the Schrödinger equation (SE) is transformed into momentum-space Lippmann-Schwinger equations (LSE). The solution of the LSE yields the scattering amplitudes for all open channels. The target and Ps states are generated using square-integrable Laguerre functions. This allows for the inclusion of as many states as necessary for convergence without having linear dependence problems.

In this chapter the basic formalism of the two-centre CCC method applied to positron scattering on helium is presented. First we separate the spatial part of the total wavefunction from the spin part. Then the derivations of the transition matrix elements are presented.

## 2.1 Two-centre close-coupling equations

Consider scattering of a positron on the helium atom. In this scattering process the positron can capture one of the electrons and form Ps. This makes the problem two-centered. We can neglect the relativistic effects and spin-orbit

interactions on the scattering energy range of our interest. The nonrelativistic Hamiltonian for the $e^+$-He system can be written as

$$H = H_0 + \frac{2}{r_0} - \frac{2}{r_1} - \frac{2}{r_2} + \frac{1}{|\boldsymbol{r}_1 - \boldsymbol{r}_2|} - \frac{1}{|\boldsymbol{r}_0 - \boldsymbol{r}_1|} - \frac{1}{|\boldsymbol{r}_0 - \boldsymbol{r}_2|}, \tag{2.1}$$

where

$$H_0 = -\frac{1}{2}\nabla^2_{\boldsymbol{r}_0} - \frac{1}{2}\nabla^2_{\boldsymbol{r}_1} - \frac{1}{2}\nabla^2_{\boldsymbol{r}_2} \tag{2.2}$$

is the free-particle Hamiltonian of three particles and $\boldsymbol{r}_0$, $\boldsymbol{r}_1$, and $\boldsymbol{r}_2$ denote the positions of the positron 0, electrons 1 and 2, respectively (see Fig. 2.1), relative to the helium nucleus.

For rearrangement processes it is convenient to use a coordinate system associated with the Ps-centre. In the corresponding set of Jacobi coordinates the Hamiltonian is written as

$$H = H_0 + \frac{2}{|\boldsymbol{R} + \frac{1}{2}\boldsymbol{\rho}|} - \frac{2}{|\boldsymbol{R} - \frac{1}{2}\boldsymbol{\rho}|} - \frac{2}{r_2} + \frac{1}{|\boldsymbol{R} - \frac{1}{2}\boldsymbol{\rho} - \boldsymbol{r}_2|} - \frac{1}{\rho} - \frac{1}{|\boldsymbol{R} + \frac{1}{2}\boldsymbol{\rho} - \boldsymbol{r}_2|}, \tag{2.3}$$

where the free Hamiltonian in $\{\boldsymbol{R}, \boldsymbol{\rho}, \boldsymbol{r}_2\}$ coordinate system is

$$H_0 = -\nabla^2_{\boldsymbol{\rho}} - \frac{1}{4}\nabla^2_{\boldsymbol{R}} - \frac{1}{2}\nabla^2_{\boldsymbol{r}_2}, \tag{2.4}$$

which describes free motions of Ps, the helium nucleus and the electron that is left in the $He^+$ ion; $\boldsymbol{R} = (\boldsymbol{r}_0 + \boldsymbol{r}_1)/2$ is the position of the Ps centre relative to the He nucleus and $\boldsymbol{\rho} = \boldsymbol{r}_0 - \boldsymbol{r}_1$ is the relative coordinate of the positron and electron 1. The two systems of coordinates $(\boldsymbol{r}_0, \boldsymbol{r}_1, \boldsymbol{r}_2)$ and $(\boldsymbol{R}, \boldsymbol{\rho}, \boldsymbol{r}_2)$ are shown in Fig. 2.1. We emphasize that since there are two electrons that can form positronium, there are two corresponding sets of Jacobi coordinates. When necessary we will refer to them explicitly as $(\boldsymbol{R}_1, \boldsymbol{\rho}_1, \boldsymbol{r}_2)$ and $(\boldsymbol{R}_2, \boldsymbol{\rho}_2, \boldsymbol{r}_1)$. Fig. 2.1 shows one of them, where Ps is formed by electron 1; the second is obtained by exchanging electrons 1 and 2.

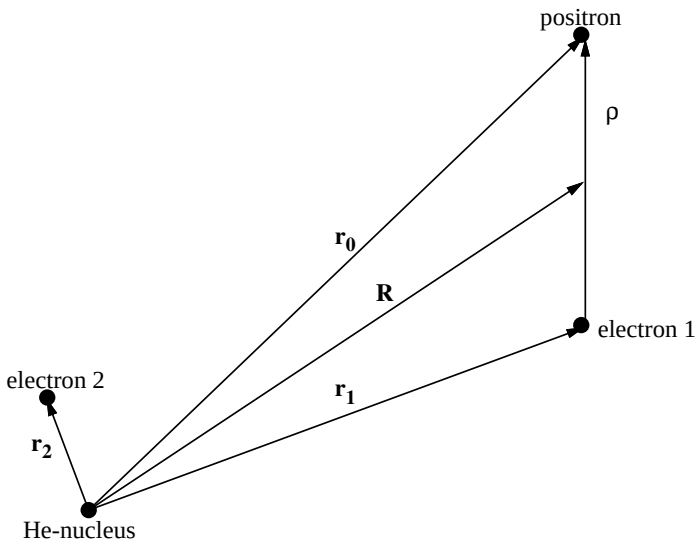


Figure 2.1: Coordinate systems for positron-helium scattering

The total scattering wavefunction $\Psi$ for the system satisfies the Schrödinger equation

$$(H - E)\Psi^{sSM}(\boldsymbol{x}_0, \boldsymbol{x}_1, \boldsymbol{x}_2) = 0, \tag{2.5}$$

where $E$ is the total energy and $\boldsymbol{x}_0, \boldsymbol{x}_1$ and $\boldsymbol{x}_2$ are the coordinates of the particles including their spin. In the absence of spin-orbit interactions it is possible to separate the spin and radial parts according to

$$\Psi^{sSM}(\boldsymbol{x}_0, \boldsymbol{x}_1, \boldsymbol{x}_2) = \Phi^{sS}(\boldsymbol{r}_0, \boldsymbol{r}_1, \boldsymbol{r}_2)\chi_{sSM}(0, (1, 2)), \tag{2.6}$$

where $\chi_{sSM}(0, (1, 2))$ is a function describing the spin state of the two electrons (with combined two-particle spin $s$) and the positron with the total spin $S$ and its projection $M$, while $\Phi^{sS}(\boldsymbol{r}_0, \boldsymbol{r}_1, \boldsymbol{r}_2)$ depends only on spatial coordinates. Since we have a system of four particles with two identical fermions, the total wavefunction must be antisymmetric against permutation of the two electrons.

### 2.1.1 Expansion of the total wavefunction

For positron scattering from atoms the system has two centers, one associated with the target atom and the other with Ps. In addition, positronium can be formed in both para (p-Ps) and ortho (o-Ps) states depending on the spin projections of the electron and the positron that form Ps. The two-centre convergent close-coupling approach to positron-He scattering is based on the expansion of the total wavefunction $\Psi^{sSM}$ in terms of states of all asymptotic channels, i.e.

$$\Psi^{sSM} \approx \frac{1}{\sqrt{2}}(1-P_{12})\Big[\sum_{\alpha}^{N_{\rm He}} F_{\alpha}^{(s)}(\boldsymbol{r}_0)\psi_{\alpha}(\boldsymbol{r}_1,\boldsymbol{r}_2)\chi_{_{sSM}}(0,(1,2)) + \sum_{s'}\sum_{\beta}^{N_{\rm Ps}} G_{\beta}^{(s')}(\boldsymbol{R}_1)\psi_{\beta}(\boldsymbol{\rho}_1)\phi_{1s}(\boldsymbol{r}_2)\chi_{s'SM}((0,1),2)\Big], \tag{2.7}$$

where the first term corresponds to expansion in terms of the helium wavefunctions $\psi_\alpha$ with expansion coefficients $F_\alpha^{(s)}$, while the second term corresponds to expansion in terms of the positronium states $\psi_\beta$ with coefficients $G_\beta^{(s')}$, which in turn depend on the spins $s$ and $s'$ of He and Ps, respectively. The $N_{\rm He}$ and $N_{\rm Ps}$ are the numbers of the atomic and Ps states, respectively. The indices $\alpha$ and $\beta$ run over all generated pseudo-states of the helium atom and Ps, including positive-energy ones corresponding to a discretized continuum. The singlet and triplet He states have $s=0$ and $s=1$, respectively. The second term allows for both electrons to form positronium and the sum over $s'$ takes into account positronium formation in para ($s'=0$) and ortho ($s'=1$) states. The residual ion of $He^+$ is described by $\phi_{1s}$. The anti-symmetrization over the two-electron permutations is included by the operator $\frac{1}{\sqrt{2}}(1-P_{12})$, where $P_{12}$ is a permutation operator which interchanges the electrons 1 and 2. The spin functions are defined as

$$\chi_{sSM}(0,(1,2)) = \sum_{\mu_0,\mu} C^{SM}_{\frac{1}{2}\mu_0\, s\mu}\chi_{\frac{1}{2}\mu_0}(0)\chi_{s\mu}(1,2) \tag{2.8}$$

for the $e^+ - He$ channel, and

$$\chi_{s'SM}((0,1),2) = \sum_{\mu_2,\mu'} C^{SM}_{\frac{1}{2}\mu_2\, s'\mu'} \chi_{s'\mu'}(0,1)\chi_{\frac{1}{2}\mu_2}(2) \tag{2.9}$$

for the $Ps - He^+$ channel, where $C^{ab}_{cd\,ef}$ are the Clebsch-Gordan coefficients of vector addition.

### 2.1.2 Separation of the spin part of the total wavefunction

As spin-orbit interactions are neglected, the initial spin of the target $s$, the total spin $S$ and consequently the total spin function must be conserved. Therefore the spatial part in Eq. (2.6) can be written as

$$\Phi^{sS}(\boldsymbol{r}_0, \boldsymbol{r}_1, \boldsymbol{r}_2) = \langle \chi_{sSM}(0,(1,2)) \mid \Psi^{sSM} \rangle. \tag{2.10}$$

In order to find the overlap on the right-hand side of Eq. (2.10) we perform the spin algebra somewhat similar to the electron-helium scattering case presented in [75]. Using Eqs. (2.8) and (2.9) and the fact that the spin functions $\chi_{sSM}$ form a complete set we get the following relations

$$\begin{aligned} \chi_{sSM}(0,(2,1)) &= \sum_{s''} \chi_{s''SM}(0,(1,2)) \langle \chi_{s''SM}(0,(1,2)) | \chi_{sSM}(0,(2,1)) \rangle \\ &= (-1)^{s+1} \chi_{sSM}(0,(1,2)), \end{aligned} \tag{2.11}$$

$$\begin{aligned} \chi_{s'SM}((0,1),2) &= \sum_{s''} \chi_{s''SM}(0,(1,2)) \langle \chi_{s''SM}(0,(1,2)) | \chi_{s'SM}((0,1),2) \rangle \\ &= \sum_{s''} c_{s's''S} \chi_{s''SM}(0,(1,2)), \end{aligned} \tag{2.12}$$

and using the above two relations we also obtain

$$\chi^{\beta}_{s'SM}((0,2),1) = \sum_{s''} (-1)^{s''+1} c_{s's''S} \chi^{\alpha}_{s''SM}(0,(1,2)), \tag{2.13}$$

where the overlap coefficients are given by the 6j-symbol

$$c_{s's''S} = (-1)^{S-\frac{1}{2}}\sqrt{(2s'+1)(2s''+1)}\left\{ \begin{array}{ccc} \frac{1}{2} & \frac{1}{2} & s' \\ S & \frac{1}{2} & s'' \end{array} \right\}. \tag{2.14}$$

Now we can rewrite the expansion (2.7) by explicitly writing the result of the $(1 - P_{12})$ operator. Then using the recoupling coefficients (2.14) we get

$$\begin{aligned}\Psi^{sSM} \approx & \frac{1}{\sqrt{2}}\sum_{\alpha}^{N_{\rm He}} F_\alpha^{(s)}(\boldsymbol{r}_0)\{\psi_\alpha(\boldsymbol{r}_1,\boldsymbol{r}_2) + (-1)^s\psi_\alpha(\boldsymbol{r}_2,\boldsymbol{r}_1)\}\chi_{sSM}(0,(1,2)) \\ & + \frac{1}{\sqrt{2}}\sum_{s's''} c_{s's''S}\sum_{\beta}^{N_{\rm Ps}}\{G_\beta^{(s')}(\boldsymbol{R}_1)\psi_\beta(\boldsymbol{\rho}_1)\phi_{1s}(\boldsymbol{r}_2) \\ & + (-1)^{s''}G_\beta^{(s')}(\boldsymbol{R}_2)\psi_\beta(\boldsymbol{\rho}_2)\phi_{1s}(\boldsymbol{r}_1)\}\chi_{sSM}(0,(1,2)).\end{aligned} \tag{2.15}$$

By projecting according to Eq. (2.10) we get the spatial part of the total wavefunction

$$\begin{aligned}\Phi^{sS}(\boldsymbol{r}_0,\boldsymbol{r}_1,\boldsymbol{r}_2) \approx & \frac{1}{\sqrt{2}}\sum_{\alpha}^{N_{\rm He}} F_\alpha^{(s)}(\boldsymbol{r}_0)\{\psi_\alpha(\boldsymbol{r}_1,\boldsymbol{r}_2) + (-1)^s\psi_\alpha(\boldsymbol{r}_2,\boldsymbol{r}_1)\} \\ & + \frac{1}{\sqrt{2}}\sum_{s'} c_{s'sS}\sum_{\beta}^{N_{\rm Ps}}\{G_\beta^{(\rm s')}(\boldsymbol{R}_1)\psi_\beta(\boldsymbol{\rho}_1)\phi_{1s}(\boldsymbol{r}_2) \\ & + (-1)^s G_\beta^{(\rm s')}(\boldsymbol{R}_2)\psi_\beta(\boldsymbol{\rho}_2)\phi_{1s}(\boldsymbol{r}_1)\}.\end{aligned} \tag{2.16}$$

The Ps spin $s'$ can be 0 or 1. Writing the sum over $s'$ explicitly we finally obtain

$$\begin{aligned}\Phi^{sS} \approx & \sum_{\alpha}^{N_{\rm He}} F_\alpha^{(s)}(\boldsymbol{r}_0)\psi_\alpha^s(\boldsymbol{r}_1,\boldsymbol{r}_2) \\ & + \frac{1}{\sqrt{2}}\sum_{\beta}^{N_{\rm Ps}}\{\tilde{G}_\beta^{(sS)}(\boldsymbol{R}_1)\psi_\beta(\boldsymbol{\rho}_1)\phi_{1s}(\boldsymbol{r}_2) + (-1)^s\tilde{G}_\beta^{(sS)}(\boldsymbol{R}_2)\psi_\beta(\boldsymbol{\rho}_2)\phi_{1s}(\boldsymbol{r}_1)\},\end{aligned} \tag{2.17}$$

where

$$\psi_\alpha^s(\boldsymbol{r}_1,\boldsymbol{r}_2) = \frac{1}{\sqrt{2}}\{\psi_\alpha(\boldsymbol{r}_1,\boldsymbol{r}_2) + (-1)^s\psi_\alpha(\boldsymbol{r}_2,\boldsymbol{r}_1)\} \tag{2.18}$$

is the antisymmetrized helium wavefunction and

$$\tilde{G}_\beta^{(sS)}(\boldsymbol{R}) = c_{0sS}G_\beta^{(0)}(\boldsymbol{R}) + c_{1sS}G_\beta^{(1)}(\boldsymbol{R}). \tag{2.19}$$

We emphasize that the superscript $s$ of $\tilde{G}_\beta$ is the spin of the target, while that of $G_\beta$ is the spin of the formed positronium.

Let us consider now particular cases. For positron scattering from the ground state of helium, i.e. when $s = 0$ and $S = \frac{1}{2}$, we get

$$c_{00\frac{1}{2}} = -1/2 \text{ and } c_{10\frac{1}{2}} = \frac{\sqrt{3}}{2}. \tag{2.20}$$

Therefore, according to Eq. (2.19) the corresponding expansion coefficient takes the form

$$\tilde{G}_\beta^{(0\frac{1}{2})}(\boldsymbol{R}) = -\frac{1}{2}G_\beta^{(0)}(\boldsymbol{R}) + \frac{\sqrt{3}}{2}G_\beta^{(1)}(\boldsymbol{R}), \tag{2.21}$$

which agrees with the result derived in [76] in a different way (also given in the Appendix B) for this particular case. For positron scattering on the metastable states of helium with $s = 1$ there are two different couplings with the incoming positron's spin, resulting in $S = \frac{1}{2}$ and $S = \frac{3}{2}$. When $S = \frac{1}{2}$ we have

$$c_{01\frac{1}{2}} = \frac{\sqrt{3}}{2} \text{ and } c_{11\frac{1}{2}} = \frac{1}{2}. \tag{2.22}$$

Therefore

$$\tilde{G}_\beta^{(1\frac{1}{2})}(\boldsymbol{R}) = \frac{\sqrt{3}}{2}G_\beta^{(0)}(\boldsymbol{R}) + \frac{1}{2}G_\beta^{(1)}(\boldsymbol{R}). \tag{2.23}$$

If the spins couple to give $S = \frac{3}{2}$ then

$$c_{01\frac{3}{2}} = 0 \text{ and } c_{11\frac{3}{2}} = 1 \tag{2.24}$$

leading to

$$\tilde{G}_\beta^{(1\frac{3}{2})}(\boldsymbol{R}) = G_\beta^{(1)}(\boldsymbol{R}). \tag{2.25}$$

Finally, since Eqs. (2.23) and (2.25) represent the same amplitude we conclude that

$$G_\beta^{(1)} = \sqrt{3}G_\beta^{(0)}. \tag{2.26}$$

This relationship is often assumed and used in the literature, however, to our best knowledge its origin remained unclear.

The wavefunction $\psi_\alpha^s(\boldsymbol{r}_1, \boldsymbol{r}_2)$ of helium is symmetrised by definition and constructed using the configuration interaction (CI) approach [68] (see Appendix A) with a frozen core (FC) or a multi-core (MC) approximation. In the FC approximation one of the electrons is described by the $He^+$ 1s orbital. In the MC approximation the core electron is described by any number of orbitals as necessary to yield as accurate He wave functions as desired. However, in the Ps-$He^+$ channels we neglect any effects of excitation of the residual ion and set the state of the residual ion to be always $1s$. Eq. (2.17) reflects this approximation.

### 2.1.3 Scattering equations

As was shown in Eqs. (2.7-2.17) the spin part of the total wavefunction can be factorized and removed from the equations. In this case, for a given total spin $S$ and target spin $s$, the Schrödinger equation (2.5) reduces to

$$(H - E)\Phi^{sS}(\boldsymbol{r}_0, \boldsymbol{r}_1, \boldsymbol{r}_2) = 0, \tag{2.27}$$

where the spatial part of the total wavefunction $\Phi^{sS}$ is given by Eq. (2.17). We note that the use of both He and Ps states in the two-centre expansion (2.17) implies required boundary conditions in the atomic and Ps channels. However, it also may lead to double counting of the continuum for the following reasons. If the sets of the He and Ps states are complete, then only one of

$$\sum_{\alpha}^{N_{\rm He}} F_\alpha^{(s)}(\boldsymbol{r}_0)\psi_\alpha^s(\boldsymbol{r}_1, \boldsymbol{r}_2)$$

and

$$\frac{1}{\sqrt{2}}\sum_{\beta}^{N_{\rm Ps}}\{\tilde{G}_\beta^{(sS)}(\boldsymbol{R}_1)\psi_\beta(\boldsymbol{\rho}_1)\phi_{1s}(\boldsymbol{r}_2) + (-1)^s\tilde{G}_\beta^{(sS)}(\boldsymbol{R}_2)\psi_\beta(\boldsymbol{\rho}_2)\phi_{1s}(\boldsymbol{r}_1)$$

alone can give the exact expansion of the total wavefunction. Then the two-centre expansion is over-complete. Additionally, the He and Ps bases are not orthogonal to each other. This may result in an ill-conditioned set of equations. However in practical calculations we use a finite number of states from both centers and thus over-completeness is avoided. The ill-conditioning appears in the process of solving the equations and can be overcome by using very accurate integration meshes. We will return to this issue later when we discuss numerical methods and results.

Substituting the expansion (2.17) into (2.27) and following [77] we can obtain momentum-space coupled-channel equations for the transition matrix elements. Below we present the basic steps of converting SE into LSE.

Substitute (2.17) into SE (2.27) to get

$$(E-H)\Big(\sum_{\alpha}^{N_{\rm He}} F_{\alpha}^{(s)}(\boldsymbol{r}_0)\psi_{\alpha}^{s}(\boldsymbol{r}_1,\boldsymbol{r}_2)+\frac{1}{\sqrt{2}}\sum_{\beta}^{N_{\rm Ps}}\{\tilde{G}_{\beta}^{(sS)}(\boldsymbol{R}_1)\psi_{\beta}(\boldsymbol{\rho}_1)\phi_{1s}(\boldsymbol{r}_2) + (-1)^{s}\tilde{G}_{\beta}^{(sS)}(\boldsymbol{R}_2)\psi_{\beta}(\boldsymbol{\rho}_2)\phi_{1s}(\boldsymbol{r}_1)\}\Big)=0. \tag{2.28}$$

Projecting Eq. (2.28) on the left side on the helium atom states $\psi_{\alpha'}^{s}$ and positronium states $\psi_{\beta'}$ respectively, we obtain the following equations for the expansion functions of $F_{\alpha'}$ and $\tilde{G}_{\beta'}$ (for brevity of the notations we drop spin superscripts from the expansion functions)

$$\begin{aligned}(E-\epsilon_{\rm He^+}-\epsilon'_{\alpha}-\frac{1}{2m_0}\nabla^2_{\boldsymbol{r}_0})F_{\alpha'}(\boldsymbol{r}_0) = &\sum_{\alpha}^{N_{\rm He}}\langle\,\psi_{\alpha'}^{s}|U_{\alpha'\alpha}|\psi_{\alpha}^{s}\,\rangle F_{\alpha}(\boldsymbol{r}_0)\\ &+\sqrt{2}\sum_{\beta}^{N_{\rm Ps}}\langle\,\psi_{\alpha'}^{s}|U_{\alpha'\beta}|\psi_{\beta}\phi_{1s}\,\rangle_{r_1,r_2}\\ &\times\tilde{G}_{\beta}(\boldsymbol{R}_1)\end{aligned} \tag{2.29}$$

and

$$(E-\epsilon_{\mathrm{He}^+}-\epsilon'_\beta-\frac{1}{2M_{Ps}}\nabla^2_{\boldsymbol{R}})\tilde{G}_{\beta'}(\boldsymbol{R}_1) = \sqrt{2}\sum_{\alpha}^{N_{\mathrm{He}}}\langle\,\psi_{\beta'}\phi_{1s}|U_{\beta'\alpha}|\psi^s_\alpha\,\rangle_{r1,r2}F_\alpha(\boldsymbol{r}_0) + \sum_{\beta}^{N_{\mathrm{Ps}}}\langle\,\psi_{\beta'}\phi_{1s}|U_{\beta\beta}|\psi_\beta\phi_{1s}\,\rangle_{r_1,r_2}\tilde{G}_\beta(\boldsymbol{R}_1) + \sum_{\beta}^{N_{\mathrm{Ps}}}\langle\,\psi_{\beta'}\phi_{1s}|U^{\mathrm{ex}}_{\beta'\beta}|\phi_{1s}\psi_\beta\,\rangle_{r_2,r_1}\tilde{G}_\beta(\boldsymbol{R}_2), \tag{2.30}$$

where the channel potentials are given by

$$U_{\alpha'\alpha}=\frac{2}{r_0}-\frac{1}{r_{01}}-\frac{1}{r_{02}}, \tag{2.31}$$

$$U_{\beta'\beta}=\frac{2}{|\boldsymbol{R}+\frac{1}{2}\boldsymbol{\rho}|}-\frac{2}{|\boldsymbol{R}-\frac{1}{2}\boldsymbol{\rho}|}+\frac{1}{|\boldsymbol{R}-\frac{1}{2}\boldsymbol{\rho}-\boldsymbol{r}|}-\frac{2}{|\boldsymbol{R}+\frac{1}{2}\boldsymbol{\rho}-\boldsymbol{r}|}, \tag{2.32}$$

$$U_{\alpha\beta}\equiv U_{\beta\alpha}=H-E, \tag{2.33}$$

$$U^{\mathrm{ex}}_{\beta'\beta}=H-E. \tag{2.34}$$

The total Hamiltonian of the system is given by Eq. (2.1) and $E$ is the total energy of the system. In order to obtain Eqs. (2.29-2.30) the following relations have been used

$$\Big(-\frac{1}{2}\nabla^2_{\boldsymbol{r}_1}-\frac{1}{2}\nabla^2_{\boldsymbol{r}_2}-\frac{2}{r_1}-\frac{2}{r_2}+\frac{1}{|\boldsymbol{r}_1-\boldsymbol{r}_2|}\Big)\phi^s_\alpha(\boldsymbol{r}_1,\boldsymbol{r}_2)=\epsilon_\alpha\phi^s_\alpha(\boldsymbol{r}_1,\boldsymbol{r}_2), \tag{2.35}$$

$$\Big(-\frac{1}{2}\nabla^2_{\boldsymbol{\rho}}-\frac{1}{\rho}\Big)\phi_\beta(\boldsymbol{\rho})=\epsilon_\beta\phi_\beta(\boldsymbol{\rho}), \tag{2.36}$$

$$\Big(-\frac{1}{2}\nabla^2_{\boldsymbol{r}}-\frac{1}{r}\Big)\phi_{1s}(\boldsymbol{r})=\epsilon_{\mathrm{He}^+}\phi_{1s}(\boldsymbol{r}). \tag{2.37}$$

Solving the differential Eqs. (2.29, 2.30) is not convenient as they do not explicitly contain scattering boundary conditions. Using the asymptotic behavior

of the total wavefunction Sloan and Moore [77] have shown that the differential close-coupling equations can be transformed into momentum-space Lippmann-Schwinger integral equation for the T-matrix.

We neglect the last term on the right-hand side of Eq. (2.30). This term corresponds to the electron exchange between the $He^+$ ion and Ps. Justification for such an approximation will be discussed in Section 2.3.2. With this approximation we can write Eqs. (2.29, 2.30) in the following way by combining the indices $\alpha$ and $\beta$ into a single index $\gamma$

$$(E - \epsilon_{\mathrm{He}^+} - \epsilon_{\gamma'} - \widehat{K}_{\gamma'})\tilde{F}_{\gamma'} = \sum_{\gamma} Z_{\gamma'\gamma}\tilde{F}_{\gamma}. \tag{2.38}$$

It can be seen that

$$\begin{aligned}
&\text{if } \gamma' = \alpha' \text{ and } \gamma = \alpha \text{ then} \\
&\quad \epsilon_\gamma = \epsilon_\alpha,\ \ \tilde{F}_\gamma = F_\alpha,\ \ \hat{K}_\gamma = \frac{1}{2m_\alpha}\nabla^2_{\boldsymbol{r}_0},\ \ \ Z_{\alpha'\alpha} = \langle\psi_{\alpha'}|U_{\alpha'\alpha}|\psi_\alpha\rangle, \\
&\text{if } \gamma' = \beta' \text{ and } \gamma = \beta \text{ then} \\
&\quad \epsilon_\gamma = \epsilon_\beta,\ \tilde{F}_\gamma = \tilde{G}_\beta,\ \widehat{K}_\gamma = \frac{1}{2m_\beta}\nabla^2_{\boldsymbol{R}},\ Z_{\beta'\beta} = \langle\psi_{\beta'}\phi_{1s}|U_{\beta'\beta}|\psi_\beta\phi_{1s}\rangle, \\
&\text{if } \gamma' = \beta \text{ and } \gamma = \alpha \text{ then } Z_{\beta\alpha} = \sqrt{2}\langle\psi_\beta\phi_{1s}|U_{\beta\alpha}|\psi_\alpha\rangle,
\end{aligned}$$

where $m_\alpha = 1$ and $m_\beta = 2$. By defining the operator of the Green's function

$$\widehat{\mathcal{G}}_\gamma = (E - \epsilon_{\mathrm{He}^+} - \epsilon_\gamma - \hat{K}_\gamma)^{-1} \tag{2.39}$$

we can write the formal solution of the differential equation (2.38) in the form of

$$\tilde{F}_{\gamma'} = \tilde{F}_0 + \widehat{\mathcal{G}}_{\gamma'}\sum_{\gamma} Z_{\gamma'\gamma}\tilde{F}_\gamma, \tag{2.40}$$

where $\tilde{F}_0$ is a solution of Eq. (2.38) when the right hand side is 0, i.e. $\widehat{\mathcal{G}}_\gamma^{-1}\tilde{F}_0 = 0$. The latter is a plane wave $|\boldsymbol{q}\rangle$ of the relative motion and is an eigenfunction of

$\widehat{\mathcal{G}}_\gamma^{-1}$

$$\mathcal{G}_\gamma^{-1}|\boldsymbol{q}\rangle = (E - \epsilon_{\mathrm{He}^+} - \epsilon_\gamma - \frac{1}{2m_\gamma}q^2)|\boldsymbol{q}\rangle, \tag{2.41}$$

where the plane wave is normalized according to

$$\langle \boldsymbol{q}|\boldsymbol{q}'\rangle = (2\pi)^3\delta(\boldsymbol{q}-\boldsymbol{q}').$$

Therefore we can write

$$\mathcal{G}_{\gamma'} = \int \frac{d\boldsymbol{q}''}{(2\pi)^3}\frac{|\boldsymbol{q}''\rangle\langle\boldsymbol{q}''|}{E^+ - \epsilon_{\gamma'} - \frac{1}{2m_{\gamma'}}q''^2 \pm i0}\,, \tag{2.42}$$

where $E^+ = E - \epsilon_{\mathrm{He}^+}$. The above integral contains a singular point at $\frac{1}{2m_{\gamma'}}q''^2 = E^+ - \epsilon_{\gamma'}$. The addition of $\pm i0$ defines the integration path around the singularity point at $q_{\gamma'} = \sqrt{2m_{\gamma'}(E^+ - \epsilon_{\gamma'})}$ and, depending on its sign, corresponds to outgoing (+) or incoming (-) boundary conditions.

The formal solution of Eq. (2.38) is

$$|\tilde{F}_{\gamma'}\rangle = |\boldsymbol{q}_{\gamma'}\rangle + \sum_\gamma \int \frac{d\boldsymbol{q}''}{(2\pi)^3}\frac{|\boldsymbol{q}''\rangle}{E^+ - \epsilon_{\gamma'} - \frac{1}{2m_{\gamma'}}q''^2 \pm i0}\langle\boldsymbol{q}''|Z_{\gamma'\gamma}|\tilde{F}_\gamma\rangle. \tag{2.43}$$

For the collision channel with initial target state $i$ and incoming wave $|\boldsymbol{q}_i\rangle$ the outgoing (with $+i0$) asymptotes of $F_\gamma(x)$ (where $x$ is $r_0$ for $\alpha$ channels and $R$ for $\beta$ channels) at $x \to \infty$ must be

$$\tilde{F}_{\gamma'}(x\to\infty) = \delta_{\gamma',i}e^{i\boldsymbol{q}_i\boldsymbol{x}} + f(\boldsymbol{q}_\gamma, \boldsymbol{q}_i)\frac{e^{iq_{\gamma'}x}}{x} \tag{2.44}$$

where $f(\boldsymbol{q}_\gamma, \boldsymbol{q}_i)$ is a scattering amplitude and $q_{\gamma'} = \sqrt{2m_{\gamma'}(E^+ - \epsilon_{\gamma'})}$. On the other hand we can find the asymptotic form of (2.43) corresponding to outgoing-wave boundary conditions [78]. By using the contour integration technique to calculate the integral with a singularity at $\frac{1}{2m_{\gamma'}}q''^2 = E^+ - \epsilon_{\gamma'}$ we get

$$\tilde{F}_{\gamma'}(x\to\infty) = \delta_{\gamma',i}e^{i\boldsymbol{q}_i\boldsymbol{x}} - \frac{m_{\gamma'}}{(2\pi)}\sum_\gamma\langle\boldsymbol{q}'|Z_{\gamma'\gamma}|\tilde{F}_\gamma\rangle\frac{e^{iq_{\gamma'}x}}{x}. \tag{2.45}$$

Comparing the last two we find that

$$f_{\gamma' i}(\boldsymbol{q}_{\gamma'}, \boldsymbol{q}_i) = -\frac{m_{\gamma'}}{(2\pi)} \sum_{\gamma} \langle \boldsymbol{q}_{\gamma'} | Z_{\gamma'\gamma} | \tilde{F}^i_{\gamma} \rangle. \tag{2.46}$$

Then from the definition of the on-shell T-matrix

$$T_{\gamma'\gamma}(\boldsymbol{q}_{\gamma}, \boldsymbol{q}_{\gamma}) = -\frac{1}{(2\pi)^2 m_{\gamma'}} f_{\gamma'\gamma}(\boldsymbol{q}_{\gamma}, \boldsymbol{q}_{\gamma})$$

it follows that

$$T_{\gamma' i}(\boldsymbol{q}_{\gamma'}, \boldsymbol{q}_i) = \frac{1}{(2\pi)^3} \sum_{\gamma} \langle \boldsymbol{q}_{\gamma'} | Z_{\gamma'\gamma} | \tilde{F}^i_{\gamma} \rangle. \tag{2.47}$$

Therefore, Eq. (2.43) can be written as

$$|\tilde{F}_{\gamma'}\rangle = \delta_{\gamma',i} |\boldsymbol{q}_i\rangle + \int d\boldsymbol{q}' \frac{|\boldsymbol{q}\rangle}{E^+ - \epsilon_{\gamma'} - \frac{1}{2m_{\gamma'}} q^2 + i0} T_{\gamma'\gamma}(\boldsymbol{q}_{\gamma'}, \boldsymbol{q}_{\gamma}). \tag{2.48}$$

Using Eq. (2.48) in Eq. (2.43) we get the Lippmann-Schwinger type equations for the T-matrices

$$T_{\gamma'\gamma}(\boldsymbol{q}_{\gamma'}, \boldsymbol{q}_{\gamma}) = \langle \boldsymbol{q}_{\gamma'} | Z_{\gamma'\gamma} | \boldsymbol{q}_{\gamma} \rangle + \sum_{\gamma''} \int \frac{d\boldsymbol{q}''}{(2\pi)^3} \frac{\langle \boldsymbol{q}_{\gamma'} | Z_{\gamma'\gamma''} | \boldsymbol{q}'' | \rangle}{E^+ - \epsilon_{\gamma''} - \frac{1}{2m_{\gamma''}} q''^2 + i0} T_{\gamma''\gamma}(\boldsymbol{q}'', \boldsymbol{q}_{\gamma}). \tag{2.49}$$

Denoting

$$V_{\gamma'\gamma}(\boldsymbol{q}_{\gamma'}, \boldsymbol{q}_{\gamma}) = \langle \boldsymbol{q}_{\gamma'} | Z_{\gamma'\gamma} | \boldsymbol{q}_{\gamma} \rangle \tag{2.50}$$

we get the LSE for the transition matrix elements

$$\begin{aligned} T_{\gamma'\gamma}(\boldsymbol{q}_{\gamma'}, \boldsymbol{q}_{\gamma}) =& V_{\gamma'\gamma}(\boldsymbol{q}_{\gamma'}, \boldsymbol{q}_{\gamma}) + \\ & \sum_{\gamma''}^{N_{\mathrm{He}}+N_{\mathrm{Ps}}} \int \frac{d\boldsymbol{q}_{\gamma''}}{(2\pi)^3} V_{\gamma'\gamma''}(\boldsymbol{q}_{\gamma'}, \boldsymbol{q}_{\gamma''}) \mathcal{G}_{\gamma''}(q^2_{\gamma''}) T_{\gamma''\gamma}(\boldsymbol{q}_{\gamma''}, \boldsymbol{q}_{\gamma}), \end{aligned} \tag{2.51}$$

where $\gamma = \alpha, \beta$ and $\boldsymbol{q}_{\gamma}$ is the momentum of free particle $\gamma$ relative to c.m. of the bound pair in channel $\gamma$. The effective two-body free Green's functions are defined as

$$\mathcal{G}_{\alpha''}(q^2_{\alpha''}) = (E - \epsilon_{\mathrm{He}^+} + i0 - q^2_{\alpha''}/2 - \epsilon_{\alpha''})^{-1}, \tag{2.52}$$

$$\mathcal{G}_{\beta''}(q^2_{\beta''}) = (E - \epsilon_{\mathrm{He}^+} + i0 - q^2_{\beta''}/4 - \epsilon_{\beta''})^{-1}, \tag{2.53}$$

and describe the free relative motion of particle $\gamma''$ and bound pair $\gamma''$ with binding energy $\epsilon_{\gamma''}$. Note that above we used the assumption that the $He^+$ ion is left in its ground state. The effective potentials used in Eq. (2.51) are given by

$$V_{\alpha'\alpha}(\boldsymbol{q}_{\alpha'}, \boldsymbol{q}_{\alpha}) = \langle \boldsymbol{q}_{\alpha'} | \langle \psi_{\alpha'} | U_{\alpha'\alpha} | \psi_{\alpha} \rangle | \boldsymbol{q}_{\alpha} \rangle, \tag{2.54}$$

$$V_{\beta'\beta}(\boldsymbol{q}_{\beta'}, \boldsymbol{q}_{\beta}) = \langle \boldsymbol{q}_{\beta'} | \langle \psi_{\beta'}\phi_{1s} | U_{\beta'\beta} + U^{\rm ex}_{\beta'\beta} | \psi_{\beta}\phi_{1s} \rangle | \boldsymbol{q}_{\beta} \rangle, \tag{2.55}$$

$$V_{\beta\alpha}(\boldsymbol{q}_{\beta}, \boldsymbol{q}_{\alpha}) = \sqrt{2}\langle \boldsymbol{q}_{\beta} | \langle \psi_{\beta}\phi_{1s} | U_{\beta\alpha} | \psi_{\alpha} \rangle | \boldsymbol{q}_{\alpha} \rangle, \tag{2.56}$$

and their derivations are given in the following sections.

The hamiltonian in Eq. (2.1) conserves the total angular momentum $J$. Therefore it is practical to solve Eq. (2.51) for a given $J$. To this end we use a partial-wave expansion in the total orbital angular momentum $J$ according to (and similar for $T_{\gamma'\gamma}(\boldsymbol{q}_{\gamma'}, \boldsymbol{q}_{\gamma})$)

$$V_{\gamma'\gamma}(\boldsymbol{q}_{\gamma'}, \boldsymbol{q}_{\gamma}) = \sum_{L',M',L,M,J,K} Y_{L'M'}(\widehat{\boldsymbol{q}}_{\gamma'}) C^{JK}_{L'M'\,l'm'} \mathcal{V}^{L'LJ}_{\gamma',\gamma}(q_{\gamma'}, q_{\gamma}) C^{JK}_{LM\,lm} Y^{*}_{LM}(\widehat{\boldsymbol{q}}_{\gamma}), \tag{2.57}$$

where $Y_{LM}(\widehat{\boldsymbol{q}}_{\gamma})$ are the spherical harmonics of unit vector $\widehat{\boldsymbol{q}}_{\gamma}$. With this Eq. (2.51) transforms to

$$\begin{aligned}\mathcal{T}^{L'LJ}_{\gamma',\gamma}(q_{\gamma'}, q_{\gamma}) =& \mathcal{V}^{L'LJ}_{\gamma',\gamma}(q_{\gamma'}, q_{\gamma}) + \sum_{\gamma''}^{N_\alpha+N_\beta} \sum_{L''} \int \frac{dq_{\gamma''} q^2_{\gamma''}}{(2\pi)^3} \mathcal{V}^{L'L''J}_{\gamma',\gamma''}(q_{\gamma'}, q_{\gamma''}) \mathcal{G}_{\gamma''}(q^2_{\gamma''}) \\ & \times \mathcal{T}^{L''LJ}_{\gamma'',\gamma}(q_{\gamma''}, q_{\gamma}),\end{aligned} \tag{2.58}$$

where $L$, $L'$ and $L''$ are the angular momenta of the free particles in channels $\gamma$, $\gamma'$ and $\gamma''$, respectively. The effective potentials in the representation of the total angular momentum are given by

$$\begin{aligned}\mathcal{V}^{L'LJ}_{\gamma',\gamma}(q_{\gamma'}, q_{\gamma}) = & \sum_{m',m,M',M} \iint d\widehat{\boldsymbol{q}}_{\gamma'} d\widehat{\boldsymbol{q}}_{\gamma} Y^{*}_{L'M'}(\widehat{\boldsymbol{q}}_{\gamma'}) C^{JK}_{L'M'\,l'm'} V_{\gamma'\gamma}(\boldsymbol{q}_{\gamma'}, \boldsymbol{q}_{\gamma}) \\ & \times C^{JK}_{LM\,lm} Y_{LM}(\widehat{\boldsymbol{q}}_{\gamma}).\end{aligned} \tag{2.59}$$

The angular momenta of pair $\gamma$ ($\gamma'$) are $l$ ($l'$), and $M$, $m$, $K$ are the projections of $L$, $l$, $J$, respectively. Accordingly, $K = M + m = M' + m'$.

## 2.2 Helium and positronium structure

The He structure is calculated using the configuration interaction expansion (see Appendix A). In this approach the He wavefunctions are represented as

$$\psi^s_\alpha(\boldsymbol{r}_1, \boldsymbol{r}_2) = \sum_{ab} \mathrm{C}^\alpha_{ab} \sum_{l_a, m_a, l_b, m_b} C^{l\,m}_{l_a m_a\, l_b m_b} \phi_a(\boldsymbol{r}_1)\phi_b(\boldsymbol{r}_2), \tag{2.60}$$

where index $\alpha$ denotes a full set of quantum numbers describing the target (He) states. The configuration interaction (CI) coefficients $\mathrm{C}^\alpha_{ab}$ are obtained from the diagonalization of the target Hamiltonian. They satisfy the symmetry property

$$\mathrm{C}^\alpha_{ab} = (-1)^{s+l_a+l_b-l}\mathrm{C}^\alpha_{ba} \tag{2.61}$$

to ensure antisymmetry of the two-electron target states. The single-particle basis functions are taken as

$$\phi_a(\boldsymbol{r}) = \frac{1}{r} R_{n_a l_a}(r) Y_{l_a m_a}(\widehat{\boldsymbol{r}}).$$

The Ps wavefunctions can be written as

$$\phi_\beta(\boldsymbol{\rho}) = Y_{lm}(\widehat{\boldsymbol{\rho}}) \sum_{k=1}^{N} B^l_{nk} R_{kl}(\rho), \tag{2.62}$$

and for a given basis size $N$ and basis function $R_{kl}$ the coefficients $B^l_{nk}$ are found by diagonalizing the Ps Hamiltonian. Index $\beta$ denotes a full set of quantum numbers describing the Ps states.

In the CCC formalism the single particle radial basis function $R_{nl}$ are taken as the square-integrable orthogonal Laguerre basis:

$$R_{nl}(r) = \Big(\frac{\lambda_l (n-1)!}{(2l+1+n)!}\Big)^{1/2} (\lambda_l r)^{l+1} e^{(-\lambda_l r)} L^{2l+2}_{n-1}(-\lambda_l r), \tag{2.63}$$

where $L_{n-1}^{2l+2}(-\lambda_l r)$ are the associated Laguerre polynomials, and $n$ ranges from 1 to the basis size $N_l = N_0 - l$, for $l = 0, 1, ..., l_{\max}$. The converged result for a given state does not depend on the fall off parameter $\lambda_l$, however the rate of convergence does. Therefore it can be chosen according to practical convenience. Usually we choose $\lambda_l$ to be 0.5 for Ps and 2 for He states. As $N_0$ increases (with the fixed value of $\lambda$) the lowest bound states of He and Ps become closer to their eigenstates while the positive-energy pseudo-states yield an increasingly denser discretization of the continuum. This will also extend the pseudo-states to higher positive energies.

## 2.3 Transition matrix elements

### 2.3.1 Direct atom-atom transitions

Channel effective potentials of the direct atom-atom ($\alpha \to \alpha$) transitions are given by Eq. (2.31). The corresponding matrix elements are written as

$$V_{\alpha'\alpha}(\boldsymbol{q}_{\alpha'}, \boldsymbol{q}_\alpha) = \iiint d^3\boldsymbol{r}_0\, d^3\boldsymbol{r}_1\, d^3\boldsymbol{r}_2\, \psi^s_{\alpha'}(\boldsymbol{r}_1, \boldsymbol{r}_2)\, e^{-i\boldsymbol{q}_{\alpha'}\boldsymbol{r}_0} U_{\alpha\alpha} \psi^s_\alpha(\boldsymbol{r}_1, \boldsymbol{r}_2) e^{i\boldsymbol{q}_\alpha \boldsymbol{r}_0}. \tag{2.64}$$

Considering the symmetry with respect to interchanging $r_1$ and $r_2$ we can write

$$V_{\alpha'\alpha}(\boldsymbol{q}_{\alpha'}, \boldsymbol{q}_\alpha) = \int\int\int d^3\boldsymbol{r}_0\, d^3\boldsymbol{r}_1\, d^3\boldsymbol{r}_2\, \psi^s_{\alpha'}(\boldsymbol{r}_1, \boldsymbol{r}_2)\, e^{-i\boldsymbol{q}_{\alpha'}\boldsymbol{r}_0} \Big(\frac{2}{r_0} - \frac{2}{|\boldsymbol{r}_0 - \boldsymbol{r}_1|}\Big) \times \psi^s_\alpha(\boldsymbol{r}_1, \boldsymbol{r}_2) e^{i\boldsymbol{q}_\alpha \boldsymbol{r}_0}. \tag{2.65}$$

Thus the definition of $U_{\alpha'\alpha}$ changes to

$$U_{\alpha'\alpha} = \frac{2}{r_0} - \frac{2}{|\boldsymbol{r}_0 - \boldsymbol{r}_1|}. \tag{2.66}$$

Taking He wavefunctions as given in Eq. (2.60) the direct atom-atom transition matrix elements are written as

$$\begin{aligned} V_{\alpha'\alpha}(\boldsymbol{q}_{\alpha'},\boldsymbol{q}_{\alpha}) =& \sum_{cd} \mathrm{C}^{\alpha'}_{cd} \sum_{l_c,m_c,l_d,m_d} C^{l'\,m'}_{l_c m_c l_d m_d} \sum_{ab} \mathrm{C}^{\alpha}_{ab} \sum_{l_a,m_a,l_b,m_b} C^{lm}_{l_a m_a l_b m_b} \\ & \times \iiint d^3\boldsymbol{r}_0\, d^3\boldsymbol{r}_1 d^3\boldsymbol{r}_2\, \phi_c(\boldsymbol{r}_1)\phi_d(\boldsymbol{r}_2) e^{-i\boldsymbol{q}_{\alpha'}\boldsymbol{r}_0} U_{\alpha\alpha} \\ & \times \phi_a(\boldsymbol{r}_1)\phi_b(\boldsymbol{r}_2) e^{i\boldsymbol{q}_{\alpha}\boldsymbol{r}_0}. \end{aligned} \tag{2.67}$$

We then expand the plane waves in (2.67) and the potential $U_{\alpha'\alpha}$ in terms of the spherical harmonics according to

$$e^{i\boldsymbol{q}_{\alpha}\boldsymbol{r}_0} = 4\pi \sum_{l_0 m_0} i^{l_0} j_{l_o}(q r_0) Y^*_{l_0 m_0}(\widehat{\boldsymbol{q}}_{\alpha}) Y_{l_0 m_0}(\widehat{\boldsymbol{r}}_0) \tag{2.68}$$

and

$$U_{\alpha'\alpha} = 4\pi \sum_{\lambda\mu} \frac{1}{2\lambda+1} \mathcal{U}^{\lambda}_{\alpha'\alpha}(r_0,r_1) Y^*_{\lambda\mu}(\widehat{\boldsymbol{r}}_0) Y_{\lambda\mu}(\widehat{\boldsymbol{r}}_1), \tag{2.69}$$

where

$$\mathcal{U}^{\lambda}_{\alpha'\alpha}(r_0,r_1) = \begin{cases} \dfrac{2\delta_{\lambda 0}}{r_0} - \dfrac{2r_0^{\lambda}}{r_1^{\lambda+1}} & \text{if} \quad r_0 \le r_1, \\ \dfrac{2\delta_{\lambda 0}}{r_0} - \dfrac{2r_1^{\lambda}}{r_0^{\lambda+1}} & \text{if} \;\; r_0 > r_1. \end{cases} \tag{2.70}$$

Substituting the expansions (2.68–2.69) into (2.67) we get

$$\begin{aligned} V_{\alpha'\alpha}(\boldsymbol{q}_{\alpha'},\boldsymbol{q}_{\alpha}) =& (4\pi)^3 \sum_{cd} \mathrm{C}^{\alpha'}_{cd} \sum_{ab} \mathrm{C}^{\alpha}_{ab} \sum_{l'_0,l_c,l_d,l_0,l_a,l_b} i^{l_0-l'_0} \frac{1}{2\lambda+1} \mathcal{I}^{\lambda l'_0 l_0}_{\alpha\alpha}(q_{\alpha'},q_{\alpha}) \\ & \times \sum_{m_c,m_d,m_a,m_b,m'_0,m_0,\mu} C^{l'm'}_{l_c m_c\, l_d m_d}\, C^{lm}_{l_a m_a\, l_b m_b} Y_{l'_0 m'_0}(\widehat{\boldsymbol{q}}_{\alpha'})\, Y^*_{l_0 m_0}(\widehat{\boldsymbol{q}}_{\alpha}) \\ & \times \int d\widehat{\boldsymbol{r}}_0\, Y^*_{l'_0 m'_0}(\widehat{\boldsymbol{r}}_0)\, Y^*_{\lambda\mu}(\widehat{\boldsymbol{r}}_0)\, Y_{l_0 m_0}(\widehat{\boldsymbol{r}}_0) \int d\widehat{\boldsymbol{r}}_1 Y^*_{l_c m_c}(\widehat{\boldsymbol{r}}_1) Y_{\lambda\mu}(\widehat{\boldsymbol{r}}_1) Y_{l_a m_a}(\widehat{\boldsymbol{r}}_1) \\ & \times \int d\widehat{\boldsymbol{r}}_2\, Y^*_{l_d m_d}(\widehat{\boldsymbol{r}}_2)\, Y_{l_b m_b}(\widehat{\boldsymbol{r}}_2), \end{aligned} \tag{2.71}$$

where the radial part is taken into

$$\begin{aligned} \mathcal{I}^{\lambda l'_0 l_0}_{\alpha'\alpha}(q_{\alpha'},q_{\alpha}) =& \langle\phi_d|\phi_b\rangle \int dr_0 r_0^2 j_{l'_0}(q_{\alpha'} r_0)\, j_{l_0}(q_{\alpha} r_0) \\ & \times \int dr_1 r_1^2\, R_{n_c l_c}(r_1) \mathcal{U}^{\lambda}_{\alpha'\alpha}(r_0,r_1) R_{n_a l_a}(r_1), \end{aligned} \tag{2.72}$$

and

$$\langle \phi_d | \phi_b \rangle = \int dr_2 r_2^2 R_{n_d l_d}(r_2) R_{n_b l_b}(r_2) \tag{2.73}$$

is an overlap between two orbitals. After the integration over angular coordinates

$$\begin{aligned}
&\int d\widehat{\boldsymbol{r}}_2\, Y^*_{l_d m_d}(\widehat{\boldsymbol{r}}_2)\, Y_{l_b m_b}(\widehat{\boldsymbol{r}}_2) = \delta_{l_b l_d}\delta_{m_b m_d},\\
&\int d\widehat{\boldsymbol{r}}_1\, Y^*_{l_c m_c}(\widehat{\boldsymbol{r}}_1)\, Y_{\lambda\mu}(\widehat{\boldsymbol{r}}_1)\, Y_{l_a m_a}(\widehat{\boldsymbol{r}}_1) = \frac{1}{\sqrt{4\pi}}\frac{[\lambda\, l_a]}{[l_c]}\, C^{l_c 0}_{\lambda 0\, l_a 0}\, C^{l_c m_c}_{\lambda\mu\, l_a m_a},\\
&\int d\widehat{\boldsymbol{r}}_0\, Y^*_{l'_0 m'_0}(\widehat{\boldsymbol{r}}_0)\, Y^*_{\lambda\mu}(\widehat{\boldsymbol{r}}_0)\, Y_{l_0 m_0}(\widehat{\boldsymbol{r}}_0) = \frac{1}{\sqrt{4\pi}}\frac{[\lambda\, l'_0]}{[l_0]}\, C^{l_0 0}_{l'_0 0\, \lambda 0}\, C^{l_0 m_0}_{l'_0 m'_0\, \lambda\mu},
\end{aligned} \tag{2.74}$$

we get

$$\begin{aligned}
V_{\alpha'\alpha}(\boldsymbol{q}_{\alpha'}, \boldsymbol{q}_\alpha) =& (4\pi)^2 \sum_{cd} \mathrm{C}^{\alpha'}_{cd} \sum_{ab} \mathrm{C}^{\alpha}_{ab} \sum_{l'_0, l_c, l_0, l_a, l_b \lambda} i^{l_0 - l'_0} \frac{[l'_0\, l_a]}{[l_0 l_c]} \cdot C^{l_c 0}_{\lambda 0\, l_a 0}\, C^{l_0 0}_{l'_0 0\, \lambda 0}\\
&\times \mathcal{I}^{\lambda l'_0 l_0}_{\alpha\alpha}(q_{\alpha'}, q_\alpha) \sum_{m'_0, m_0} Y_{l'_0 m'_0}(\widehat{\boldsymbol{q}}_{\alpha'})\, Y^*_{l_0 m_0}(\widehat{\boldsymbol{q}}_\alpha) C^{l_0 m_0}_{l'_0 m'_0}\\
&\times \sum_{m_c, m_a, m_b, \mu} C^{l' m'}_{l_c m_c\, l_b m_b}\, C^{l m}_{l_a m_a\, l_b m_b}\, C^{l_c m_c}_{\lambda\mu\, l_a m_a},
\end{aligned} \tag{2.75}$$

where $[l] \equiv \sqrt{2l+1}$. In (2.75) we take a sum over projections $m_c, m_b$ and $m_a$:

$$\begin{aligned}
\sum_{m_c, m_b, m_a} C^{l' m'}_{l_c m_c\, l_b m_b}\, C^{l m}_{l_a m_a\, l_b m_b} C^{l_c m_c}_{l_a m_a\, \lambda\mu} (-1)^{l_a + \lambda - l_c} =& (-1)^{l_a + l_b + l}\, [l\, l_c]\, C^{l' m'}_{l m\, \lambda\mu}\\
&\times \left\{ \begin{array}{ccc} l_a & l_b & l \\ l' & \lambda & l_c \end{array} \right\}.
\end{aligned} \tag{2.76}$$

Using (2.76) in (2.75) we get

$$\begin{aligned}
V_{\alpha'\alpha}(\boldsymbol{q}_{\alpha'}, \boldsymbol{q}_\alpha) =& (4\pi)^2 \sum_{cd} \mathrm{C}^{\alpha'}_{cd} \sum_{ab} \mathrm{C}^{\alpha}_{ab} \sum_{l'_0, l_c, l_0, l_a, l_b \lambda} i^{l_0 - l'_0}\, (-1)^{l_a + l_b + l}\, \frac{[l'_0\, l_a\, l]}{[l_0]}\\
&\times \mathcal{I}^{\lambda l'_0 l_0}_{\alpha\alpha}(q_{\alpha'}, q_\alpha)\, C^{l_c 0}_{\lambda 0\, l_a 0}\, C^{l_0 0}_{l'_0 0\, \lambda 0} \left\{ \begin{array}{ccc} l_a & l_b & l \\ l' & \lambda & l_c \end{array} \right\}\\
&\times \sum_{m'_0, m_0, \mu} C^{l' m'}_{l m\, \lambda\mu}\, C^{l_0 m_0}_{l'_0 m'_0\, \lambda\mu}\, Y_{l'_0 m'_0}(\widehat{\boldsymbol{q}}_{\alpha'})\, Y^*_{l_0 m_0}(\widehat{\boldsymbol{q}}_\alpha).
\end{aligned} \tag{2.77}$$

Substituting this into (2.59) and integrating over $\widehat{\boldsymbol{q}}_{\alpha'}$ and $\widehat{\boldsymbol{q}}_{\alpha}$ we get the partial-wave expanded form

$$\begin{aligned}\mathcal{V}^{L'L}_{\alpha'\alpha}(q_{\alpha'},q_\alpha) =&(4\pi)^2\sum_{cd}\mathrm{C}^{\alpha'}_{cd}\sum_{ab}\mathrm{C}^{\alpha}_{ab}\sum_{l_c,l_a,l_b\lambda} i^{L-L'}\,(-1)^{l_a+l_b+l}\,\frac{[L'\,l_a\,l]}{[L]}\\ &\times\mathcal{I}^{\lambda L'L}_{\alpha'\alpha}(q_{\alpha'},q_\alpha)\,C^{l_c0}_{\lambda0\,l_a0}\,C^{L0}_{L0\,\lambda0}\begin{Bmatrix} l_a & l_b & l\\ l' & \lambda & l_c\end{Bmatrix}\\ &\times\sum_{m',M',m,M,\mu} C^{JK}_{L'M'\,l'm'}C^{JK}_{LM\,lm}\,C^{l'm'}_{lm\,\lambda\mu}\,C^{LM}_{L'M'\,\lambda\mu}.\end{aligned}\tag{2.78}$$

Then we take the sum over the angular projections in (2.78):

$$\begin{aligned}\sum_{m',M',m,M,\mu} C^{JK}_{L'M'\,l'm'}C^{JK}_{LM\,lm}\,C^{l'm'}_{lm\,\lambda\mu}\,C^{LM}_{L'M'\,\lambda\mu} &= (-1)^{\lambda+l-l'+\lambda+L'-L}\\ &\times\sum_{m',M'} C^{JK}_{L'M'\,l'm'}\sum_{m,M,\mu} C^{JK}_{LM\,lm}\,C^{l'm'}_{lm\,\lambda\mu}\,C^{LM}_{L'M'\,\lambda\mu}\\ &=\sum_{m',M'} C^{JK}_{L'M'\,l'm'}\,C^{JK}_{l'm'\,L'M'}\begin{Bmatrix} L' & \lambda & L\\ l & J & l'\end{Bmatrix}[l'L]\\ &=(-1)^{L'+l'-J}\,[l'\,L]\begin{Bmatrix} L' & \lambda & L\\ l & J & l'\end{Bmatrix}.\end{aligned}\tag{2.79}$$

Using (2.79) in (2.78) and writing $i^{L-L'}=(-1)^{\frac{L}{2}-\frac{L'}{2}}$ we finally get

$$\begin{aligned}\mathcal{V}^{L'L}_{\alpha'\alpha}(q_{\alpha'},q_\alpha) =&(4\pi)^2\,(-1)^{J+l'+(L+L')/2}[L'\,l\,l']\sum_{cd}\mathrm{C}^{\alpha'}_{cd}\sum_{ab}\mathrm{C}^{\alpha}_{ab}\sum_{l_c,l_a,l_b\lambda}(-1)^{l_a+l_b}[l_a]\\ &\times\mathcal{I}^{\lambda L'L}_{\alpha'\alpha}(q_{\alpha'},q_\alpha)\,C^{l_c0}_{\lambda0\,l_a0}\,C^{L0}_{L'0\,\lambda0}\begin{Bmatrix} l' & \lambda & l\\ l_a & l_b & l_c\end{Bmatrix}\begin{Bmatrix} L' & \lambda & L\\ l & J & l'\end{Bmatrix},\end{aligned}\tag{2.80}$$

where the radial part now is

$$\begin{aligned}\mathcal{I}^{\lambda L'L}_{\alpha'\alpha}(q_{\alpha'},q_\alpha) =&\langle\phi_d|\phi_b\rangle\int dr_0 r_0^2 j_{L'}(q_{\alpha'}r_0)\,j_L(q_\alpha r_0)\\ &\times\int dr_1 r_1^2\,R_{n_cl_c}(r_1)\mathcal{U}^{\lambda}_{\alpha'\alpha}(r_0,r_1)R_{n_al_a}(r_1).\end{aligned}\tag{2.81}$$

### 2.3.2 Direct Ps-Ps transitions

In the Ps-$He^+$ channels, Ps $\rightarrow$ Ps transitions can occur in two ways. First by the static potential from the $He^+$ ion given by Eq. (2.32). Secondly by electron exchange between Ps and the $He^+$ ion given in Eq. (2.34). For the simplicity of the calculations we neglect the electron exchange term. This approximation is supported by the studies of Van Reeth and Humberston [79] who observed similarity in the S-wave Ps formation from hydrogen and helium. They suggested that the electron of the $He^+$ ion is strongly bound, which makes the latter similar to a proton. At the same time a big difference (a factor of eight) between the mean kinetic energies of the electron in $He^+$ ion and that in Ps makes them effectively distinguishable. The neglected exchange effect should be of more importance in the static exchange and s-wave model calculations, as in these cases direct transitions due to the static potential are exactly zero. In the real problem the direct Ps $\rightarrow$ Ps transitions should be dominated by the static potential rather than electron exchange. Therefore we consider the direct Ps $\rightarrow$ Ps transitions only via the static potential of the $He^+$ ion. The $He^+$ ion in its ground state is described by

$$\phi_{1s}(\boldsymbol{r}_2) = \sqrt{\frac{2}{\pi}} e^{-2r_2}. \tag{2.82}$$

As we mentioned earlier we neglect $He^+$ excitation. Within this approximation the static potential that causes Ps $\rightarrow$ Ps direct transitions is

$$\begin{aligned} W(\boldsymbol{R},\boldsymbol{\rho}) &\equiv \langle \phi_{1s}|U_{\beta'\beta}|\phi_{1s}\rangle \\ &= \int d\boldsymbol{r_2}\phi^*_{1s}(\boldsymbol{r}_2)\Big(\frac{2}{|\boldsymbol{R}+\frac{\boldsymbol{\rho}}{2}|} - \frac{2}{|\boldsymbol{R}-\frac{\boldsymbol{\rho}}{2}|} + \frac{1}{|\boldsymbol{R}+\frac{\boldsymbol{\rho}}{2}-\boldsymbol{r}_2|} - \frac{1}{|\boldsymbol{R}-\frac{\boldsymbol{\rho}}{2}-\boldsymbol{r}_2|}\Big) \\ &\quad \times \phi_{1s}(\boldsymbol{r}_2) \\ &= \frac{1}{|\boldsymbol{R}+\frac{\boldsymbol{\rho}}{2}|} + \Big(2+\frac{1}{|\boldsymbol{R}+\frac{\boldsymbol{\rho}}{2}|}\Big)e^{-4|\boldsymbol{R}+\frac{\boldsymbol{\rho}}{2}|} - \frac{1}{|\boldsymbol{R}-\frac{\boldsymbol{\rho}}{2}|} - \Big(2+\frac{1}{|\boldsymbol{R}-\frac{\boldsymbol{\rho}}{2}|}\Big) \\ &\quad \times e^{-4|\boldsymbol{R}-\frac{\boldsymbol{\rho}}{2}|}. \end{aligned} \tag{2.83}$$

Then the transition matrix elements are written as

$$V_{\beta'\beta}(\boldsymbol{q}_{\beta'},\boldsymbol{q}_{\beta}) = \iint d^3\boldsymbol{R}\, d^3\boldsymbol{\rho}\, e^{-i\boldsymbol{q}_{\beta'}\boldsymbol{R}}\psi^*_{\beta'}(\boldsymbol{\rho})W(\boldsymbol{R},\boldsymbol{\rho})\psi_{\beta}(\boldsymbol{\rho})\, e^{i\boldsymbol{q}_{\beta}\boldsymbol{R}}. \tag{2.84}$$

We expand the potential $W(\boldsymbol{R},\boldsymbol{\rho})$ according to

$$W(\boldsymbol{R},\boldsymbol{\rho}) = 4\pi\sum_{\lambda\mu}\frac{1}{[\lambda^2]}\,\mathcal{U}^{\lambda}_{\beta'\beta}(R,\rho)Y^*_{\lambda\mu}(\widehat{\boldsymbol{R}})Y_{\lambda\mu}(\widehat{\boldsymbol{\rho}}), \tag{2.85}$$

where

$$\mathcal{U}^{\lambda}_{\beta'\beta}(R,\rho) = [(-1)^{\lambda}-1]\begin{cases}\dfrac{2^{\lambda+1}R^{\lambda}}{\rho^{\lambda+1}} + \mathcal{W}_{\lambda}(R,\rho) & \text{if } R\le\rho,\\[2ex] \dfrac{\rho^{\lambda}}{2^{\lambda}R^{\lambda+1}} + \mathcal{W}_{\lambda}(R,\rho) & \text{if } R>\rho,\end{cases} \tag{2.86}$$

and

$$\mathcal{W}_{\lambda}(R,\rho) = \frac{2\lambda+1}{2}\int_{-1}^{+1} d\widehat{z}\left(\frac{2}{r}+\frac{1}{|\boldsymbol{R}-\frac{1}{2}\boldsymbol{\rho}|}\right)e^{-2Z|\boldsymbol{R}-\frac{1}{2}\boldsymbol{\rho}|}P_{\lambda}(\widehat{z}). \tag{2.87}$$

Here $\widehat{z}$ is the cosine of the angle between $\boldsymbol{R}$ and $\boldsymbol{\rho}$. Substituting (2.85) and the expansions of the plane waves (see Eq. (2.68)) into Eq. (2.84) and taking the configuration space bound-state wavefunction in the form

$$\psi_{\beta}(\boldsymbol{\rho}) = R_{nl}(\rho)Y_{lm}(\widehat{\boldsymbol{\rho}}),$$

with $R_{nl}(\rho)$ being the square-integrable radial part, we get

$$\begin{aligned}V_{\beta'\beta}(\boldsymbol{q}_{\beta'},\boldsymbol{q}_{\beta}) =& (4\pi)^3\sum_{l_0,m_0,l'_0,m'_0,\lambda} i^{l_0-l'_0}\frac{1}{\widehat{\lambda}^2}I^{\lambda}_{\beta'\beta}(q_{\beta'},q_{\beta})\,Y_{l'_0m'_0}(\widehat{\boldsymbol{q}}_{\beta'})\,Y^*_{l_0m_0}(\widehat{\boldsymbol{q}}_{\beta})\\ &\times\int d\widehat{\rho}\,Y^*_{l'm'}(\widehat{\boldsymbol{\rho}})Y_{lm}(\widehat{\boldsymbol{\rho}})Y_{\lambda\mu}(\widehat{\boldsymbol{\rho}})\int d\widehat{\boldsymbol{R}}\,Y^*_{l'_0m'_0}(\widehat{\boldsymbol{R}})Y_{l_0m_0}(\widehat{\boldsymbol{R}})Y^*_{\lambda\mu}(\widehat{\boldsymbol{R}}),\end{aligned} \tag{2.88}$$

where the radial part is separated into the function

$$I^{\lambda l'_0 l_0}_{\beta'\beta}(q_{\beta'},q_{\beta}) = \int_0^{\infty} dR\,R^2\,j_{l'_0}(q_{\beta'}R)\,j_{l_0}(q_{\beta}R)\int_0^{\infty} d\rho\,\rho^2\,R^*_{n'l'}(\rho)\,\mathcal{U}^{\lambda}_{\beta'\beta}(R,\rho)\,R_{nl}(\rho). \tag{2.89}$$

Integrating over the angles of $\boldsymbol{R}$ and $\boldsymbol{\rho}$ results in

$$V_{\beta'\beta}(\boldsymbol{q}_{\beta'},\boldsymbol{q}_{\beta}) = (4\pi)^2 \sum_{l_0,m_0,l_0',m_0',\lambda} i^{l_0-l_0'} \frac{[l\,l_0']}{[l'\,l_0]} C^{l'm'}_{lm\,\lambda\mu} C^{l_0m_0}_{l_0'm_0'\,\lambda\mu} I^{\lambda}_{\beta'\beta}(q_{\beta'},q_{\beta}) \times Y_{l_0'm_0'}(\widehat{\boldsymbol{q}}_{\beta'})\, Y^{*}_{l_0m_0}(\widehat{\boldsymbol{q}}_{\beta}). \tag{2.90}$$

Substituting the latter into Eq. (2.59) we obtain the partial-wave expanded form

$$\mathcal{V}^{L'L}_{\beta'\beta}(q_{\beta'},q_{\beta}) = (4\pi)^2 i^{L-L'} \sum_{m',m,M',M} C^{L'l'J}_{M'm'K} C^{LlJ}_{MmK} \times \sum_{\lambda}{}^{(2)} \frac{[L']}{[L]} C^{L'\lambda L}_{M'\mu M} C^{L'\lambda L}_{000} \frac{[l]}{[l']} C^{l\lambda l'}_{m\mu m'} C^{l\lambda l'}_{000}\, I^{\lambda}_{\beta'\beta}(q_{\beta'},q_{\beta}), \tag{2.91}$$

where all radial information is now contained in the integral

$$I^{\lambda L'L}_{\beta'\beta}(q_{\beta'},q_{\beta}) = \int_0^{\infty} dR\, R^2\, j_{L'}(q_{\beta'}R)\, j_L(q_{\beta}R) \int_0^{\infty} d\rho\, \rho^2\, R_{n'l'}(\rho) \mathcal{U}^{\lambda}_{\beta'\beta}(R,\rho)\, R_{nl}(\rho). \tag{2.92}$$

Summing over the angular momenta projections one finally arrives at

$$\mathcal{V}^{L'L}_{\beta'\beta}(q_{\beta'},q_{\beta}) = (4\pi)^2\,(-1)^{J+(L+L')/2}\,[L'\,l] \sum_{\lambda}{}^{(2)} C^{l'0}_{l0\,\lambda0}\, C^{L0}_{L'0\,\lambda0} \times \begin{Bmatrix} \lambda & l & l' \\ J & L' & L \end{Bmatrix} I^{\lambda L'L}_{\beta'\beta}(q_{\beta'},q_{\beta}), \tag{2.93}$$

where the braces denote a $6j$-symbol. Step 2 of the sum points to the fact that only the terms corresponding to $\lambda$ of the same parity as that of $l'+l$ (or, equivalently, of $L'+L$) contribute.

### 2.3.3 Rearrangement transitions

Calculations of the effective potentials for the rearrangement (atom $\rightarrow$ Ps) transitions are relatively more complicated. Using the CI approximation for the helium wavefunctions, the rearrangement matrix elements also can be calculated in a similar way as in the positron hydrogen case [4].

The effective potentials for rearrangement $\alpha \to \beta$ transitions are written as

$$V_{\beta\alpha}(\boldsymbol{q}_\beta, \boldsymbol{q}_\alpha) \equiv \sqrt{2}\langle \boldsymbol{q}_\beta | \langle \psi_\beta \phi_{1s} | U_{\beta\alpha} | \psi_\alpha \rangle | \boldsymbol{q}_\alpha \rangle$$
$$= \sqrt{2} \iiint d\boldsymbol{r}_0 d\boldsymbol{r}_1 d\boldsymbol{r}_2 e^{-i\boldsymbol{q}_\beta \boldsymbol{R}_1} \psi^*_\beta(\boldsymbol{\rho}_1) \phi^*_{1s}(\boldsymbol{r}_2)(H - E)\psi_\alpha(\boldsymbol{r}_1, \boldsymbol{r}_2) e^{i\boldsymbol{q}_\alpha \boldsymbol{r}_0}. \tag{2.94}$$

Using the helium wavefunctions given in Eq. (2.60) the rearrangement matrix elements are written as

$$V_{\beta\alpha}(\boldsymbol{q}_\beta, \boldsymbol{q}_\alpha) = \sqrt{2} \sum_{ab} \mathrm{C}^\alpha_{ab} \sum_{l_a, m_a, l_b, m_b} C^{l\,m}_{l_a m_a\, l_b m_b} \iiint d\boldsymbol{r}_0 d\boldsymbol{r}_1 d\boldsymbol{r}_2 e^{-i\boldsymbol{q}_\beta \boldsymbol{R}_1}$$
$$\times \psi^*_\beta(\boldsymbol{\rho}_1) \phi^*_{1s}(\boldsymbol{r}_2)[H - E]\phi_a(\boldsymbol{r}_1)\phi_b(\boldsymbol{r}_2) e^{i\boldsymbol{q}_\alpha \boldsymbol{r}_0}. \tag{2.95}$$

Integrating over $\boldsymbol{r}_2$ we get

$$\int d\boldsymbol{r}_2 \phi^*_{1s}(\boldsymbol{r}_2)[H - E]\phi_b(\boldsymbol{r}_2) = \delta_{b,1s}\Big( -\frac{1}{2}\nabla^2_{\boldsymbol{r}_0} - \frac{1}{2}\nabla^2_{\boldsymbol{r}_1} + \frac{2}{r_0} - \frac{2}{r_1} - \frac{1}{\rho_1} - E\Big)$$
$$+ \epsilon_b - f_b(\boldsymbol{r}_0) + f_b(\boldsymbol{r}_1), \tag{2.96}$$

where

$$\epsilon_b = \int d\boldsymbol{r}_2 \phi^*_{1s}(\boldsymbol{r}_2)\Big( -\frac{1}{2}\nabla^2_{\boldsymbol{r}_2} - \frac{2}{r_2}\Big)\phi_b(\boldsymbol{r}_2), \tag{2.97}$$

and

$$f_b(\boldsymbol{r}) = \int d\boldsymbol{r}_2 \phi^*_{1s}(\boldsymbol{r}_2) \frac{1}{|\boldsymbol{r} - \boldsymbol{r}_2|} \phi_b(\boldsymbol{r}_2). \tag{2.98}$$

Because of the orthogonality of $\phi_b$ to $\phi_{1s}$ we can take $\epsilon_b = \delta_{b,1s}\epsilon_{1s}$ where $\epsilon_{1s}$ is the binding energy of the electron of the $\mathrm{He}^+$ ion described by $\phi_{1s}(\boldsymbol{r})$ given in Eq. (2.82). In particular, when $b = 1s$ the function $f_b$ reduces to

$$f_{1s}(\boldsymbol{r}) = \int d\boldsymbol{r}_2 \phi^*_{1s}(\boldsymbol{r}_2) \frac{1}{|\boldsymbol{r} - \boldsymbol{r}_2|} \phi_{1s}(\boldsymbol{r}_2) = \Big[ -\frac{1}{r} + \Big(2 + \frac{1}{r}\Big)e^{-4r}\Big]. \tag{2.99}$$

Substituting Eq. (2.96) into (2.95) we get

$$\begin{aligned}V_{\beta\alpha}(\boldsymbol{q}_\beta,\boldsymbol{q}_\alpha) =&\sqrt{2}\sum_{ab}\mathrm{C}^{\alpha}_{ab}\sum_{l_a,m_a,l_b,m_b}C^{l\,m}_{l_a m_a\, l_b m_b}\Big[\delta_{b,1s}\iint d\boldsymbol{r}_0 d\boldsymbol{r}_1 e^{-i\boldsymbol{q}_\beta\boldsymbol{R}_1}\psi^*_\beta(\boldsymbol{\rho}_1)\\ &\times\Big(-\frac{1}{2}\nabla^2_{\boldsymbol{r}_0}-\frac{1}{2}\nabla^2_{\boldsymbol{r}_1}+\frac{1}{r_0}-f_{1s}(r_0)-\frac{1}{\rho_1}-E+\epsilon_{1s}-\frac{2}{r_1}+f_{1s}(r_1)\Big)\\ &\times\phi_a(\boldsymbol{r}_1)e^{i\boldsymbol{q}_\alpha\boldsymbol{r}_0}+(1-\delta_{b,1s})\iint d\boldsymbol{r}_0 d\boldsymbol{r}_1 e^{-i\boldsymbol{q}_\beta\boldsymbol{R}_1}\psi^*_\beta(\boldsymbol{\rho}_1)\big(f_b(\boldsymbol{r}_1)\\ &-f_b(\boldsymbol{r}_0)\big)\phi_a(\boldsymbol{r}_1)e^{i\boldsymbol{q}_\alpha\boldsymbol{r}_0}\Big]. \qquad (2.100)\end{aligned}$$

Here we make an approximation by neglecting $f_b(\boldsymbol{r}_0)$ under the second integral. This approximation is indeed reasonable as this term corresponds to the secondary transition which is the transition from a higher (than 1s) state to the 1s state at the same time with the other electron jumping to the positronium state. The derivation for this term would be more complicated as it involves more virtual momenta than for other terms that are considered below. We have evaluated the contribution of this term for the s-state calculations and the results have shown that the term can indeed be neglected.

With the aforementioned approximation we can take sum over the configurational orbitals to get

$$\begin{aligned}V_{\beta\alpha}(\boldsymbol{q}_\beta,\boldsymbol{q}_\alpha) =&\iint d\boldsymbol{r}_0 d\boldsymbol{r}_1 e^{-i\boldsymbol{q}_\beta\boldsymbol{R}_1}\psi^*_\beta(\boldsymbol{\rho}_1)\Big[-\frac{1}{2}\nabla^2_{\boldsymbol{r}_0}-\frac{1}{2}\nabla^2_{\boldsymbol{r}_1}+\frac{2}{r_0}-f_{1s}(r_0)\\ &-\frac{1}{\rho_1}-E+\epsilon_{1s}-\frac{2}{r_1}+f_{1s}(r_1)\Big)\Big]\xi_\alpha(\boldsymbol{r}_1)e^{i\boldsymbol{q}_\alpha\boldsymbol{r}_0}\\ &+\iint d\boldsymbol{r}_0 d\boldsymbol{r}_1 e^{-i\boldsymbol{q}_\beta\boldsymbol{R}_1}\psi^*_\beta(\boldsymbol{\rho}_1)\zeta_\alpha(\boldsymbol{r}_1)e^{i\boldsymbol{q}_\alpha\boldsymbol{r}_0}, \qquad (2.101)\end{aligned}$$

where

$$\begin{aligned}\xi_\alpha(\boldsymbol{r}_1) =&\sqrt{2}\sum_{ab}\mathrm{C}^{\alpha}_{ab}\sum_{l_a,m_a,l_b,m_b}C^{l\,m}_{l_a m_a\, l_b m_b}\delta_{b,1s}\phi_a(\boldsymbol{r}_1)\\ =&\sqrt{2}\sum_{ab}\mathrm{C}^{\alpha}_{ab}\delta_{b,1s}R_a(r_1)\,Y_{lm}(\widehat{\boldsymbol{r}}_1)=B_{nl}(r_1)\,Y_{lm}(\widehat{\boldsymbol{r}}_1), \qquad (2.102)\end{aligned}$$

and

$$\begin{aligned}\zeta_\alpha(\boldsymbol{r}_1) =&\sqrt{2}\sum_{a,\,b}(1-\delta_{b,1s})\mathrm{C}^\alpha_{ab}\sum_{l_a,m_a,l_b,m_b} C^{lm}_{l_a m_a\, l_b m_b} f_b(\boldsymbol{r}_1)\phi_a(\boldsymbol{r}_1)\\ =&\sqrt{2}\sum_{a,\,b}(1-\delta_{b,1s})\mathrm{C}^\alpha_{ab}F_b(r_1)R_a(r_1)\,Y_{lm}(\widehat{\boldsymbol{r}}_1)\\ =&D_{nl}(r_1)\,Y_{lm}(\widehat{\boldsymbol{r}}_1)\end{aligned} \tag{2.103}$$

with

$$F_b(r_1) = \int_0^\infty dr_2 R_{1s}(r_2)\frac{r_<^{l_b}}{r_>^{l_b+1}}R_b(r_2). \tag{2.104}$$

We now change the integration variables from $(\boldsymbol{r}_0, \boldsymbol{r}_1)$ to $(\boldsymbol{R}_1, \boldsymbol{\rho}_1)$. Hereafter we can drop the index 1. As the Jacobian of this transformation is equal to 1, we get

$$\begin{aligned}V_{\beta\alpha}(\boldsymbol{q}_\beta,\boldsymbol{q}_\alpha) = &\iint d\boldsymbol{R}d\boldsymbol{\rho}e^{-i\boldsymbol{q}_\beta\boldsymbol{R}}\psi^*_\beta(\boldsymbol{\rho})\Big[-\frac{1}{2}\nabla^2_{\boldsymbol{R}}-\frac{1}{2}\nabla^2_{\boldsymbol{\rho}}+\frac{2}{r_0}-f_{1s}(r_0)-\frac{1}{\rho}-E\\ &+\epsilon_{1s}-\frac{2}{r}+f_{1s}(r)\Big)\Big]\xi_\alpha(\boldsymbol{r})e^{i\boldsymbol{q}_\alpha\boldsymbol{r}_0}\\ &+\iint d\boldsymbol{R}d\boldsymbol{\rho}e^{-i\boldsymbol{q}_\beta\boldsymbol{R}}\psi^*_\beta(\boldsymbol{\rho})\zeta_\alpha(\boldsymbol{r})e^{i\boldsymbol{q}_\alpha\boldsymbol{r}_0}.\end{aligned} \tag{2.105}$$

The hamiltonian $H'_0 = -\frac{1}{4}\nabla_{\boldsymbol{R}} - \nabla^2_{\boldsymbol{\rho}}$ can be taken in variables of either channel $\alpha$ or $\beta$

$$q^2_\alpha/2 + p^2_\alpha/2 \equiv q^2_\beta/4 + p^2_\beta, \tag{2.106}$$

where $\boldsymbol{p}_\gamma$ is the momentum of the internal relative motion of the particles of pair $\gamma$

$$\boldsymbol{p}_\beta = \boldsymbol{q}_\beta/2 - \boldsymbol{q}_\alpha \text{ and } \boldsymbol{p}_\alpha = \boldsymbol{q}_\beta - \boldsymbol{q}_\alpha. \tag{2.107}$$

We split Eq. (2.105) into two parts

$$\begin{aligned}V_{\beta\alpha}(\boldsymbol{q}_\beta,\boldsymbol{q}_\alpha) = &\iint d\boldsymbol{R}d\boldsymbol{\rho}e^{-i\boldsymbol{q}_\beta\boldsymbol{R}}\psi^*_\beta(\boldsymbol{\rho})\Big[\Big(\mathcal{E}(\boldsymbol{q}_\beta,\boldsymbol{q}_\alpha)+\frac{1}{\rho}+\frac{2}{r}+f_{1s}(r)\Big)\xi_\alpha(\boldsymbol{r})\\ &+\zeta_\alpha(\boldsymbol{r})\Big]e^{i\boldsymbol{q}_\alpha\boldsymbol{r}}+\iint d\boldsymbol{R}d\boldsymbol{\rho}e^{-i\boldsymbol{q}_\beta\boldsymbol{R}}\psi^*_\beta(\boldsymbol{\rho})\Big(\frac{2}{r_0}-f_{1s}(r_0)\Big)\xi_\alpha(\boldsymbol{r}_1)e^{i\boldsymbol{q}_\alpha\boldsymbol{r}}\\ \equiv &\, V^{(I)}_{\beta\alpha}(\boldsymbol{q}_\beta,\boldsymbol{q}_\alpha)+V^{(II)}_{\beta\alpha}(\boldsymbol{q}_\beta,\boldsymbol{q}_\alpha),\end{aligned} \tag{2.108}$$

where

$$\mathcal{E}(\boldsymbol{q}_\beta, \boldsymbol{q}_\alpha) = q_\alpha^2/2 + p_\alpha^2/2 - E + \epsilon_{1s}.$$

Now using the momentum-space representations for the wavefunctions the parts can be written as

$$\begin{aligned} V_{\beta\alpha}^{(I)}(\boldsymbol{q}_\beta, \boldsymbol{q}_\alpha) =& \mathcal{E}(\boldsymbol{q}_\beta, \boldsymbol{q}_\alpha)\widetilde{\psi}_\beta^*(\boldsymbol{p}_\beta)\widetilde{\xi}_\alpha(\boldsymbol{p}_\alpha) + \widetilde{g}_\beta^*(\boldsymbol{p}_\beta)\widetilde{\xi}_\alpha(\boldsymbol{p}_\alpha) \\ &+ \widetilde{\psi}_\beta^*(\boldsymbol{p}_\beta)\widetilde{g}_\alpha(\boldsymbol{p}_\alpha) + \widetilde{\psi}_\beta^*(\boldsymbol{p}_\beta)\widetilde{\zeta}_\alpha(\boldsymbol{p}_\alpha) \end{aligned} \tag{2.109}$$

and

$$V_{\beta\alpha}^{(II)}(\boldsymbol{q}_\beta, \boldsymbol{q}_\alpha) = \int \frac{d\boldsymbol{q}}{(2\pi)^3}\widetilde{\psi}_\beta^*(\boldsymbol{p}'_\beta)\Big[\frac{4\pi}{(\boldsymbol{q}-\boldsymbol{q}_\alpha)^2} + 4\pi\frac{32+|\boldsymbol{q}-\boldsymbol{q}_\alpha|^2}{(16+|\boldsymbol{q}-\boldsymbol{q}_\alpha|^2)^2}\Big]\widetilde{\xi}_\alpha(\boldsymbol{p}'_\alpha), \tag{2.110}$$

where $\widetilde{\psi}_\beta$, $\widetilde{\xi}_\alpha$, $\widetilde{\zeta}_\alpha$ are pseudo-state wavefunctions in momentum-space, $\widetilde{g}_\beta$, $\widetilde{g}_\alpha$ are pseudo-state formfactors (we will call them simply pseudoformfactors) corresponding to $\psi_\beta$, $\xi_\alpha$, respectively. Here $\boldsymbol{p}'_\alpha = \boldsymbol{q}_\beta - \boldsymbol{q}$ and $\boldsymbol{p}'_\beta = \boldsymbol{q}_\beta/2 - \boldsymbol{q}$ are the momenta of relative motion of the particles of the corresponding pairs immediately before and after the actual rearrangement via the modified Coulomb potential

$$\frac{4\pi}{(\boldsymbol{q}-\boldsymbol{q}_\alpha)^2} + 4\pi\frac{32+|\boldsymbol{q}-\boldsymbol{q}_\alpha|^2}{(16+|\boldsymbol{q}-\boldsymbol{q}_\alpha|^2)^2}, \tag{2.111}$$

where $\boldsymbol{q}$ is the momentum of the relative motion of fragments in virtual channel $e$.

Now we transform $V_{\beta\alpha}^{(I)}(\boldsymbol{q}_\beta, \boldsymbol{q}_\alpha)$ into the representation of total angular momentum $J$, then separate the radial parts of the momentum-space pseudo-states and pseudoformfactors according to

$$\widetilde{\psi}_\beta(\boldsymbol{p}) = \widetilde{R}_{\beta nl}(p)Y_{lm}(\widehat{\boldsymbol{p}}),$$

$$\widetilde{g}_\beta(\boldsymbol{p}) = \widetilde{u}_{\beta nl}(p)Y_{lm}(\widehat{\boldsymbol{p}})$$

and

$$\widetilde{\xi}_\alpha(\boldsymbol{p}) = \widetilde{B}_{nl}(p) Y_{lm}(\widehat{\boldsymbol{p}}),$$

$$\widetilde{g}_\alpha(\boldsymbol{p}) = \widetilde{u}_{\alpha nl}(p) Y_{lm}(\widehat{\boldsymbol{p}}),$$

$$\widetilde{\zeta}_\alpha(\boldsymbol{p}) = \widetilde{D}_{nl}(p) Y_{lm}(\widehat{\boldsymbol{p}}).$$

The radial parts $\widetilde{R}_{n'l'}(p), \widetilde{B}_{nl}(p), \widetilde{D}_{nl}(p)$ and $\widetilde{u}_{nl}(p)$ will be calculated in the following subsection. Then we have (for given $J$)

$$\begin{aligned}\mathcal{V}^{L'L(I)}_{\beta,\alpha}(q_\beta, q_\alpha) = & \sum_{m',m,M',M} C^{JK}_{L'M'\,l'm'} C^{JK}_{LM\,lm} \iint d\widehat{\boldsymbol{q}}_\beta d\widehat{\boldsymbol{q}}_\alpha Y^*_{L'M'}(\widehat{\boldsymbol{q}}_\beta) Y_{LM}(\widehat{\boldsymbol{q}}_\alpha) \\ & \times Y^*_{l'm'}(\widehat{\boldsymbol{p}}_\beta) Y_{lm}(\widehat{\boldsymbol{p}}_\alpha) \left[\mathcal{E}(\boldsymbol{q}_\beta, \boldsymbol{q}_\alpha) \widetilde{R}^*_{n'l'}(p_\beta) \widetilde{B}_{nl}(p_\alpha)\right. \\ & \left. + \widetilde{R}^*_{n'l'}(p_\beta) \widetilde{u}_{\alpha nl}(p_\alpha) + \widetilde{u}^*_{n'l'}(p_\beta) \widetilde{B}_{nl}(p_\alpha) + \widetilde{R}^*_{n'l'}(p_\beta) \widetilde{D}_{nl}(p_\alpha)\right].\end{aligned} \tag{2.112}$$

Decomposing the spherical harmonics of the direction of the relative motion in pairs $\alpha$ and $\beta$ one gets

$$\begin{aligned}\mathcal{V}^{L'L(I)}_{\beta,\alpha}(q_\beta, q_\alpha) = & 4\pi \sum_{m',m,M',M} C^{JK}_{L'M'\,l'm'} C^{JK}_{LM\,lm} \sum_{l'_1,m'_1,m'_2} C^{l'\,m'}_{l'_1 m'_1\, l'_2 m'_2 m'} \frac{[l'!]}{[l'_1! l'_2!]} q_\beta^{l'_1} \\ & \times (-q_\alpha)^{l'_2} 2^{-l'_1} \sum_{l_1,m_1,m_2} C^{l\,m}_{l_1 - m_1\, l_2 - m_2 m} \frac{[l!]}{[l_1! l_2!]} q_\beta^{l_1} (-q_\alpha)^{l_2} \\ & \times \iint d\widehat{\boldsymbol{q}}_\beta d\widehat{\boldsymbol{q}}_\alpha F^{(I)}(\boldsymbol{q}_\beta, \boldsymbol{q}_\alpha) Y^*_{L'M'}(\widehat{\boldsymbol{q}}_\beta) Y_{LM}(\widehat{\boldsymbol{q}}_\alpha) Y_{l_1 - m_1}(\widehat{\boldsymbol{q}}_\beta) \\ & \times Y^*_{l'_1 m'_1}(\widehat{\boldsymbol{q}}_\beta) Y_{l_2 - m_2}(\widehat{\boldsymbol{q}}_\alpha) Y^*_{l'_2 m'_2}(\widehat{\boldsymbol{q}}_\alpha),\end{aligned} \tag{2.113}$$

where

$$\begin{aligned}F^{(I)}(\boldsymbol{q}_\beta, \boldsymbol{q}_\alpha) = & \mathcal{E}(\boldsymbol{q}_\beta, \boldsymbol{q}_\alpha) \frac{\widetilde{R}^*_{n'l'}(p_\beta) \widetilde{B}_{nl}(p_\alpha)}{p'^{l'}_\beta p^l_\alpha} + \frac{\widetilde{R}^*_{n'l'}(p_\beta) \widetilde{D}_{nl}(p_\alpha)}{p'^{l'}_\beta p^l_\alpha} \\ & + \frac{\widetilde{R}^*_{n'l'}(p_\beta) \widetilde{u}_{\alpha nl}(p_\alpha)}{p'^{l'}_\beta p^l_\alpha} + \frac{\widetilde{u}^*_{n'l'}(p_\beta) \widetilde{B}_{nl}(p_\alpha)}{p'^{l'}_\beta p^l_\alpha},\end{aligned} \tag{2.114}$$

and $l'_1 + l'_2 = l'$, $l_1 + l_2 = l$. Combining two spherical harmonics of the same

relative motion in channels $\alpha$ and $\beta$ we get

$$\begin{aligned}\mathcal{V}^{L'L(I)}_{\beta,\alpha}(q_\beta,q_\alpha) = &\sum_{m',m,M',M} C^{JK}_{L'M'\,l'm'} C^{JK}_{LM\,lm} \sum_{l'_1,m'_1,m'_2} C^{l'\,m'}_{l'_1 m'_1\,l'_2 m'_2} \frac{[l'!]}{[l'_1!l'_2!]} q^{l'_1}_\beta (-q_\alpha)^{l'_2} \\ &\times 2^{-l'_1} \sum_{l_1,m_1,m_2} C^{lm}_{l_1-m_1\,l_2-m_2} \frac{[l!]}{[l_1!l_2!]} q^{l_1}_\beta (-q_\alpha)^{l_2} \sum_{l''_1,m''_1}{}^{(2)} C^{l''_1 m''_1}_{l_1 m_1\,l'_1 m'_1} C^{l''_1 0}_{l_1 0\,l'_1 0} \\ &\times \frac{[l_1 l'_1]}{[l''_1]} \sum_{l''_2,m''_2}{}^{(2)} C^{l''_2\,m''_2}_{l_2-m_2\,l'_2-m'_2} C^{l''_2\,0}_{l_2 0\,l'_2 0} \frac{[l_2 l'_2]}{[l''_2]} (-1)^{m'_2-m_1} \iint d\widehat{\boldsymbol{q}}_\beta d\widehat{\boldsymbol{q}}_\alpha \\ &\times F^{(I)}(\boldsymbol{q}_\beta,\boldsymbol{q}_\alpha) Y^*_{L'M'}(\widehat{\boldsymbol{q}}_\beta) Y_{LM}(\widehat{\boldsymbol{q}}_\alpha) Y^*_{l''_1 m''_1}(\widehat{\boldsymbol{q}}_\beta) Y_{l''_2 m''_2}(\widehat{\boldsymbol{q}}_\alpha). \end{aligned} \tag{2.115}$$

Now we expand $F^{(I)}(\boldsymbol{q}_\beta,\boldsymbol{q}_\alpha)$ according to

$$F^{(I)}(\boldsymbol{q}_\beta,\boldsymbol{q}_\alpha) = 2\pi \sum_{\lambda,\mu} \mathcal{F}^{(I)}_\lambda(q_\beta,q_\alpha) Y^*_{\lambda\mu}(\widehat{\boldsymbol{q}}_\beta) Y_{\lambda\mu}(\widehat{\boldsymbol{q}}_\alpha), \tag{2.116}$$

where the expansion coefficients are given by

$$\mathcal{F}^{(I)}_\lambda(q_\beta,q_\alpha) = \int_{-1}^{1} dz F^{(I)}(\boldsymbol{q}_\beta,\boldsymbol{q}_\alpha) P_\lambda(z), \tag{2.117}$$

and $z = \widehat{\boldsymbol{q}}_\beta.\widehat{\boldsymbol{q}}_\alpha$. Using the latter we arrive at

$$\begin{aligned}\mathcal{V}^{L'L(I)}_{\beta,\alpha}(q_\beta,q_\alpha) = &\sum_{l'_1} \frac{[l'!]}{[l'_1!l'_2!]} q^{l'_1}_\beta q^{l'_2}_\alpha 2^{-l'_1-1} \sum_{l_1} \frac{[l!]}{[l_1!l_2!]} q^{l_1}_\beta q^{l_2}_\alpha \sum_{l''_1}{}^{(2)} C^{l''_1 0}_{l_1 0\,l'_1 0} \frac{[l_1 l'_1]}{[l''_1]} \\ &\times \sum_{l''_2}{}^{(2)} C^{l''_2 0}_{l_2 0\,l'_2 0} \frac{[l_2 l'_2]}{[l''_2]} \sum_{\lambda}{}^{(2)} \mathcal{F}^{(I)}_\lambda(q_\beta,q_\alpha) \frac{[L'\lambda]}{[l''_1]} C^{l''_1 0}_{L'0\,\lambda 0} \frac{[L\lambda]}{[l''_2]} C^{l''_2 0}_{L0\,\lambda 0} \\ &\times \sum_{m',m,M',M,m'_1,m_1,m''_1,m''_2,\mu} (-1)^{l'_2+l_2+m'_2-m_1+m''_1+m''_2} C^{JK}_{L'M'\,l'm'} C^{JK}_{LM\,lm} \\ &\times C^{l'\,m'}_{l'_1 m'_1\,l'_2 m'_2} C^{lm}_{l_1-m_1\,l_2-m_2} C^{l''_1 m''_1}_{l_1 m_1\,l'_1 m'_1} C^{l''_2 m''_2}_{l_2-m_2\,l'_2-m'_2} C^{l''_1-m''_1}_{L'M'\,\lambda\mu} C^{l''_2-m''_2}_{LM\,\lambda\mu}. \end{aligned} \tag{2.118}$$

Summing over all the projections of the angular momenta, which is techni-

cally rather involved but straightforward, we finally get

$$\begin{aligned}\mathcal{V}^{L'L(I)}_{\beta,\alpha}(q_\beta,q_\alpha) =&[l'lL'Ll'!l!](-1)^{J+L'}\sum_{l'_1}\frac{[l'_1l'_2]}{[l'_1!l'_2!]}2^{-l'_1-1}\sum_{l_1}\frac{[l_1l_2]}{[l_1!l_2!]}q_\beta^{l'_1+l_1}q_\alpha^{l'_2+l_2}\\ &\times\sum_{l''_1}{}^{(2)}C^{l''_10}_{l_10\,l'_10}\sum_{l''_2}{}^{(2)}C^{l''_20}_{l_20\,l'_20}\sum_{\lambda}{}^{(2)}[\lambda]^2C^{l'''0}_{L0\,'\lambda0}C^{l'''}_{L0\,\lambda0}\\ &\times\left\{\begin{array}{ccccc} l_1 & & l & & J & & l' \\ & l_2 & & L & & L' & & l'_1 \\ l'_2 & & l''_2 & & \lambda & & l''_1 \end{array}\right\}\mathcal{F}^{(I)}_\lambda(q_\beta,q_\alpha),\end{aligned}\tag{2.119}$$

where the braces denote the $12j$-symbol of the first kind [80].

Next we transform $V^{(II)}_{\beta\alpha}(\boldsymbol{q}_\beta,\boldsymbol{q}_\alpha)$ into partial-wave form

$$\begin{aligned}\mathcal{V}^{L'L(II)}_{\beta,\alpha}(q_\beta,q_\alpha) =&\sum_{m',m,M',M}C^{JK}_{L'M'\,l'm'}C^{JK}_{LM\,lm}\iint d\widehat{\boldsymbol{q}}_\beta d\widehat{\boldsymbol{q}}_\alpha Y^*_{L'M'}(\widehat{\boldsymbol{q}}_\beta)Y_{LM}(\widehat{\boldsymbol{q}}_\alpha)\\ &\times\int\frac{d\boldsymbol{q}}{(2\pi)^3}\widetilde{\psi}^*_\beta(\boldsymbol{p}'_\beta)\Big[\frac{4\pi}{(\boldsymbol{q}-\boldsymbol{q}_\alpha)^2}+\frac{32+|\boldsymbol{q}-\boldsymbol{q}_\alpha|^2}{(16+|\boldsymbol{q}-\boldsymbol{q}_\alpha|^2)^2}\Big]\widetilde{\xi}_\alpha(\boldsymbol{p}'_\alpha).\end{aligned}\tag{2.120}$$

To this end we first expand the modified Coulomb potentials (2.111) according to

$$\frac{1}{(\boldsymbol{q}_\alpha-\boldsymbol{q})^2}=\frac{2\pi}{kq}\sum_{\lambda\mu}Q_\lambda\left(\frac{q_\alpha^2+q^2}{2q_\alpha q}\right)Y^*_{\lambda\mu}(\widehat{\boldsymbol{q}}_\alpha)\,Y_{\lambda\mu}(\widehat{\boldsymbol{q}})$$

and

$$\frac{32+|\boldsymbol{q}-\boldsymbol{q}_\alpha|^2}{(16+|\boldsymbol{q}-\boldsymbol{q}_\alpha|^2)^2}=2\pi\sum_{\lambda\mu}\mathcal{A}_\lambda(q_\alpha,q)\,Y^*_{\lambda\mu}(\widehat{\boldsymbol{q}}_\alpha)Y_{\lambda\mu}(\widehat{\boldsymbol{q}}),$$

where $Q_\lambda$ is the Legendre function of the second kind and

$$\mathcal{A}_\lambda(q_\alpha,q)=\int_{-1}^{1}dz\,\frac{32+|\boldsymbol{q}-\boldsymbol{q}_\alpha|^2}{(16+|\boldsymbol{q}-\boldsymbol{q}_\alpha|^2)^2}P_\lambda(z).$$

With this expansion we arrive at

$$\begin{aligned}\mathcal{V}^{L'L(II)}_{\beta,\alpha}(q_\beta,q_\alpha) =&\frac{1}{\pi}\int_0^\infty dq\,q^2\Big[\frac{1}{q\,q_\alpha}Q_L\left(\frac{q^2+q_\alpha^2}{2qq_\alpha}\right)+\mathcal{A}_L(q,q_\alpha)\Big]\sum_{m',m,M',M}C^{JK}_{L'M'\,l'm'}\\ &\times C^{JK}_{LM\,lm}\iint d\widehat{\boldsymbol{q}}_\beta\,d\widehat{\boldsymbol{q}}\,Y^*_{L'M'}(\widehat{\boldsymbol{q}}_\beta)Y_{LM}(\widehat{\boldsymbol{q}})\widetilde{\psi}^*_\beta(\boldsymbol{p}'_\beta)\widetilde{\xi}_\alpha(\boldsymbol{p}'_\alpha).\end{aligned}\tag{2.121}$$

This shows that the rest is the same as for $\mathcal{V}^{(I)}_{\beta\alpha}(q_\beta, q_\alpha)$. The only difference is that $F^{(II)}(\boldsymbol{q}_\beta, \boldsymbol{q}_\alpha)$ is now given by

$$F^{(II)}(\boldsymbol{q}_\beta, \boldsymbol{q}) = \frac{\widetilde{R}^*_{n'l'}(p'_\beta)\widetilde{B}_{nl}(p'_\alpha)}{{p'_\beta}^{l'}{p'_\alpha}^{l}}. \tag{2.122}$$

Finally, combining $\mathcal{V}^{(I)}_{\beta,\alpha}(q_\beta, q_\alpha)$ and $\mathcal{V}^{(II)}_{\beta,\alpha}(q_\beta, q_\alpha)$ we get the partial-wave expanded form of $V_{\beta\alpha}(\boldsymbol{q}_\beta, \boldsymbol{q}_\alpha)$ (2.94)

$$\begin{aligned}\mathcal{V}^{L'L}_{\beta,\alpha}(q_\beta, q_\alpha) =& [l'lL'Ll'!l!](-1)^{J+L'}\sum_{l'_1}\frac{[l'_1 l'_2]}{[l'_1!l'_2!]}2^{-l'_1-1}\sum_{l_1}\frac{[l_1 l_2]}{[l_1!l_2!]}q_\beta^{l'_1+l_1}\\ &\times\sum_{l''_1}{}^{(2)}C^{l''_1 0}_{l_1 0\, l'_1 0}\sum_{l''_2}{}^{(2)}C^{l''_2 0}_{l_2 0\, l'_2 0}\sum_{\lambda}{}^{(2)}[\lambda]^2 C^{l''_1 0}_{L0'\lambda 0}C^{l''_2 0}_{L0\,\lambda 0}\\ &\times\begin{Bmatrix} l_1 & l & J & l' \\ l_2 & L & L' & l'_1 \\ l'_2 & l''_2 & \lambda & l''_1 \end{Bmatrix} I^\lambda_{\beta\alpha}(q_\beta, q_\alpha),\end{aligned} \tag{2.123}$$

where

$$\begin{aligned}I^\lambda_{\beta\alpha} =& q_\alpha^{l'_2+l_2}\mathcal{F}^{(I)}_\lambda(q_\beta, q_\alpha) + \int_0^\infty \frac{dq}{\pi}q^{l'_2+l_2+2}\Big[\frac{1}{q\,q_\alpha}Q_L\left(\frac{q^2+q_\alpha^2}{2qq_\alpha}\right) + \mathcal{A}_L(q, q_\alpha)\Big]\\ &\times\mathcal{F}^{(II)}_\lambda(q_\beta, q).\end{aligned} \tag{2.124}$$

Eqs. (2.123-2.124) are similar in form to those in the positron-hydrogen case [4], except that in our case the pseudo-formfactors and additional function $A_L$ in (2.124) are calculated numerically. The function $Q_L$ has a singularity at $q = q_\alpha$. The numerical method to calculate this integral with a singularity will be discussed in the next section.

## 2.4 Numerical methods to solve the scattering equation

One useful feature of the CCC formalism is that the method of solution of the coupled equations (2.58) is essentially independent of the choice of the target, and is similar to that given for hydrogen [4].

In order to calculate the transition matrix elements we have to solve a system of coupled momentum-space integral equations (2.58) with the effective potentials given by Eqs. (2.80), (2.93) and (2.123). To avoid complex-number arithmetic we introduce the K-matrix as in the case of electron scattering [67]. First we rewrite Eq. (2.58) as

$$\mathcal{T}^{L'LJ}_{\gamma',\gamma}(q_{\gamma'},q_\gamma) = \mathcal{V}^{L'LJ}_{\gamma',\gamma}(q_{\gamma'},q_\gamma) + \sum_{L''}\Big[\sum_{\gamma''}^{N_{\rm He}+N_{\rm Ps}}\mathcal{P}\int\frac{dq_{\gamma''}q^2_{\gamma''}}{(2\pi)^3}\mathcal{V}^{L'L''J}_{\gamma',\gamma''}(q_{\gamma'},q_{\gamma''})\omega_{\gamma''}(q^2_{\gamma''}) \times \mathcal{T}^{L''LJ}_{\gamma'',\gamma}(q_{\gamma''},q_\gamma) + i\pi\sum_{\gamma''}^{N^{(o)}} q^{(o)}_{\gamma''}\mathcal{V}^{L'L''J}_{\gamma',\gamma''}(q_{\gamma'},q_{\gamma''})\mathcal{T}^{L''LJ}_{\gamma'',\gamma}(q_{\gamma''},q_\gamma)\Big], \tag{2.125}$$

where the symbol $\mathcal{P}$ indicates that the integral is of the principal value type,

$$\omega_{\gamma''}(q^2_{\gamma''}) = (E - \epsilon_{\rm He^+} - \frac{1}{2m_{\gamma''}}q^2_{\gamma''} - \epsilon_{\gamma''})^{-1} \tag{2.126}$$

is a real function, and $q^{(o)}_{\gamma''}$ is defined for $\gamma'' \le N^{(o)} \le (N_{\rm He}+N_{\rm Ps})$ for which

$$q^{(o)}_{\gamma''} = \sqrt{2m_{\gamma''}(E - \epsilon_{\rm He^+} - \epsilon_{\gamma''})} \tag{2.127}$$

is real. In this case the channel $\gamma''$ is called open (and there are $N^{(o)}$ of them). Channels for which $\epsilon_{\gamma''} \ge E - \epsilon_{\rm He^+}$ are called closed channels.

We can use pure real arithmetic if we introduce the K-matrix by letting

$$\mathcal{K}^{L'LJ}_{\gamma'\gamma}(q_{\gamma'},q_\gamma) = \sum_{L''}\sum_{\gamma''}^{N^{(o)}}\mathcal{T}^{L''LJ}_{\gamma'',\gamma}(q_{\gamma''},q_\gamma)(\delta_{\gamma'',\gamma}\delta_{L'',L} + i\pi\, q^{(o)}_{\gamma''}\,\mathcal{K}^{L''LJ}_{\gamma''\gamma}(q^{(o)}_{\gamma'},q_\gamma)). \tag{2.128}$$

With this definition Eq. (2.58) transforms to the following system of equations for the K-matrix amplitudes

$$\mathcal{K}^{L'LJ}_{\gamma'\gamma}(q_{\gamma'},q_\gamma) = \mathcal{V}^{L'LJ}_{\gamma'\gamma}(q_{\gamma'},q_\gamma) + \sum_{\gamma''}^{N_{\rm He}+N_{\rm Ps}}\sum_{L''}\mathcal{P}\int\frac{dq_{\gamma''}q^2_{\gamma''}}{(2\pi)^3}\mathcal{V}^{L'L''J}_{\gamma'\gamma''}(q_{\gamma'},q_{\gamma''})\mathcal{G}_{\gamma''\gamma} \times \mathcal{K}^{L''LJ}_{\gamma''\gamma}(q_{\gamma''},q_\gamma). \tag{2.129}$$

This equation is solved by using purely real arithmetic and then the T-matrix is obtained by solving a much smaller set of equations (2.128).

For the numerical solution of Eq. (2.129) we use standard quadrature rules. The kernel of the equations containing principal value integrals is discretized using a Gauss-Legendre quadrature. The problem of channel-dependent singularities is overcome by using a unique quadrature in each channel containing the singularity. The accuracy of the integral in the sense of the principal value was ensured by using a subquadrature consisting of an even number of Gauss-Legendre points, symmetrically distributed in the immediate vicinity of the singular point. This procedure is similar to the widely used subtraction method with the subtraction being numerically zero.

As a result of the two-centre expansion the system of equations (2.129) is highly ill-conditioned. This makes it impossible to use arbitrarily high basis sizes. The ill-conditioning in this case is very similar to the positron-hydrogen case reported in [4]. The experience with the hydrogen case has shown that the ill-conditioning can be overcome by employing double precision accuracy in calculations of matrix elements given in Eqs. (2.80,2.93, 2.123) and by using sufficiently dense mesh on $q''_\gamma$ integration in Eq. (2.129).

Calculations of the effective potentials for the direct transitions, Eq. (2.80) and (2.93), require evaluation of the integrals in Eq. (2.81) and (2.92). These integrals can be calculated to a desired accuracy by integrating out to 400 a.u. on a sufficiently fine radial mesh. The calculations of direct transition potential matrix elements are relatively quick.

As shown in the previous section the positronium formation matrix elements have been written as a coupling of 12 actual and virtual angular momenta, leading to finite angular momentum sums and two and three-dimensional integrals.

We utilize the singularity subtraction method that was also used by Mitroy [3] to evaluate the integral over the momentum of the virtual electron involving the Coulomb singularity in Eq. (2.124). The integral in Eq. (2.124) can, in general, be written as

$$\mathcal{I}(q_\alpha) = \int_0^\infty dq h(q) Q_L \left( \frac{q^2 + q_\alpha^2}{2qq_\alpha} \right), \tag{2.130}$$

and it has singularity at $q = q_\alpha$. We can write

$$\begin{aligned} \mathcal{I}(q_\alpha) = &\int_0^{q_\alpha - \varepsilon} dq h(q) Q_L \left( \frac{q^2 + q_\alpha^2}{2qq_\alpha} \right) + \int_{q_\alpha + \varepsilon}^\infty dq h(q) Q_L \left( \frac{q^2 + q_\alpha^2}{2qq_\alpha} \right) \\ &+ \int_{q_\alpha - \varepsilon}^{q_\alpha + \varepsilon} dq h(q) Q_L \left( \frac{q^2 + q_\alpha^2}{2qq_\alpha} \right), \end{aligned} \tag{2.131}$$

where $\varepsilon$ is a small positive number. The first two integrals are singularity free. Only the last integral contains a singularity, for which we apply singularity subtraction method

$$\begin{aligned} \int_{q_1}^{q_2} dq h(q) Q_L \left( \frac{q^2 + q_\alpha^2}{2qq_\alpha} \right) = &\int_{q_1}^{q_2} dq \left[ h(q) Q_L \left( \frac{q^2 + q_\alpha^2}{2qq_\alpha} \right) - h(q_\alpha) Q_0 \left( \frac{q^2 + q_\alpha^2}{2qq_\alpha} \right) \right] \\ &+ h(q_\alpha) \int_{q_1}^{q_2} dq\, Q_0 \left( \frac{q^2 + q_\alpha^2}{2qq_\alpha} \right), \end{aligned} \tag{2.132}$$

where $q_1 = q_\alpha - \varepsilon$ and $q_2 = q_\alpha + \varepsilon$. In this equation the first integral on the right-hand side can be calculated numerically, as $Q_L(x \to 1) - Q_0(x \to 1)$ is a constant. The last integral can be evaluated analytically

$$\begin{aligned} \int_{q_1}^{q_2} dq\, Q_0 \left( \frac{q^2 + q_\alpha^2}{2qq_\alpha} \right) = &\frac{q_2}{q_\alpha} \left[ \left( \frac{q_2}{q_\alpha} + 1 \right) \ln \left( 1 + \frac{q_2}{q_\alpha} \right) - 2\ln(2) - \left( \frac{q_2}{q_\alpha} - 1 \right) \right. \\ &\left. \times \ln \left( \frac{q_2}{q_\alpha} - 1 \right) \right] + \frac{q_1}{q_\alpha} \left[ \left( \frac{q_1}{q_\alpha} - 1 \right) \ln \left( 1 - \frac{q_1}{q_\alpha} \right) \right. \\ &\left. + 2\ln(2) - \left( \frac{q_1}{q_\alpha} + 1 \right) \ln \left( 1 + \frac{q_1}{q_\alpha} \right) \right]. \end{aligned} \tag{2.133}$$

For numerical evaluation of the above subtraction method we generate the $q$ integration composite mesh for each given channel $\alpha$ from its $q_\alpha$ grid with $n_{\rm com}$ points located in symmetrical positions around each point (including the first

and the last points) in the $q_\alpha$ grid. $n_{\rm com}$ can be chosen to achieve the desired accuracy in the integration over $q$.

The calculations are performed for a limited number of partial-waves $J$. Extrapolation to infinite $J$ is done using the Born subtraction method for the direct scattering cross sections and a geometric series method for the positronium formation cross sections. A number of test runs at intermediate energies showed that the first 10 partial-waves were sufficient for reliable extrapolation in the Ps formation channels. For the same in the direct scattering channels, however, we had to include a further 10 partial-waves that were calculated numerically.

The momentum-space pseudo-state wavefunctions and pseudoformfactors of Ps ($\widetilde{R}_{\beta nl}$, $\widetilde{u}_{\beta nl}$) are calculated analytically as derived in [4]. But in case of He these functions ($\widetilde{B}_{nl}$, $\widetilde{D}_{nl}$ and $\widetilde{u}_{\alpha nl}$) are given as

$$\widetilde{B}_{nl}(p) = \int_0^\infty dr\, r^2\, j_l(pr) B_{nl}(r), \tag{2.134}$$

$$\widetilde{D}_{nl}(p) = \int_0^\infty dr\, r^2\, j_l(pr) D_{nl}(r), \tag{2.135}$$

$$\widetilde{u}_{\alpha nl}(p) = \int_0^\infty dr\, r^2\, j_l(pr) \left( -\frac{1}{r} - \left(2 + \frac{1}{r}\right) e^{-4r} \right) B_{nl}(r), \tag{2.136}$$

where $B_{nl}(r)$ and $D_{nl}(r)$ are defined in Eq. (2.102) and (2.103), respectively. The above integrals are calculated numerically using a composite mesh created using Simpson's rule. The number of grid points and the integration limits are chosen to achieve a sufficient accuracy. This extra numerical integration slows down the calculation of rearrangement V-matrix elements. The integrand and the results of the integrations in Eqs. (2.134-2.136) are well-defined smooth functions. Therefore, to speed up the calculations we can generate these functions once on a given logarithmic mesh and then use interpolation with the stored values. By taking sufficiently dense storage points we can achieve the desired accuracy in the interpolation.

## 2.5 Experimental observables

In positron scattering experiments the main observables of interest are angle-differential cross sections (DCS) and integrated cross sections for various transitions including elastic, target excitation, ionization and Ps-formation. All these physical observables can be calculated from the scattering amplitudes $f_{\gamma'\gamma}$.

Scattering amplitudes for a particular transition are related to on-shell values of the corresponding $T$-matrix elements. By solving the equations (2.128-2.129) we obtain reduced $\mathcal{T}^{L'LJ}_{\gamma'\gamma}$-matrix elements for various transitions of interest, which depend on partial-waves of total orbital angular momentum $J$. In the collision frame, where the quantization axis is taken along the incident projectile direction, the relation between scattering amplitudes (from state $\gamma$ to state $\gamma'$ with magnetic sublevels $m$ and $m'$, respectively) and reduced on-shell T-matrix can be written as

$$\begin{aligned} f_{\gamma' m',\gamma m}(\theta,\varphi) &= \frac{1}{\sqrt{4\pi}}\frac{1}{\sqrt{2l+1}}\sqrt{\frac{q_{\gamma'}}{q_\gamma}}\sum_{L',L,J}\sqrt{(2L+1)}C^{Jm}_{L' m-m'\ lm} \\ &\quad \times C^{Jm}_{L0\,lm}\mathcal{T}^{L'LJ}_{\gamma'\gamma}(q_\gamma,q_{\gamma'})Y_{L'\,m-m'}(\theta,\varphi), \end{aligned} \tag{2.137}$$

where $l, m$ and $l', m'$ are the orbital angular momentum and its projection of the initial and final states, respectively. The initial and final linear and orbital angular momenta of the projectile are denoted by $q_\gamma, L$ and $q_{\gamma'}, L'$. Considering positron measurements performed in the scattering plane, we set $\varphi = 0$ and drop it from the notation.

With the assumption that initial target is not polarized the angle-differential cross section is given by averaging over magnetic sublevels of the initial state orbital angular momentum $l$ (the factor $1/\sqrt{2l+1}$ is included in (2.137)) and

summing over the magnetic sublevels of the final-state orbital angular momentum

$$\sigma(\theta) = \frac{d\sigma}{d\Omega} = \sum_{mm'} |f_{\gamma' m', \gamma m}(\theta, 0)|^2. \tag{2.138}$$

The integrated cross sections are calculated by integrating the corresponding angle-differential cross section over all scattering angles, i.e.,

$$\sigma = \int_0^\pi \sigma(\theta)\, \sin(\theta)\, d\theta. \tag{2.139}$$

By substituting Eq. (2.137) and Eq. (2.138) into Eq. (2.139) the above integral can be taken analytically and then the integrated cross sections can be directly calculated from the on-shell values of the reduced T-matrix elements

$$\sigma \;=\; \frac{1}{4\pi(2l+1)} \frac{q_{\gamma'}}{q_\gamma} \sum_{J,L',L} (2J+1) |\mathcal{T}^{L'LJ}_{\gamma'\gamma}(q_\gamma, q_{\gamma'})|^2. \tag{2.140}$$

The total cross section $\sigma_t$ is obtained by summing the individual integrated cross sections for each state included in the close-coupling expansion, or utilizing the unitarity of the close-coupling formalism by applying the optical theorem. We calculate $\sigma_t$ in both ways (which should give the same result) to check that the optical theorem is satisfied. The total ionization cross section is calculated as a sum of the integrated cross sections for positive energy states (of both atom and Ps). The total Ps-formation cross sections are calculated as a sum of cross sections for electron capture into Ps-bound states.

## 2.6 Chapter summary

In this chapter we have presented the basic formalism of the two-centre CCC method applied to positron scattering on helium. It has been shown that spatial and spin parts can be separated if spin-orbit interactions are neglected. The Schrödinger equation, written for the spatial part, has then been transformed into Lippmann-Schwinger integral equations in momentum-space. To solve these equations one needs to calculate the effective potentials. Their derivation has also been given in detail. Calculations of the effective potentials for the direct transitions are relatively easy. The effective potentials for the rearrangement (Ps-formation) channels are more complicated to calculate. The use of the configuration interaction (CI) approach for the He wavefunctions makes it possible to write the two-particle He wavefunctions in terms of single particle functions. This, in turn, makes it possible to derive the rearrangement effective potentials in a way similar to the positron-hydrogen case. Numerical methods used in the formalism have been discussed. Next, we apply the presented formalism to positron scattering from helium in its ground state and the $2^3$S excited state, and compare the obtained results with those from other available theories and experiments.

# Chapter 3

# Positron scattering on the ground state of helium

Helium in its ground state is the most frequently used target in experimental studies of positron-atom scattering. First measurements on positron-helium scattering were carried out by Canter et al. [24] in 1972. Since then many other experimental studies have been conducted including Stein et al. [41], Kauppila et al. [81], Mori and Sueoka [82], Fromme et al. [16], Fornari et al. [58], Diana et al. [59], Jacobsen et al. [83]. Moxom et al. [18]. Further developments of positron beams in terms of energy resolution and beam intensities have recently motivated more experimental studies. Recently such measurements have been carried out by Murtagh et al. [84, 85], G.P. Karwasz [86], Karwasz et al. [87] and Caradonna et al. [55, 88], Sullivan et al. [89, 90]. In general, the results from the experiments mentioned above agree with each other. However, in some cases there are a few particular differences that generate motivation for further studies.

In this chapter we present our theoretical results on positron scattering on the ground state of helium. First, we demonstrate the convergence of the results. Then we compare the converged results with available theory and experiments

and indicate differences if there are any and the possible sources of such discrepancies.

## 3.1 Convergence studies

In general, the main stages of calculations are as follows. At the first step effective potentials (V-matrix), given in Eqs. (2.80, 2.93, 2.123), are generated and stored in the computer's operative memory. Then, on the second stage, using these V-matrix elements we solve the equation for the K-matrix given in Eq. (2.129) from which then we find the T-matrix by solving Eq. (2.128). All the observables can then be found by using only on-shell values of the T-matrix as described in Section 2.5. Because of the coupling between different channels the results may depend on the size of the basis. Therefore we must first check the convergence of the results. For this we need to carry out calculations with different basis sizes $N = \sum_l N_l$, where $N_l = N_0 - l$. The convergence of the obtained results is checked by increasing the values of $N_0$ and $l$, independently. We take the same number of Laguerre-basis states for both centers at each point in energy. We check the convergence in the calculated cross sections only in the frozen-core model for He-states. There are two reasons for doing this. Firstly, calculations within the FC model are a few times faster than those in the MC model. At the same time, the main difference between the FC and MC model calculations is in the He ground state energy, which affects the results for cross sections but not their convergence rate. The convergence rate mainly depends on the number of excited states included, which are almost the same for the FC and MC models.

We present here calculations with the following basis sizes for both the

atomic and Ps centers:

(a) $N_l = 10 - l$, $l_{max} = 0$,

(b) $N_l = 10 - l$, $l_{max} = 1$,

(c) $N_l = 10 - l$, $l_{max} = 2$,

(d) $N_l = 10 - l$, $l_{max} = 3$,

(e) $N_l = 9 - l$, $l_{max} = 2$,

(f) $N_l = 12 - l$, $l_{max} = 2$.

For all bases the fall-off parameter $\lambda$ for He is set to 2.0. Table 3.1 shows the lowest ionization energies of He calculated in the FC and MC models with basis (c). The experimental values are also given in the table. We see that the MC model gives very accurate energies for the ground and excited states. Though the ground state calculated in the FC model is not very satisfactory, the corresponding excited states are very close to the MC ones and the experimental data. The MC model with the basis (c) has 8 bound states and 19 positive energy states with the highest energy of 245.76 eV corresponding to the pseudo-state $\overline{10}$P. In case of the FC model with the basis (c), there are 7 bound states and 20 positive energy states among which the highest energy of 422.4 eV corresponding to the pseudo-state $\overline{10}$S.

Table 3.1: Ionization energies of He in units of eV. FC and MC model calculations are obtained using the basis (c).

| State | FC model | MC model | Experiment |
|---|---|---|---|
| $1^1$S | 23.74 | 24.51 | 24.58 |
| $2^1$S | 3.82 | 3.88 | 3.97 |
| $2^1$P | 3.33 | 3.31 | 3.37 |
| $3^1$S | 1.59 | 1.61 | 1.66 |
| $3^1$P | 1.43 | 1.42 | 1.50 |
| $3^1$D | 1.49 | 1.49 | 1.51 |

The fall-off parameter $\lambda$ of Ps is taken to be 0.5. With this value for $\lambda$ the

Ps states generated with the aforementioned bases give nearly exact ground and lowest excited states of Ps.

In addition to the above bases, which are equal for both centers, we have also performed calculations with basis (e) for He and 3 lowest (1s, 2s and 2p) states from Ps centers. Results of this basis are denoted as CC($\overline{24}$,3). Therefore, this basis has 24 ($\overline{9}$s, $\overline{8}$p, $\overline{7}$d) pseudo-states of He and 3 eigenstates of Ps; and it is similar to the basis used by Campbell et al. [56].

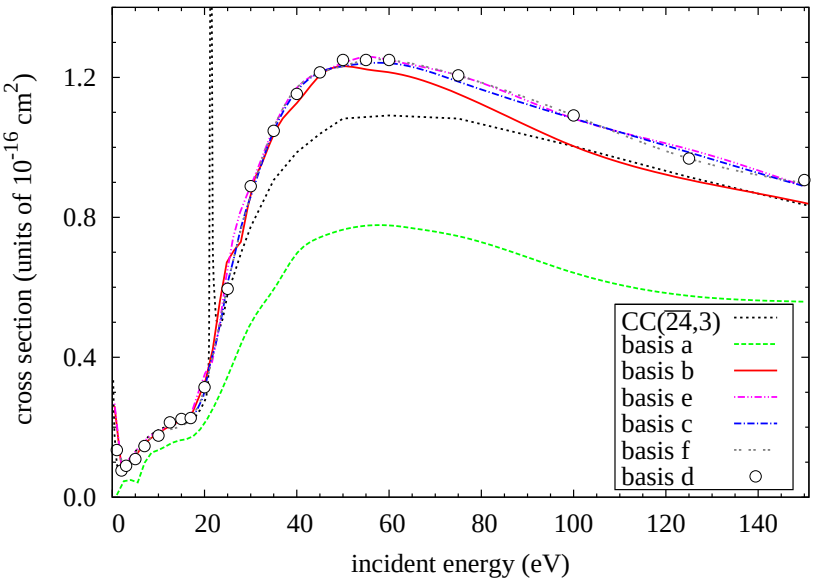


Figure 3.1: Total cross section for positron scattering from the ground state of helium. The basis descriptions are given in the text.

The grand total, total Ps-formation and direct ionization cross sections calculated with different basis sizes are shown in Figs. 3.1-3.3. The rapid convergence rate with increasing $l$ can be seen by comparing the results using bases (a), (b), (c) and (d). We can see that including p-states (basis (b)) has made quite a significant change in the calculated cross sections while including d-states had a rather small (typically less than 5%) effect while adding f-states had almost no effect (less than 1%).

Comparing the results of bases (e), (c) and (f) we can assess the convergence rate with increasing $N$. We see that the basis (c) is sufficient to get accurate results for the cross sections we are interested in. Further we use this basis for calculations with the MC model and compare the obtained results with those from the other methods and experimental data. We have provided more detailed convergence studies in the elastic region in Ref. [91].

The CC($\overline{24}$,3) results for all presented cross sections in Figs. 3.1-3.3 are below the converged results. This indicates that the basis is not sufficient to obtain converged result. There is an unphysical resonance-like behavior in the total cross section obtained in our CC($\overline{24}$,3) calculations around 22 eV, similar to that found by Campbell et al. [56]. Although not presented, our calculations show that adding more Ps eigenstates slowly changes the cross sections towards the two-center CCC results. However, this procedure was not able to remove the pseudo-resonances completely. In positron-hydrogen case presented in Ref. [4] similar pseudo-resonances were obtained when such a basis was used. It has been concluded that the use of similar bases from both centers eliminates such resonances. Our pseudo-resonance-free results of bases (a) - (e) also confirm this conclusion.

In addition to a sufficiently large basis we also need a denser k-integration grid to get an accurate solution with increasing number of included states. In the present calculations we chose k-grids and basis sizes to satisfy convergence in the grand total, total Ps-formation and total ionization cross sections.

It is interesting to note that the convergence rates and the cross-section behavior are very similar to that observed in the $e^+$-H case [4]. For example, when Ps formation is calculated using only s-states, the maximum in the cross section is around 10% lower than the converged results and positioned at an

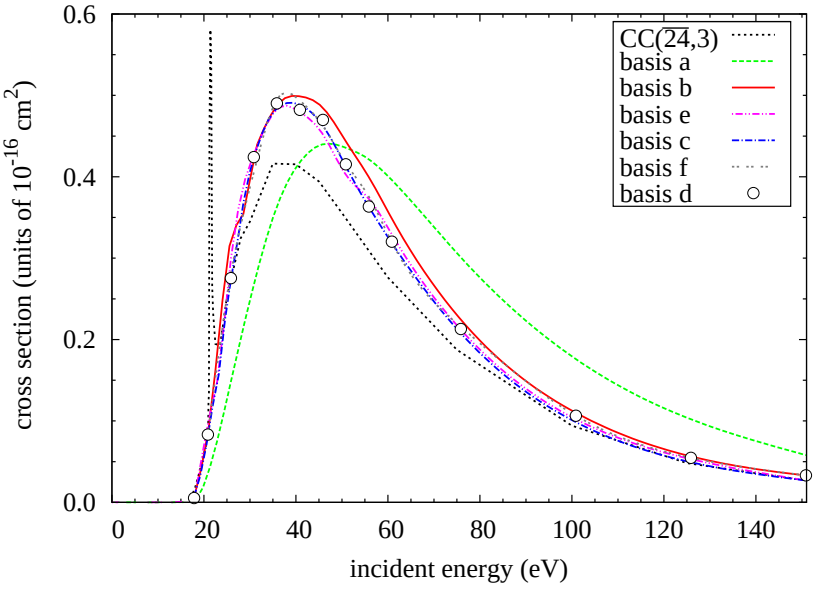


Figure 3.2: Ps-formation cross sections for positron scattering from the ground state of helium.

energy about 10 eV higher. It would be interesting to see if this feature holds for more complex targets.

From the above discussion we conclude that converged results for the presented cross sections can be obtained by using the basis c. However, we need to note that the small cross sections (e.g. excitation, near-threshold ionization) might be not sufficiently converged even if the summed cross sections are. Very small cross sections usually require even larger basis sizes for convergence and thus require more computing resources. In the following subsection we compare the results of basis (c) with other theoretical and experimental data.

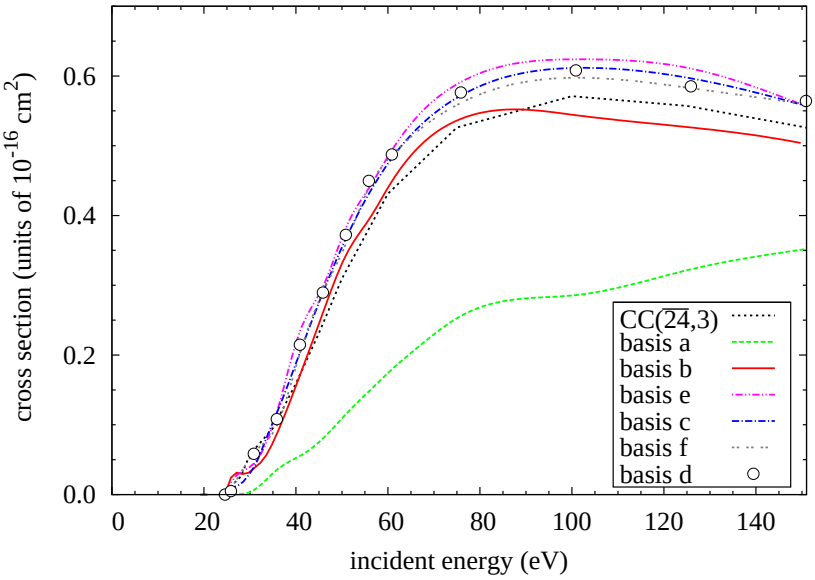


Figure 3.3: Total ionization cross sections for positron scattering from the ground state of helium.

## 3.2 Comparison with experimental data and other theories

### 3.2.1 Integrated cross sections

A vast amount of experimental data is available for integrated cross sections for positron scattering from the helium ground state. The total CCC-calculated cross section is shown in Fig. 3.4 in comparison with experimental data and other calculations. The CCC results have no pseudo-resonances and are in very good agreement with the low-energy experiments by Stein et al. [41] and Sullivan et al. [89] and the medium- to high-energy experimental data by Kauppila et al. [81] and Caradonna et al. [88]. The FC CCC results given in Ref. [92] were overestimating the data, due to a less accurate He ground state in the FC model. As we can see here the difference between the FC and MC results are around

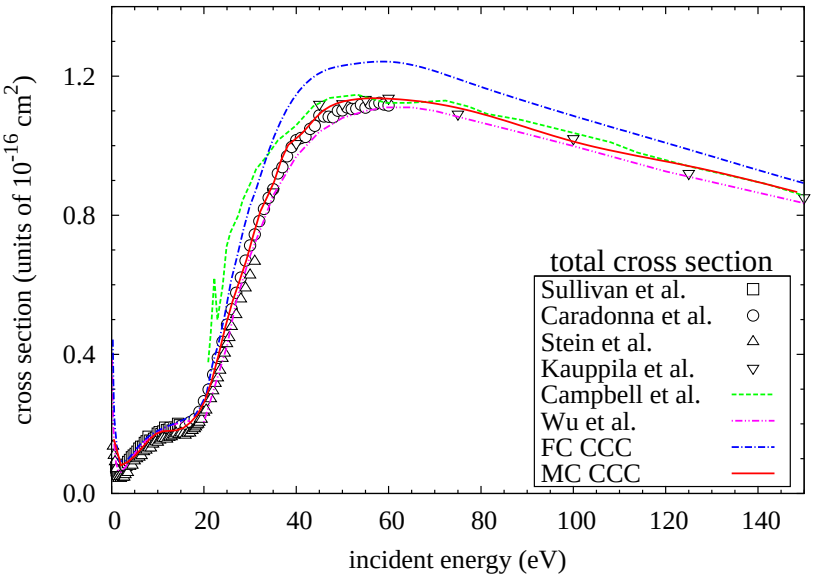


Figure 3.4: Total cross sections. Experimental data are due to Stein et al. [41], Sullivan et al. [89], Kauppila et al. [57], and Caradonna et al. [88]. The calculations are due to Campbell et al. [56] and Wu et al. [72]. The present results, denoted as FC CCC and MC CCC, are described in the text.

10%. This behavior was first observed in the single-center FC and MC results of Wu et al. [72]. Note that the MC results of Wu et al. [72] agree well with the two-center MC CCC results.

The close-coupling results by Campbell et al. [56] are also in good agreement with the experimental data above 22.0 eV. However, they show an unphysical resonance around 22 eV and overestimate the total cross section below 40 eV. Our method has also produced a similar pseudo-resonance (see the previous Section) when a similar basis had been used.

The total Ps-formation, breakup and electron-loss cross sections are shown in Fig. 3.5(a), (b) and (c), respectively. The CCC results for the Ps-formation cross sections are in excellent agreement with the most recent measurements by Caradonna et al. [88] but underestimate earlier experimental data by Fornari et al. [58], Diana et al. [59] and Murtagh et al. [84]. We emphasize that in the case of the FC model the picture was opposite, the results being in agreement with the experiments of Fornari et al. [58], Diana et al. [59], Murtagh et al. [84] but overestimating the recent data by Caradonna et al. [88]. We believe that the present CCC results calculated in the MC model using better He wave functions are more accurate and preferable. Results by Campbell et al. [56] are in very good agreement with the recent experimental data by Caradonna et al. [88], except for a slight overestimation at the peak.

The experimental data for breakup of Jacobsen et al. [83] and Murtagh et al. [84] are well described by the close-coupling calculations of Campbell et al. [56]. The MC CCC results for breakup are lower than the FC ones, though they are still higher than the experimental data of Jacobsen et al. [83] and Murtagh et al. [84]. We emphasize that the convergence in the cross sections is only possible when two independent and sufficiently large Laguerre bases are employed to

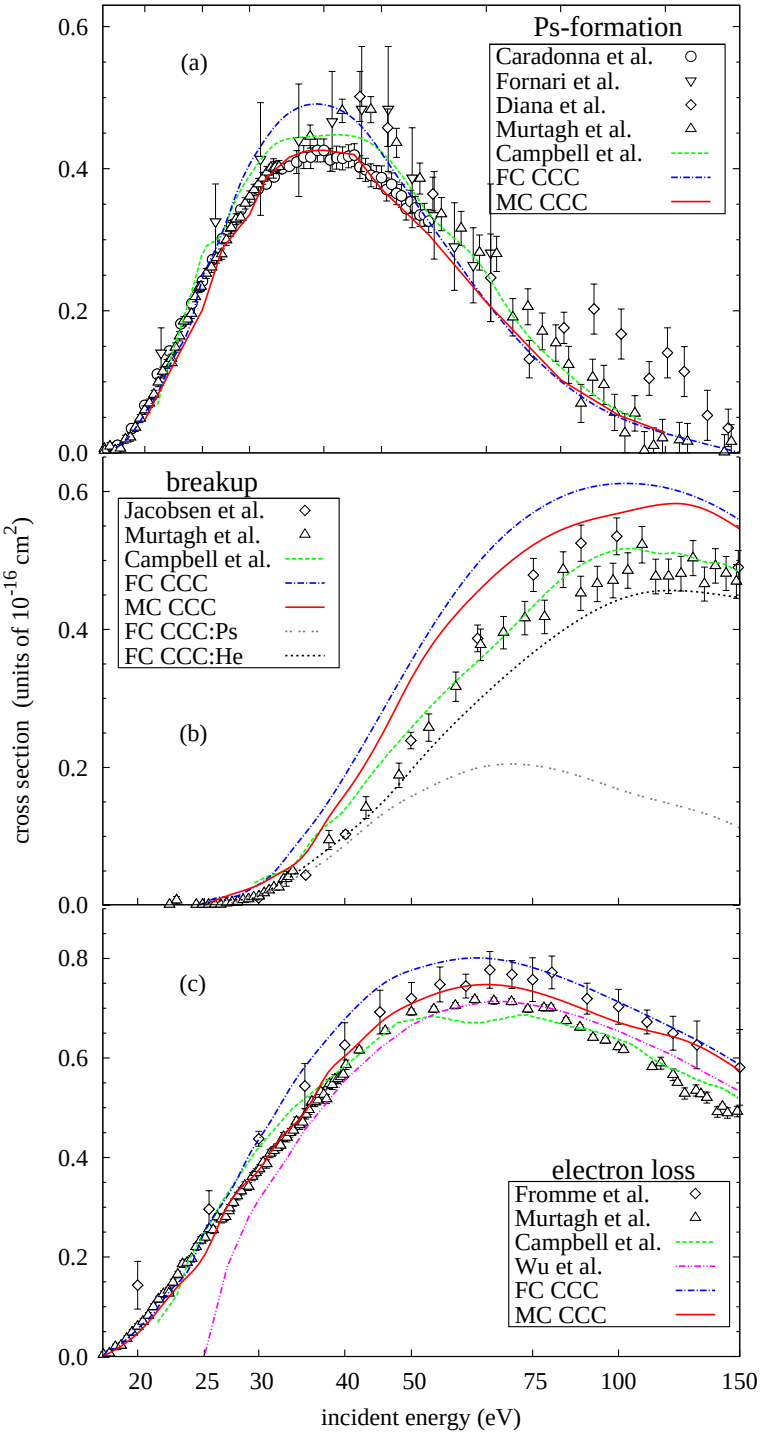


Figure 3.5: (a) Ps-formation, (b) breakup, and (c) electron-loss (sum of the other two) cross sections. The measurements are due to Caradonna et al. [88], Fornari et al. [58], Diana et al. [59], Murtagh et al. [84], and Knudsen et al. [17]. The calculations are due to Campbell et al. [56], Wu et al. [72], and the present results are described in the text.

both of the centers. One consequence of this is that the breakup cross section has two independently converged contributions: ionization of the helium atom (denoted as FC CCC:He) and electron capture into the Ps continuum (denoted as FC CCC:Ps). These two contributions approach each other near the breakup threshold. This behavior, also observed in the positron-hydrogen case, has been discussed in detail by Kadyrov and Bray [4]. We interpret such a threshold ionization feature as an absence of any numerical problems due to non-orthogonal two-center expansions in the three-body breakup channel.

However, does the two-center expansion lead to double counting of the continuum? As mentioned earlier, the breakup cross section is calculated as a combination of the cross sections for direct ionization of the target and electron capture into the Ps continuum. Though this is the most consistent way of treating the two centers of the problem on an equal footing, our approach seems to overestimate the data on the total breakup cross section. Therefore, the method of calculating the breakup cross section may require further investigation as it neglects possible interference effects between contributions from the two centers. In this connection, we recall that a similar trend was observed in the CCC calculations of positron-hydrogen breakup [4]. However, the aforementioned discrepancy between our results for the breakup of helium and the experiment should be considered in light of the observation described below.

The total cross section for electron-loss by He, which is calculated as a sum of Ps-formation and breakup cross sections, is compared with the calculations of Campbell et al. [56], the single-center CCC results of Wu et al. [72] and the experimental data of Fromme et al. [16], Murtagh et al. [84] in Fig. 3.5c. These independent measurements serve as a consistency check regarding these two collision processes. The results of Campbell et al. [56] are in good agreement with the measurements of Murtagh et al. [84], but underestimate the data of Fromme

et al. [16]. The CCC results are in very good agreement with measurements by Fromme et al. [16] on the entire energy range. They are a little higher than the more recent data by Murtagh et al. [84] at energies above 75 eV. Given the small variation between the measurements for these processes and internal self-consistency of the theory, we are hopeful that the presented CCC results are accurate for both the Ps-formation and breakup processes. The single-center CCC results [72] are in good agreement with the experimental data of Murtagh et al. [84] above 35 eV. Below this region they are lower than all the other theories and experiments. In general, the single-center CCC results for electron-loss are in good agreement with the two-centre CCC results. This fact may indicate that double-counting is unlikely. If there is a double counting in the two-center calculations then one would expect much bigger differences between the single-center and the two-center results.

The cross sections for excitation of helium into the $2^1$S and $2^1$P states are presented in Fig. 3.6a and b, respectively. The MC CCC result for $2^1$S is in good agreement with the recent high resolution data of Caradonna et al. [88] while $2^1$P is lower than experiment. The better agreement between FC CCC results and the experimental data is coincidental. Further independent theoretical and experimental investigations are desirable to understand these discrepancies. The CC($\bar{5}$,3) calculations by Hewitt et al. [62] were limited to energies above 30 eV due to the presence of pseudo-resonances in the calculated cross sections at the lower energies. The CC(5,3) calculations of Adhikari and Ghosh [93] have difficulty in describing $2^1$S excitation. The CC($\overline{24}$,3) result for the $2^1$P state of Campbell et al. [56] are between FC CCC and MC CCC results and have a resonance structure around 22 eV. As was shown in Ref. [92] our CC($\overline{24}$,3) calculations exhibit large pseudo-resonances both in the $2^1$S and $2^1$P cross sections below 24 eV, indicating the importance of a commensurate treatment of both

centers even for atomic excitation. Results of Igarashi et al. [66], obtained using a single-electron approximation to He, overestimate both $2^1$S and $2^1$P excitation cross sections.

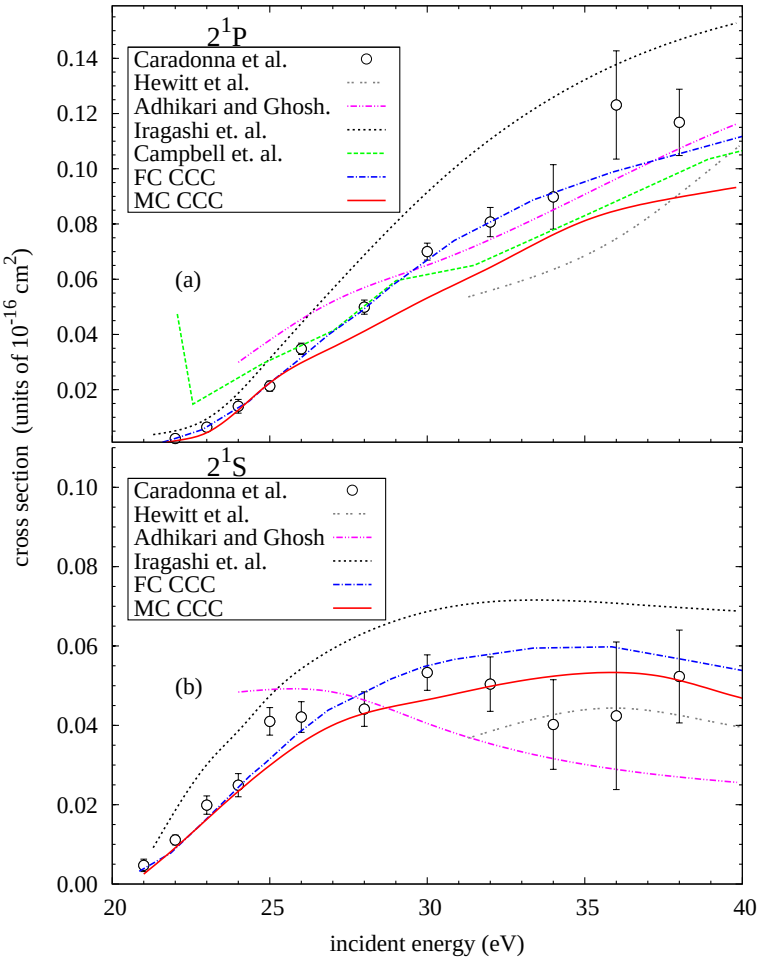


Figure 3.6: Integrated cross sections for (a) He($2^1$S) and (b) He($2^1$P) excitations. Experiment is due to Caradonna et al. [88]. The present calculations are described in the text, and others are due to Hewitt et al. [62], Adhikari and Ghosh [93], Igarashi et al. [66] and Campbell et al. [56].

The cross sections for Ps formation in the 2s and 2p excited states are presented in Fig. 3.7(a) and (b) respectively. Our results are compared with the recent measurements of Murtagh et al. [85] and the CC($\overline{24}$,3) type calculations of Campbell et al. [56]. The FC CCC and MC CCC results for Ps 2p excitation

are not too different from each other and agree well with the experimental data. Ps formation in the 2p state calculated by Igarashi et al. [66], where He was treated as single electron atom, is also in good agreement with the experimental data. No experimental data are available yet for Ps 2s excitation. We compare our results with Ps 2s excitation calculations by Igarashi et al. [66], which show different behavior above 40 eV.

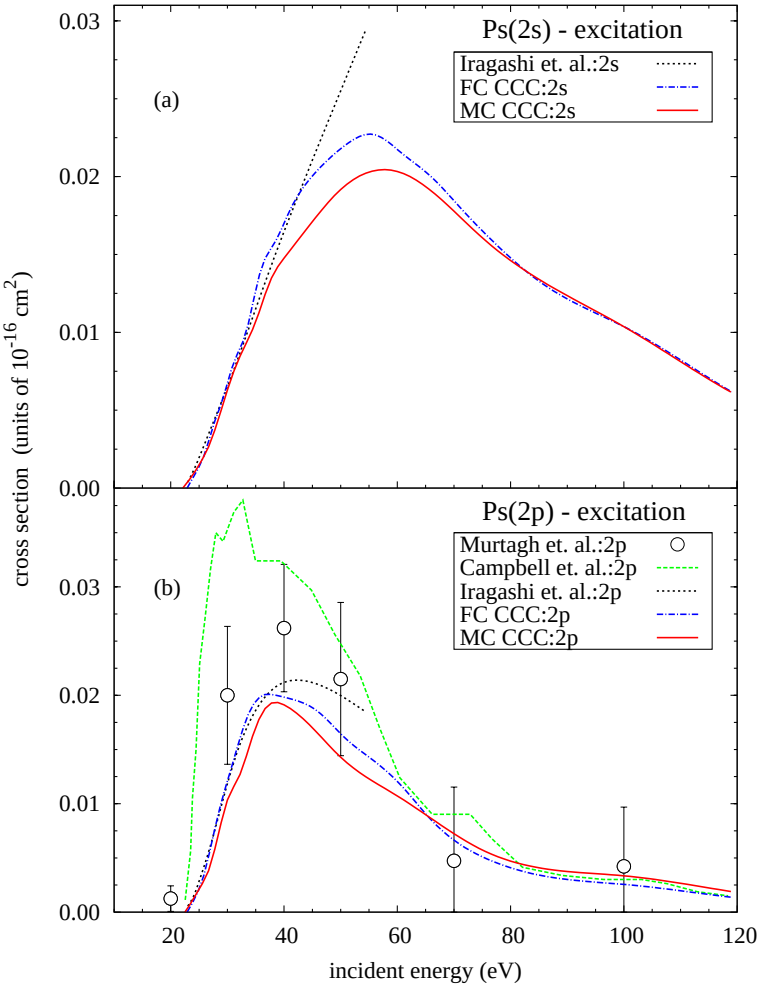


Figure 3.7: Integrated cross sections for Ps formation in the (a) 2s and (b) 2p states. Experimental data for Ps(2p) are due to Murtagh et al. [85]. The present calculations are described in the text, and others are due to Campbell et al. [56] and Igarashi et al. [66].

### 3.2.2 Angle-differential cross sections

As we have seen in the previous section there is good agreement between theory and experiment for the integrated cross sections. However, integrated cross sections may not contain enough information for critical tests of theories. Information about angle-differential cross sections could be more useful for such tests and sometimes for other practical applications.

In the CCC method, after solving Eqs. (2.128, 2.129) the calculations of angle-differential cross sections are straightforward by use of Eq. (2.138). However, the measurements are often more challenging than in the case of integrated cross sections. The experimental group at the Australian National University has recently developed a new positron beam for experimental and practical applications [94]. Using this new experimental setup they have, for the first time, measured the angle-differential cross sections for elastic scattering in positron collisions with helium in its ground state. Figures 3.8-3.11 show their preliminary results compared to various theories. Note that the measured data from Ref. [94] were reported with folded angles. In order to compare theories with these experimental data, we need to transform the calculated angle-differential cross section into folded angles according to

$$\sigma^{\rm f}(\theta) = \sigma(\theta) + \sigma(\pi - \theta), \tag{3.1}$$

where $\sigma^{\rm f}(\theta)$ is the angle-differential cross section for folded angles $0 \leq \theta \leq \pi/2$; $\sigma(\theta)$ is the calculated angle-differential cross sections for $0 \leq \theta \leq \pi$.

Our results obtained in the multi-core approximation are denoted as CCC. The polarized-orbital approximation (POA) results are due to McEachran et al. [95]. Variational method calculations of Reeth et al. [96] are denoted as VM.

Figure 3.8 shows the angle-differential cross section for elastic scattering at

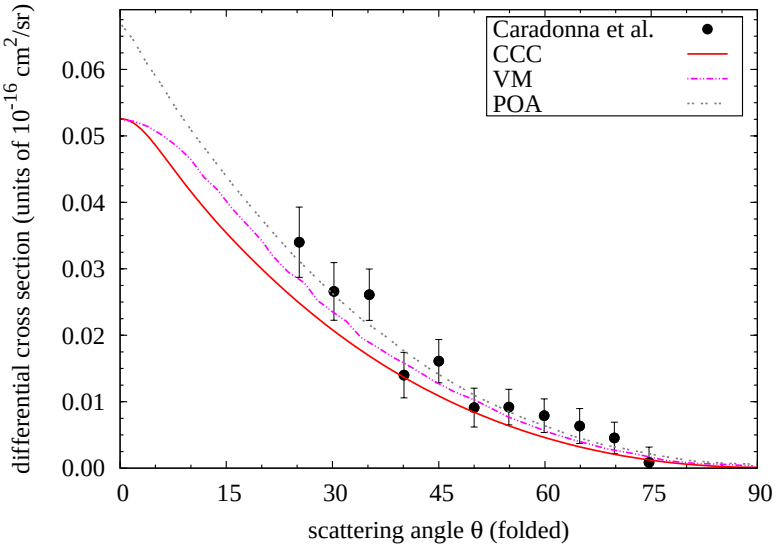


Figure 3.8: The angle-differential cross section for elastic scattering at 1.7 eV. Dots are experimental value by the ANU group, see Ref. [94]. The calculations are described in the text.

1.7 eV. This scattering energy corresponds to the Ramsauer minimum, where the elastic cross section is the smallest. There is good agreement between the experimental data of Caradonna et al. [94] and the calculations. However our results are slightly lower than the experiment and the other theories near the forward angles.

The angle-differential cross section at 5 eV scattering energy is given in Figure 3.9. For this case our results are in very good agreement with the experiment, and this time a little better than the other two theories.

Figure 3.10 shows the elastic scattering DCS at 10 eV. Theories are in good agreement with the experiment for scattering angles above 30°. The two measured points at scattering angles of 20° and 25°, however, are much higher than all of the presented theories. We do not believe that there is any cause for alarm due to the relatively large experimental uncertainty.

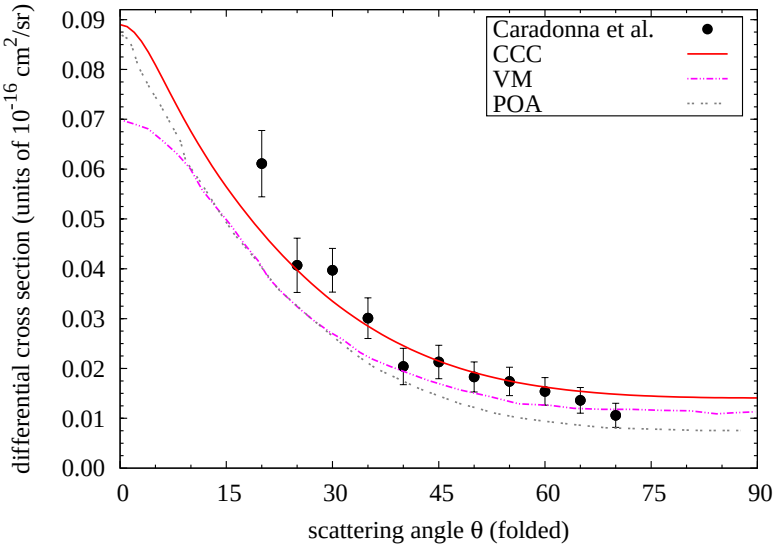


Figure 3.9: The same as in Fig. 3.8, but for 5 eV.

Figure 3.11 shows the elastic scattering DCS at 24 eV, where excitation and Ps-formation channels are also open. The experimental data are in good quantitative agreement with the given theories.

As seen from the above figures the agreement between theory and experiment is satisfactory at intermediate and large angles. However, at near-forward angles the theories predict different results. The absence of experimental data and the loss of accuracy in the measurements at such small angles do not allow to test the theories thoroughly. Moreover, the discrepancy at small angles does not contribute much to the integrated cross sections (because of $\sin(\theta)$ in Eq. (2.139)).

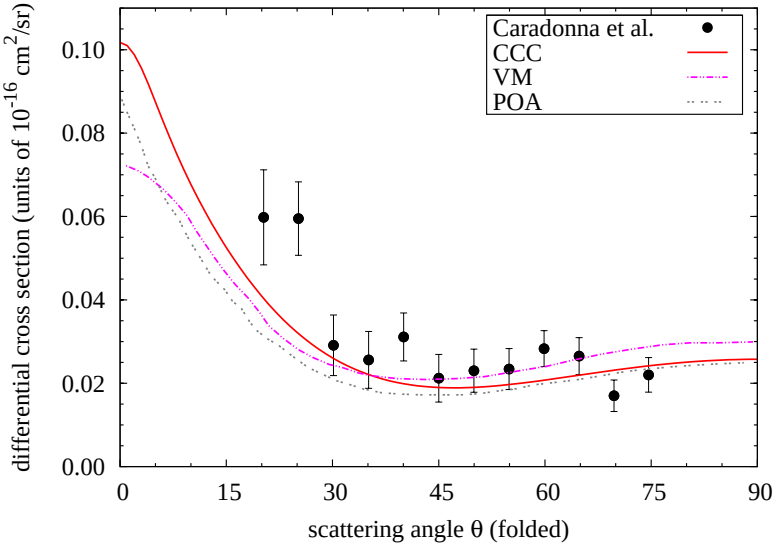


Figure 3.10: The same as in Fig. 3.8, but for 10 eV.

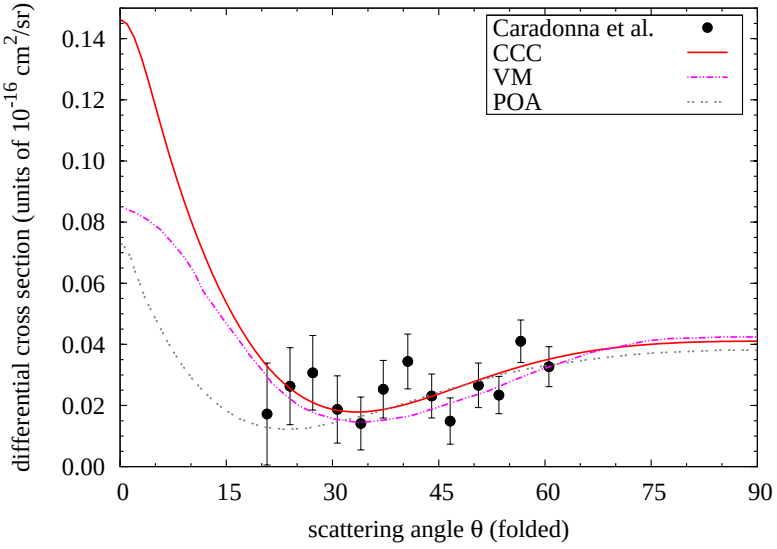


Figure 3.11: The same as in Fig. 3.8, but for 24 eV.

## 3.3 Chapter summary

In this chapter we have presented results of the CCC method applied to positron scattering on the ground state of helium. Direct-scattering, positronium-formation and breakup cross sections have been calculated on a broad range of energies of practical interest. Convergence in the calculated cross sections was demonstrated by increasing the basis sizes and orbital angular momentum of the included states for each of the centers. The calculations were performed for both frozen-core and multi-core description of helium wavefunctions. A better agreement with experimental data is found when a multiconfigurational description is used for the helium wavefunctions in comparison with the recent frozen-core results. Frozen-core results are in good qualitative agreement with experiment, however they often cause overestimation by about 10% near the maximum of calculated cross sections. The total breakup cross section is calculated as the sum of direct ionization of the target and positronium formation in the continuum states. Positronium formation is taken into account explicitly as electron capture into the positronium states. Angle-differential cross sections for elastic scattering below and above the Ps-formation threshold agree well with recent experimental data. We shall next apply the method to positron scattering from helium in its $2^3$S metastable excited state.

# Chapter 4

# Positron scattering on the $2^3S$ metastable state of helium

For many targets the Ps-formation channel is open starting from zero collision energy. Positron scattering from the $2^3S$ metastable state of helium is an example of such a system where the Ps threshold is negative (-2.06 eV). This collisional system has not been yet studied theoretically at low incident positron energies. To the best of our knowledge, only a few calculations [97–99] have been reported at higher energies where the Ps-formation contribution is negligible. More recently Hanssen et al. [100] studied Ps formation in positron-metastable-He collisions at incident energies above 50 eV by including the Ps(1s) state in their expansions. Ryzhikh and Mitroy [101] have reported that positron may form bound state with helium in the $2^3S$ metastable state. Though the estimated binding energy is small, about 0.0161 eV, the existence of bound state may substantially increase the scattering cross sections.

As we have seen in the previous chapter, two-centre CCC results of positron-scattering from the ground state of helium are in good agreement with experimental data. In this chapter we apply this formalism to positron scattering on the $2^3S$ metastable helium. As yet, no experimental studies have been con-

ducted for positron-metastable helium scattering. The motivation for this study is mainly based on the following. First, we would like to check the applicability of the two-centre CCC approach to a system with a negative Ps threshold. Second, the recent experimental achievements on electron scattering from metastable helium [102], in a group that also has a positron beam, may suggest that in future there might be experimental data to test our calculations. Moreover, there are still unresolved differences between theory and experiment regarding electron scattering from metastable states of He [103, 104]. Alternative studies using positrons instead of electrons may therefore shed more light on the reasons for such discrepancies.

## 4.1 Results

The CCC code developed for positron scattering from helium can be applied for any initial state of the target including singlet or triplet states. In Chapter 3 we have presented the results for positron scattering from the ground state of helium. In this case for positron scattering from $2^3$S metastable state of helium the only difference is that the radial part of the total and He wave functions are now antisymmetric. Other differences are the thresholds for excitation, ionization and Ps-formation processes. These differences do not require any changes in the code. However, with these different characteristics of the initial target we may need different basis sizes to get converged results. Therefore, as in the previous case, we start from convergence studies.

Based on our previous results for positron scattering from hydrogen [4] and helium (see Chapter 3), we know that cross sections smooth and free of pseudo-resonances can be obtained if both centers are treated on an equal footing, e.g. by taking the same number ($N_l = N_0 - l$, $l \leq l_{\max}$) of Laguerre-basis states for

both centers. We present here calculations with the following basis sizes from both the atomic and the Ps centers:

(a) $N_0 = 15, l_{\max} = 0$,

(b) $N_0 = 15, l_{\max} = 1$,

(c) $N_0 = 15, l_{\max} = 2$,

(d) $N_0 = 15, l_{\max} = 3$,

(e) $N_0 = 17, l_{\max} = 1$.

Note that we need larger $N_0$ for this case, in comparison to scattering from the ground state. The reason for this is that the results are strongly dependent from the initial state of the target. In case of the ground state the wave function of the ground state converges relatively fast and reaches its converged value even at small values of $N_0$. In case of the excited states, however, the convergence is relatively slow. Therefore, larger $N_0$ is required to get converged results.

As we know from the cases of other targets, close-coupling calculations with pseudo-states on a target centre and only few eigenstates on Ps may produce unphysical resonance-features in the cross sections. To check whether or not this occurs with the metastable helium target, we also have performed calculations with the basis (c) for He and only the three lowest eigenstates (1s, 2s and 2p) of Ps. We denote the results of this basis as CC($\overline{41}$,3). Results of the first four bases, (a)–(d), will illustrate the convergence over increasing $l_{\max}$. The convergence over increasing $N_0$ can be seen by comparing the results of bases (e) and (b).

For simplicity, all bases are generated with the Laguerre fall-off parameter set equal to $\lambda = 2$ for He, and $\lambda = 0.5$ for Ps. We used a frozen-core configuration interaction model to construct the triplet-state He wave functions. The lowest excited states are described sufficiently well within this model. Table 4.1 shows the lowest ionization energies of metastable-He used in our calculations

and compared to experimental values [105]. As seen from the Table 4.1, the lowest triplet states of He are sufficiently well described, and thus represent true

Table 4.1: Ionization energies of the lowest triplet states of He in eV. Values denoted as FC are obtained by using the basis (c).

| State | FC model | Experiment |
|---|---|---|
| $2^3$S | 4.742 | 4.767 |
| $2^3$P | 3.573 | 3.622 |
| $3^3$S | 1.864 | 1.868 |
| $3^3$P | 1.566 | 1.580 |
| $3^3$D | 1.512 | 1.513 |
| $4^3$S | 0.944 | 0.993 |
| $4^3$P | 0.792 | 0.879 |
| $4^3$D | 0.791 | 0.851 |

eigenstates. Higher-lying states diverge from the true eigenstates and are referred to as pseudo-states. By increasing the basis size $N_l$ the number of true eigenstates can be increased to any given accuracy. The Ps states generated with the above basis give a nearly exact ground and the lowest excited states of Ps.

In addition to calculations with the above bases we also present single-centre convergent-close coupling results that were obtained with the basis size $N_0 = 14$ and $l_{\max} = 8$ and will be referred to as CCC1.

Figure 4.1 shows the grand total cross sections calculated with different bases. As seen from Figure 4.1 the single-centre expansion approach, though converged, can yield accurate results only above 10 eV. At lower energies the approach cannot be relied upon. Results of CC($\overline{41}$,3) are almost indistinguishable from the fully converged ones, except around 2 eV where there is a narrow pseudo-resonance. Results with different bases (a), (b), (c), (d) and (e) show that convergence is achieved in both $N_0$ and $l_{\max}$. The most interesting feature

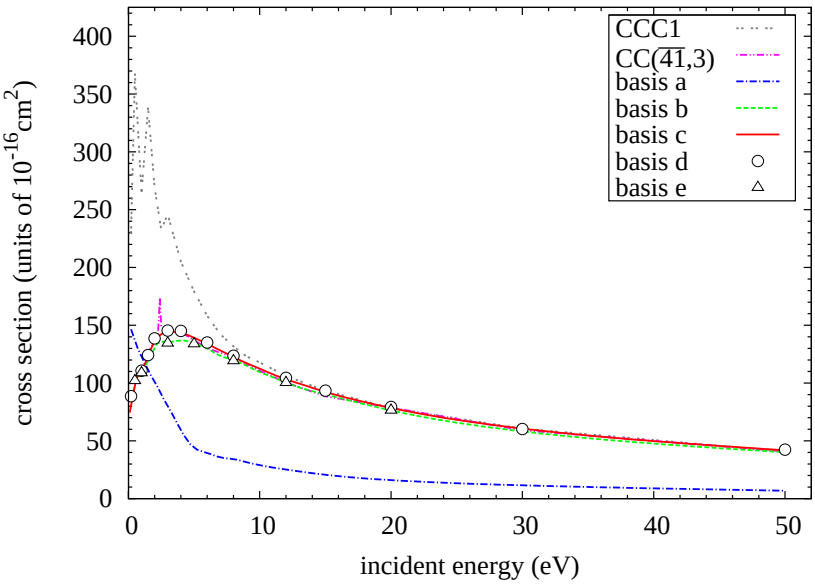


Figure 4.1: $e^+$-He($2^3S$) total cross sections. Descriptions of the calculations are given in the text.

with increasing $l_{\max}$ is the sudden change of the results from basis (a), which is the s-wave model, to basis (b) with $l_{\max} = 1$. The reason for this is the large contribution of $2^3$P excitation, which is neglected in the s-wave calculations. We see that the basis (b), which only has s and p states, is quite sufficient to obtain the total scattering cross sections within 10% accuracy. Convergence is achieved with basis (c), which has 14 $^3$S, 14 $^3$P, and 13 $^3$D states. Adding F-states (basis (d)) changes the results by no more than 1%.

Ps-formation cross sections are given in Figure 4.2. The single-centre model does not provide Ps-formation cross sections. Adding only three Ps states as in CC($\overline{41}$,3) exhibits pseudo-resonance features, which indicate the necessity of treating both centers with extended bases. Note that a similar pseudo-resonance was obtained in positron scattering on the ground state as given in Chapter 3. Results of the s-wave calculations (basis (a)) are too low near the peak and are not smooth around the Ps(2s) excitation threshold at 3.04 eV. The basis

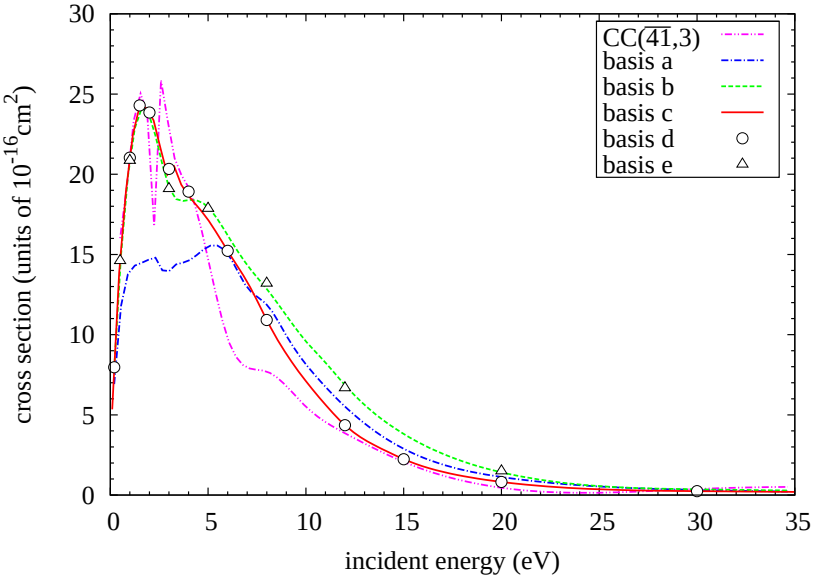


Figure 4.2: $e^+$-He($2^3$S) total Ps-formation cross sections. The calculations are described in the text.

(b) seems sufficient to obtain reasonably converged total Ps-formation cross sections. However it still shows some instability around the Ps($n$=2) excitation threshold and overestimates the converged results at high energies. As in the case of the total cross section, basis (c) is sufficient to obtain converged Ps-formation cross sections. The converged total Ps-formation cross section have a shallow and very narrow local minimum at the Ps($n$=2) excitation threshold. This minimum appears as a result of sharply decreasing Ps(1s) cross sections and fast rising Ps(2s) and Ps(2p) cross sections.

Figure 4.3 shows the total breakup cross section calculated as the sum of the cross sections for excitation of positive-energy pseudo-states of He and electron capture into the Ps pseudo-continuum. As we go down to the ionization threshold region these two contributions approach each other, thus confirming similar behavior observed in positron scattering from the helium ground state (given in Chapter 3) and hydrogen (Ref. [106]) cases. The CC($\overline{41}$,3) results are almost

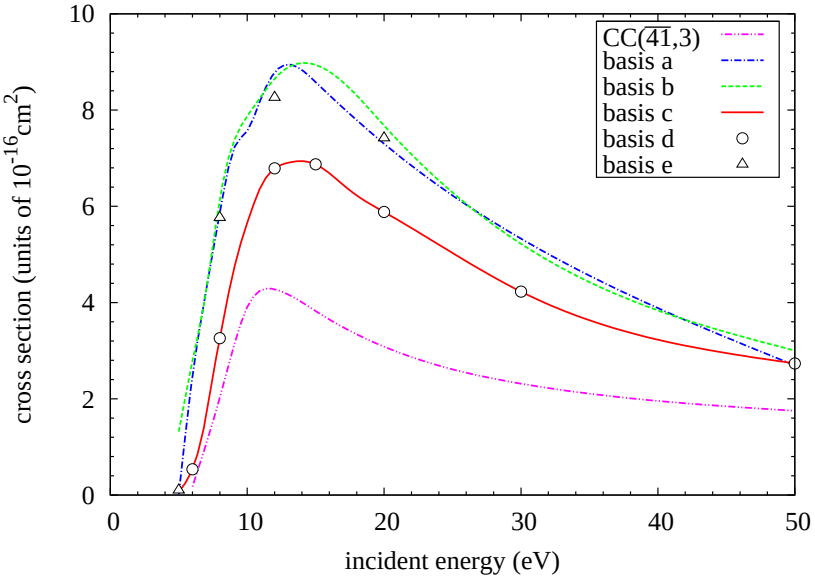


Figure 4.3: $e^+$-He($2^3$S) total breakup cross sections. The calculations are described in the text.

half the converged results of the bases (c) and (d). Interestingly, the results from bases (a) and (b) are close to each other, suggesting p-states play little role in the total breakup process. Adding D-states is significant, however, and has changed the results by around 20%. Adding even larger orbital momentum states (basis (e)) has not had a noticeable effect.

As can be seen from the results for the total, Ps-formation and breakup cross sections, the basis (c) (that includes s, p, d states) is sufficient to get results convergent in $l$. Therefore, unless otherwise stated, we only give results of basis (c) in the cross sections presented below.

The elastic He($2^3$S) and first excitation He($2^3$P) cross sections are given in Figure 4.4. As seen from the figure, the elastic cross section reaches its maximum at 1 eV and then drops fast and stays stable starting from 20 eV. The large value of the elastic cross section may be indicating the existence of a positron bound-state to this system, as predicted by Ryzhikh and Mitroy [101]. In order

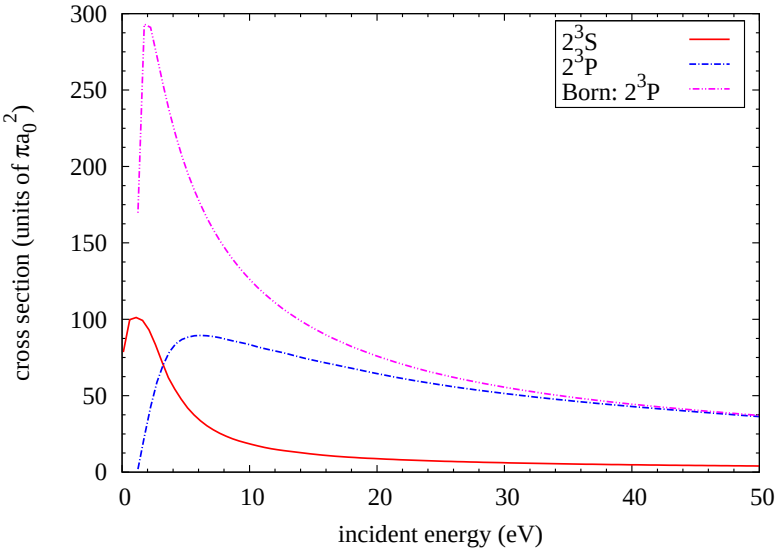


Figure 4.4: Elastic - He($2^3$S) and He($2^3$P)-excitation cross sections calculated using basis (c), see text.

to investigate the existence of such a bound state, some modifications to our computer code are required.We are planning to implement them in the near future.

Figure 4.4 shows that the excitation to $2^3$P reaches its maximum around 6 eV and then slowly decreases. If we compare this figure with Figure 4.1 we see that at higher energies the main contribution to total scattering comes from $2^3$P excitation. Convergence in this channel requires inclusion of very high partial-waves. We overcome this by implementing the Born subtraction method, using that we can get sufficiently accurate results by performing full close-coupling calculations only up to 20 partial waves. The figure also shows the Born cross section for the He($2^3$P) excitation. It can be seen that the Born approximation for the He($2^3$P) excitation can be accurate at collision energies higher than 40eV.

Recently, Murtagh et al. [85] have reported cross sections for Ps-formation

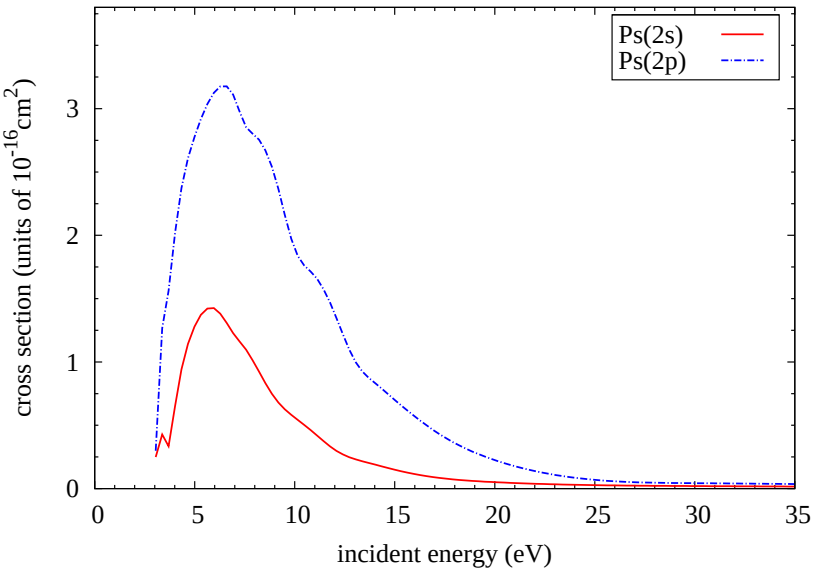


Figure 4.5: Ps(2s,2p) excitation cross sections.

in excited states in positron scattering from the ground state of He, which are in good agreement with our calculations (see Chapter 3 and Ref. [76]). We present the corresponding results for He($2^3$S) in Figure 4.5. We note that Ps(2p) excitation is two to three times higher than Ps(2s) excitation. This is unlike the positron-He($1^1$S) case, where they have comparable magnitudes. The minor oscillations are usually an indication that an even larger basis is required for greater accuracy for a relatively small cross sections.

The angle- differential cross sections are calculated according to Eq. (2.138). We compare our results with the calculations of Verma and Srivastava [98] for $n^3$S and $n^3$P excitations, where $n = 2, 3$, obtained by a distorted-wave approximation. Figure 4.6 shows DCS of $2^3\text{S} \rightarrow n^3\text{P}$ transitions at final positron energy of 20 eV (which corresponds to 21.2 and 23.2 eV scattering energy for $2^3$P and $3^3$P, respectively). At this relatively high energy the contribution of Ps-formation is negligible and the two-centre results for atomic excitation become much the same as the single-centre ones. We can see qualitative agreement

between our results and the calculations of Verma and Srivastava [98]. Our results for $2^3S \rightarrow 2^3P$ are a bit lower above 20°. In the case of $2^3S \rightarrow 3^3P$ both methods predict a minimum at around 10-15°.

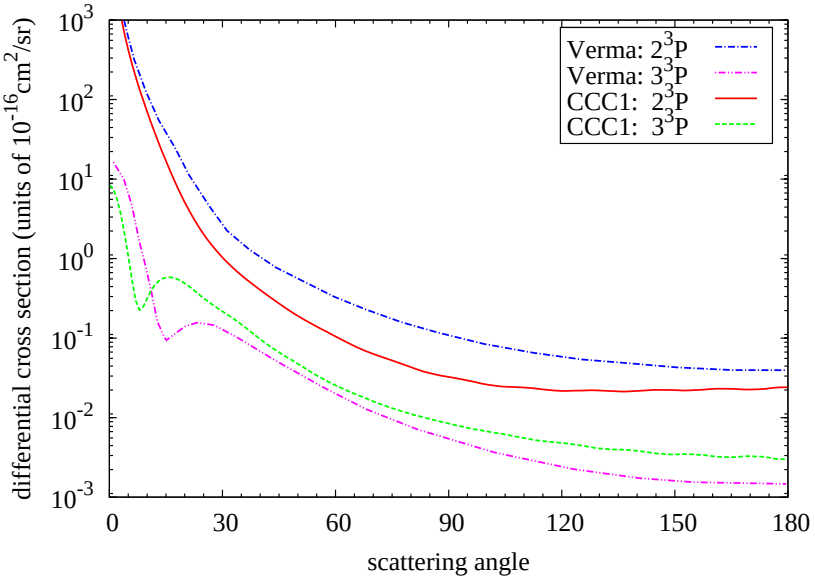


Figure 4.6: Angle-differential cross section. The calculations are due to Verma and Srivastava [98] and present results are described in the text.

Comparison of the integrated cross sections for positron scattering from He($2^3S$) and He($1^1S$) is given in Figure 4.7. The relative magnitudes of cross sections vary substantially depending on the process. The breakup cross section for He($2^3S$) is around 10 times higher than for He($1^1S$) at its peak, while for Ps formation this difference is around 50 times. The total scattering cross section for He($2^3S$) is almost 100 times larger than for He($1^1S$). This large ratio of cross sections in the He($2^3S$) and He($1^1S$) cases shows the importance of studies including excited states.

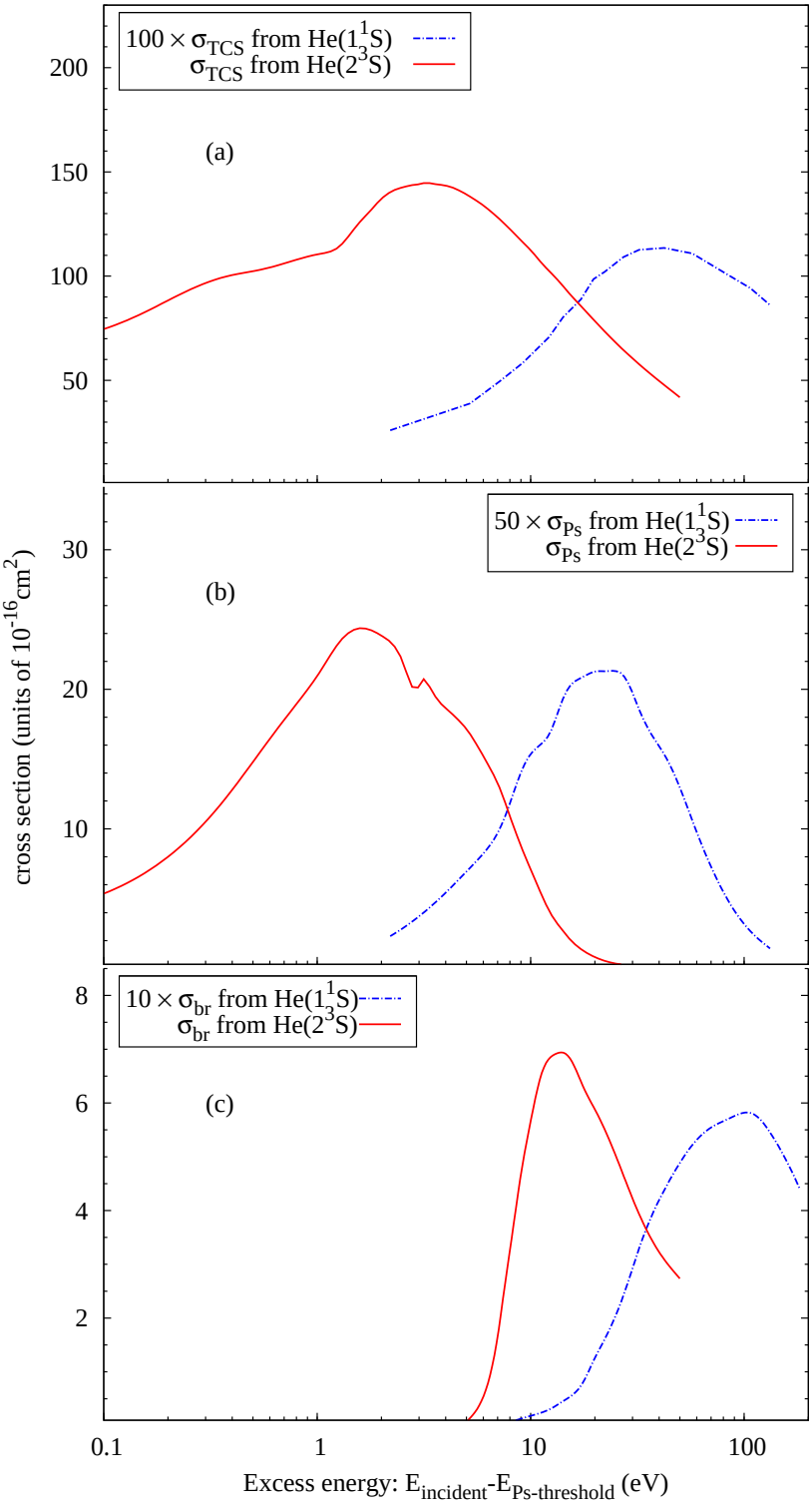


Figure 4.7: Comparison of (a) grand total, (b) total Ps-formation and (c) total breakup cross sections for $e^+$-He($1^1$S) and $e^+$-He($2^3$S) scattering as a function of excess energy above Ps-threshold.

## 4.2 Chapter summary

Positron scattering from the helium $2^3$S metastable state has been theoretically studied for the first time at low and intermediate energies. Converged results for the total, Ps-formation and breakup cross sections have been obtained with a high degree of convergence. The obtained cross sections are significantly larger than those for scattering from the helium ground state. This fact shows that the presence of excited states in the experimental target gas chamber may significantly enhance the apparent cross sections, thereby demonstrating the importance of this process in understanding positron scattering from helium. Another noticeable feature in this collision system is that the total Ps formation cross section exhibits a shoulder arising from the interplay of formation of Ps in its ground and first excited-state. We hope that the present results will generate interest in the considered collision system from both experimentalists and other theorists.

The studies presented in this chapter confirm the applicability of the two-centre convergent close-coupling method to systems with negative Ps-formation threshold. The main conclusions of previous two-centre CCC studies also apply to the $e^+ - He(2^3S)$ system. For example, it is necessary to use a similar number of pseudo-states from both centers to avoid unphysical resonances. In addition, contributions to the breakup cross section from the atomic and Ps centers become equal as the threshold is approached.

# Chapter 5

# Conclusions

The two-centre convergent close-coupling method has been developed and applied to positron scattering on the ground and the $2^3$S metastable excited states of helium. The method utilizes frozen-core or multi-core descriptions of helium wave functions. Positronium formation is taken into account explicitly as electron capture into the positronium states. The total breakup cross section is calculated as direct ionization of the target and positronium formation in the continuum state. Convergence in the calculated cross sections was demonstrated by increasing the basis sizes and orbital angular momenta of the included states for each of the centers. A good agreement between the single-centre and the two-centre CCC results for the total and the electron-loss cross sections above the ionization threshold indicates that double-counting is unlikely.

Positron scattering from the helium ground state has been calculated in both the frozen-core and multi-core expanded helium wavefunctions. Both approximations give good qualitative agreement with the available experimental data. However frozen-core wavefunctions often produce around 10% overestimated cross sections. A better quantitative agreement with the experimental data is found when a multiconfigurational description is used. Differential cross sections for elastic scattering agree well with recent experimental data and pre-

dictions from other sophisticated theories.

Positron scattering from the $2^3$S metastable state of helium has been theoretically studied for the first time at low energies. Converged results were obtained by using larger basis sizes than in the case of the helium ground state. Due to the much larger cross sections, the results show that the presence of excited states in the experimental target gas chamber may significantly enhance the apparent measured cross sections, thus demonstrating the importance of this process in understanding positron scattering from helium. Therefore, we hope that the present work will generate interest in the considered collision system from both experimentalists and other theorists. Converged results for total, Ps-formation and breakup cross sections have been obtained with high accuracy of convergence. Our studies also confirm the applicability of the two-centre convergent close-coupling method to systems with zero Ps-formation threshold.

Positron scattering from the helium ground and metastable states together with the results of positron scattering from hydrogen [4] indicate some important and common features. One of them is the necessity of using a similar number of pseudo-states from both centers to avoid unphysical resonances. Another common feature that we have observed in those targets are the equal contributions from atomic and Ps centers to breakup cross sections near the breakup threshold. Future studies on other targets will show whether these features are common for all targets.

The computer code developed in this project is constructed on top of the existing CCC code that has also been used for electron-atom and positron-hydrogen scattering calculations. We plan to upgrade the code for other He-like targets in the near future. Another planned development is the inclusion of electron exchange between Ps and the residual ion. The method can also be

applied to $e^+$-$H^-$, Ps-H, and Ps-$He^{+1}$ collisions.

# Appendix A

# Helium structure

The CCC approach uses target wave-functions that are square-integrable. They produce sufficiently accurate low-lying bound states and discretized positive energy states to resemble the continuum. Because of two-electron correlations, obtaining the He structure is a complicated process with no analytical solution. Below a configuration interaction (CI) approximation to He structure is presented.

In the nonrelativistic approach the Hamiltonian $H_{\rm T}$ of the helium atom can be written as

$$H_{\rm T} = \sum_{i=1}^{2} \left( \frac{1}{2}\nabla_i^2 + \frac{2}{r_i} \right) + \frac{1}{|\mathbf{r}_1 - \mathbf{r}_2|}. \tag{A.1}$$

As the spin-orbit interactions are neglected in the nonrelativistic Hamiltonian $H_{\rm T}$, it conserves the parity $\pi$ and the total orbital $l$ and spin $s$ angular momenta. Therefore it is convenient to use the $LS$-coupling scheme in which the helium wave functions $\Psi_\alpha$ are characterized by the orbital angular momentum $l$, spin $s$, and parity $\pi$. For brevity of notations we use index $\alpha$ to denote the full set of quantum numbers $(n, l, s, \pi)$. The He wavefunctions are obtained from the solution of the Schrödinger equation

$$H_{\rm T}\, \Psi_\alpha = \epsilon\, \Psi_\alpha. \tag{A.2}$$

An analytical solution of (A.2) does not exist and therefore several approximations have been used to solve it numerically. One such approach is the configuration interaction (CI) method. In the CI approach it is assumed that the helium wave function can be represented as

$$\Psi_\alpha = \sum_{i=1}^{N} C_i^\alpha \Phi_i^{ls\pi}, \tag{A.3}$$

where $\Phi_i^{ls\pi}$ are antisymmetrized two-electron functions (configurations), $C_i^\alpha$ are the CI coefficients and $N$ is the number of configurations.

The target states and energies are obtained by solving the generalized eigenvalue problem for a given CI basis $\Phi_i^{ls\pi}$

$$\sum_{i=1}^{N} \left( \langle \Phi_j^{ls\pi} | H_{\mathrm{T}} | \Phi_i^{ls\pi} \rangle - \epsilon \langle \Phi_j^{ls\pi} | \Phi_i^{ls\pi} \rangle \right) C_i^\alpha = 0. \tag{A.4}$$

Note that the latter equation is written in its general form which does not require CI basis to be an orthogonal basis. By solving the eigenvalue problem (A.4) we obtain $N$ partial solutions which correspond to $N$ helium target states. These states may be written as

$$\Psi_\alpha = \sum_{i=1}^{N} C_i^\alpha \Phi_i^{ls\pi}, \tag{A.5}$$

and satisfy

$$\langle \Psi_\alpha | H_{\mathrm{T}} | \Psi_{\alpha'} \rangle = \epsilon_\alpha \delta_{\alpha\alpha'}. \tag{A.6}$$

Here the indices $\alpha$ and $\alpha'$ denote the helium states for the given combination $(l, s, \pi)$.

Each configuration $\Phi_i^{ls\pi}$ is constructed from antisymmetric combinations of one-electron functions coupled to yield total orbital angular momentum $l$, total spin $s$ and parity $\pi$ by writing

$$\Phi_i^{lms\nu\pi} = \frac{1}{\sqrt{2(1+\delta_{ab})}} \sum_{m_a m_b \sigma_1 \sigma_2} C^{lm}_{l_1 m_1 l_2 m_2} C^{s\nu}_{\frac{1}{2}\sigma_1 \frac{1}{2}\sigma_2} \left[ \phi_a(x_1)\phi_b(x_2) - \phi_a(x_2)\phi_b(x_1) \right], \tag{A.7}$$

where $C^{j_3 m_3}_{j_1 m_1 j_2 m_2}$ is a Clebsch-Gordan coefficient and $x$ denotes spatial and spin coordinates. The one-electron orbital $\phi_{a(b)}(x_i)$ is a product of a radial function, a spherical harmonic, and a spin function, i.e.

$$\phi_{a(b)}(x_i) = \phi_{a(b)}(\mathbf{r}_i)\chi_{\frac{1}{2}\sigma_i} = \frac{1}{r_i} R_{k a l_i}(r_i) Y_{l_i m_i}(\widehat{\mathbf{r}_i})\chi_{\frac{1}{2}\sigma_i}. \tag{A.8}$$

The parity of the configuration (A.7) is defined by

$$\pi = (-1)^{l_a + l_b}. \tag{A.9}$$

It is convenient to separate the spin functions in (A.7) and recouple the orbital angular momenta to obtain

$$\begin{aligned}\Phi_i^{lms\nu\pi} =& \chi_{s\nu}(12)\frac{1}{\sqrt{2(1+\delta_{ab})}}\left(1 + (-1)^s(-1)^{l_a+l_b-l}P_{ab}\right) \\ &\times \sum_{m_a m_b} C^{lm}_{l_a m_a\, l_b m_b}\phi_a(\mathbf{r}_1)\phi_b(\mathbf{r}_2),\end{aligned} \tag{A.10}$$

where the operator $P_{ab}$ interchanges the indices a and b, and the two-electron spin function is defined by

$$\chi_{s\nu}(12) = \sum_{\sigma_1\sigma_2} C^{s\nu}_{\frac{1}{2}\sigma_1\frac{1}{2}\sigma_2}\chi_{\frac{1}{2}\sigma_1}(1)\chi_{\frac{1}{2}\sigma_2}(2). \tag{A.11}$$

The orbitals $\phi_\alpha$ and $\phi_\beta$ form a configuration $\Phi_i^{ls\pi}$ that is included in the CI expansion (A.3) if the following selection rules are satisfied

$$\begin{aligned}|l_\alpha - l_\beta| &\leq l \leq l_\alpha + l_\beta, \\ \pi &= (-1)^{l_\alpha + l_\beta}, \\ (-1)^{l+s} &= 1 \text{ if } \varphi_\alpha = \varphi_\beta.\end{aligned} \tag{A.12}$$

Using Eq. (A.10) we can write matrix elements of $H_{\mathrm{T}}$ in the following way

$$\begin{aligned}\langle\Phi_j^{ls\pi}|H_{\mathrm{T}}|\Phi_i^{ls\pi}\rangle &= \frac{1}{2\sqrt{(1+\delta_{\alpha\beta})(1+\delta_{\gamma\delta})}}\left(1 + (-1)^s(-1)^{l_\alpha+l_\beta-l}P_{\alpha\beta}\right) \\ &\times \left(1 + (-1)^s(-1)^{l_\gamma+l_\delta-l}P_{\gamma\delta}\right)\left[2V_1 + V_{12}\right],\end{aligned} \tag{A.13}$$

where antisymmetry of the configurations $\Phi_j^{ls\pi}$ has been used. The one-electron matrix elements $V_1$ can easily be reduced to

$$V_1 = \langle\phi_\beta|\phi_\delta\rangle\delta_{l_\alpha l_\gamma}\int dr_1 R_\alpha(r_1)[-\frac{1}{2}(\frac{d^2}{dr_1^2} - \frac{l_\alpha(l_\alpha+1)}{r_1^2}) - \frac{Z}{r_1}]R_\gamma(r_1), \qquad (A.14)$$

where the overlap integral between the one-electron orbitals is given by

$$\langle\phi_\beta|\phi_\delta\rangle = \delta_{l_\beta l_\delta}\int dr\ R_\beta(r)R_\delta(r). \qquad (A.15)$$

Calculating two-electron matrix elements $V_{12}$ is a little more challenging. To calculate two-electron matrix elements we first use the multipole expansion of the electron-electron potential

$$\frac{1}{|\mathbf{r}_1 - \mathbf{r}_2|} = 4\pi\sum_{\lambda,\mu}\frac{1}{2\lambda+1}\frac{r_<^\lambda}{r_>^{\lambda+1}}Y_{\lambda\mu}(\hat{\boldsymbol{r}}_1)Y^*_{\lambda\mu}(\hat{\boldsymbol{r}}_2)). \qquad (A.16)$$

Using (A.16) and after some angular momenta algebra we get

$$V_{12} = \sum_\lambda(-1)^{l_\beta+l_\gamma+l}\sqrt{(2l_\gamma+1)(2l_\delta+1)}C^{l_\alpha 0}_{l_\gamma 0\,\lambda 0}C^{l_\beta 0}_{l_\delta 0\,\lambda 0}\left\{\begin{array}{ccc} l_\alpha & l_\beta & l \\ l_\delta & l_\gamma & \lambda\end{array}\right\}\mathcal{R}_\lambda(\alpha,\beta,\gamma,\delta), \qquad (A.17)$$

where the radial integral is given by

$$\mathcal{R}_\lambda(\alpha,\beta,\gamma,\delta) = \int\int dr_1 dr_2\,\frac{r_<^\lambda}{r_>^{\lambda+1}}R_\alpha(r_1)R_\beta(r_2)R_\gamma(r_1)R_\delta(r_2). \qquad (A.18)$$

The range of allowed values of $\lambda$ is determined by the triangle rule for Clebsch-Gordan coefficients in (A.18).

The matrix element $V_{12}$ is symmetric over simultaneous interchange of indices $\alpha$ with $\beta$ and $\delta$ with $\gamma$. This property is used to speed up the calculations.

In order to calculate the radial integrals in (A.18) and (A.14) we must choose the radial functions $R_\alpha(r)$. We take the radial part of the single-particle functions to be the Laguerre basis

$$R_{kl}(r) \;=\; \left(\frac{\lambda_l(k-1)!}{(2l+1+k)!}\right)^{1/2}(\lambda_l r)^{l+1}\exp(-\lambda_l r/2)L^{2l+2}_{k-1}(\lambda_l r), \quad (A.19)$$

where the $L_{k-1}^{2l+2}(\lambda_l r)$ are the associated Laguerre polynomials, and $k$ ranges from 1 to the basis size $N_l$. For a given $\lambda_l$, the Laguerre functions $R_{kl}(r)$ form an orthonormal basis which leads to an orthonormal CI basis $\Phi_i^{ls\pi}$.

The two-electron radial integrals (A.18) are evaluated numerically. In the calculation of the one-electron matrix elements (A.14) the differentiation is first taken analytically according to the following relation

$$\begin{aligned}\frac{d^2}{dr^2}\phi_{kl}(r) &= \left(\frac{\lambda_l(k-1)!}{(2l+1+k)!}\right)^{1/2}\lambda^2(\lambda_l r)^l \exp(-\lambda_l r/2)L_{k-2}^{2l+3}(\lambda_l r) \\ &\quad + \left(\frac{l(l+1)}{r^2} - \frac{\lambda(k+l)}{r} + \frac{\lambda^2}{4}\right)\phi_{kl}, \end{aligned} \tag{A.20}$$

and the integral is then evaluated numerically.

# Appendix B

# Separation of the spin-part in positron scattering on singlet states of helium

For positron scattering from atoms the system has two centers, one associated with the target atom and another with Ps. In addition, as we consider the target of helium to be in its ground state (the general case for scattering from arbitrary, singlet or triplet, states is given in Section 2.1.2) with two electrons of opposite spins, positronium can be formed in both para (p-Ps) and ortho (o-Ps) states depending on which one of the electrons is captured. The two-centre convergent close-coupling approach is based on the expansion of the total wave function $\Psi$ in terms of states of all asymptotic channels, i.e.

$$\begin{aligned}\Psi \approx & \sum_{\alpha}^{N_{\rm He}} F_\alpha(\boldsymbol{r}_0)\psi_\alpha(\boldsymbol{r}_1,\boldsymbol{r}_2)\chi_{SM}^{\rm e^+-He}(0,(1,2)) + \sum_{\beta}^{N_{\rm Ps}} \Big\{ \psi_\beta(\boldsymbol{\rho}_1)\phi_{1s}(\boldsymbol{r}_2) \\ & \times \Big[ G_\beta^{\rm p-Ps-He^+}(\boldsymbol{R}_1)\chi_{SM}^{\rm p-Ps-He^+}((0,1),2) + G_\beta^{\rm o-Ps-He^+}(\boldsymbol{R}_1)\chi_{SM}^{\rm o-Ps-He^+}((0,1),2) \Big] \\ & - \psi_\beta(\boldsymbol{\rho}_2)\phi_{1s}(\boldsymbol{r}_1) \Big[ G_\beta^{\rm p-Ps-He^+}(\boldsymbol{R}_2)\chi_{SM}^{\rm p-Ps-He^+}((0,2),1) \\ & + G_\beta^{\rm o-Ps-He^+}(\boldsymbol{R}_2)\chi_{SM}^{\rm o-Ps-He^+}((0,2),1) \Big] \Big\}, \end{aligned} \tag{B.1}$$

where the first term corresponds to expansion in terms of the helium wave functions $\psi_\alpha$ with expansion coefficients being $F_\alpha$, while the second term corresponds

to expansion in terms of the positronium states $\psi_\beta$ with coefficients $G_\beta^{\mathrm{p-Ps-He^+}}$ and $G_\beta^{\mathrm{o-Ps-He^+}}$ corresponding to para-Ps and ortho-Ps, respectively. The $N_{\mathrm{He}}$ and $N_{\mathrm{Ps}}$ are the numbers of the atomic and Ps states, respectively. The indices $\alpha$ and $\beta$ run over all generated pseudo-states of the helium atom and Ps, including positive-energy ones corresponding to the discretized continuum. The second term allows for both electrons to form positronium, thus taking into account positronium formation in para and ortho states. The residual $He^+$ ion is described by $\phi_{1s}$.

We construct the total wave function of the $e^+$-He system to be antisymmetric with regards to permutation of the two electrons. Therefore, both terms in the expansion (B.1) individually satisfy the antisymmetry condition. The first term on the right hand side corresponds to the positron-He channel where He is in the singlet spin state. The spin part of the wave function for the helium singlet state is antisymmetric and given as

$$\chi_{00}^{\mathrm{He}}(1,2) = \frac{1}{\sqrt{2}}(\alpha_1\beta_2 - \beta_1\alpha_2). \tag{B.2}$$

Consequently, the radial part of the helium wave function is symmetric

$$\psi_\alpha(\boldsymbol{r}_1, \boldsymbol{r}_2) = \psi_\alpha(\boldsymbol{r}_2, \boldsymbol{r}_1). \tag{B.3}$$

The total spin state in the positron-He channel can be written as a product of the He and positron spin functions. As helium is in the spin-zero state, the total channel spin $S$ and its projection $M$ are defined by that of the incoming positron. Considering the positron coming in with up spin (which means $S = \frac{1}{2}$, $M = \frac{1}{2}$) we get

$$\chi_{\frac{1}{2}\frac{1}{2}}^{\mathrm{e^+-He}}(0,(1,2)) = \frac{1}{\sqrt{2}}\alpha_0(\alpha_1\beta_2 - \beta_1\alpha_2). \tag{B.4}$$

This wave function is antisymmetric. We emphasize that knowing the spin projection direction of the incoming positron is not essential and the calculations

below can be done equally well for the positron spin down case. The final result will be the same.

As the spin interactions are neglected the total spin is conserved. We take the second term in Eq. (B.1) to be antisymmetric by construction in its very general form. Here the radial and spin parts of the para- and ortho-positronium formation channels come in a mixed form and altogether combine into an anti-symmetric function. After the collision only the part of this term that conserves the total spin can be excited. Such a part can be separated from the second term of Eq. (B.1) by projecting the latter on the initial channel spin function given by Eq. (B.4). As the initial channel spin function is antisymmetric, this, of course, should lead to a symmetric radial part in the positronium formation channel as a consistency check.

The total wave function of Ps, with a spin $S_0$ and its projection $M_0$, is

$$\phi_\beta(\boldsymbol{\rho})\chi^{\rm Ps}_{S_0M_0}(0,1), \tag{B.5}$$

where $\chi^{\rm Ps}_{S_0M_0}(0,1)$ is a spin function of Ps which is defined as

$$\begin{aligned}\chi^{\rm p-Ps}_{00}(0,1) =& \sum_{m_0,m_1} C^{0\,0}_{\frac{1}{2}m_0\,\frac{1}{2}m_1}\,\chi_{\frac{1}{2}m_0}(0)\chi_{\frac{1}{2}m_1}(1)\\ =& \frac{1}{\sqrt{2}}(\alpha_0\beta_1-\beta_0\alpha_1)\end{aligned} \tag{B.6}$$

for para-Ps and

$$\begin{aligned}\chi^{\rm o-Ps}_{1M_0}(0,1) =& \sum_{m_0,m_1} C^{1\,M_0}_{\frac{1}{2}m_0\,\frac{1}{2}m_1}\,\chi_{\frac{1}{2}m_0}(0)\chi_{\frac{1}{2}m_1}(1)\\ =& \begin{cases}\alpha_0\alpha_1 & \text{if } M_0=1\\ \frac{1}{\sqrt{2}}(\alpha_0\beta_1+\beta_0\alpha_1) & \text{if } M_0=0\\ \beta_0\beta_1 & \text{if } M_0=-1\end{cases}\end{aligned} \tag{B.7}$$

for ortho-Ps. Here $C^{ab}_{cdef}$ are the Clebsch-Gordan coefficients of vector addition. Now we couple the Ps spin function with the one-electron spin function of the

$He^+$ ion in order to get possible spin functions of Ps-$He^+$:

$$\chi^{\mathrm{Ps-He^+}}_{\frac{1}{2}\frac{1}{2}}((0,1),2) = \sum_{M_0,m_2} C^{\frac{1}{2}\,\frac{1}{2}}_{S_0 M_0\ \frac{1}{2} m_2} \chi_{S_0 M_0}(0,1) \times \chi_{\frac{1}{2} m_2}(2), \tag{B.8}$$

where $m_2$ is a spin projection of the second electron. For the para-Ps-$He^+$ the above function becomes

$$\chi^{\mathrm{p-Ps-He^+}}_{\frac{1}{2}\frac{1}{2}}((0,1),2) = \frac{1}{\sqrt{2}}(\alpha_0\beta_1 - \beta_0\alpha_1)\alpha_2 \tag{B.9}$$

and for ortho-Ps-$He^+$

$$\chi^{\mathrm{o-Ps-He^+}}_{\frac{1}{2}\frac{1}{2}}((0,1),2) = -\frac{1}{\sqrt{6}}(\alpha_0\beta_1 + \beta_0\alpha_1)\alpha_2 + \frac{2}{\sqrt{6}}\alpha_0\alpha_1\beta_2. \tag{B.10}$$

In order to extract the spatial part of the wave function we project the total wave function of Eq. (B.1) onto the spin function of the initial channel $\chi^{\mathrm{e^+-He}}_{\frac{1}{2}\frac{1}{2}}$ given in (B.4). Then, using the following overlap coefficients

$$\begin{aligned}
&< \chi^{\mathrm{p-Ps-He^+}}_{\frac{1}{2}\frac{1}{2}}((0,1),2)\,|\,\chi^{\mathrm{e^+-He}}_{\frac{1}{2}\frac{1}{2}}(0,(1,2)) >= -\frac{1}{2},\\
&< \chi^{\mathrm{o-Ps-He^+}}_{\frac{1}{2}\frac{1}{2}}((0,1),2)\,|\,\chi^{\mathrm{e^+-He}}_{\frac{1}{2}\frac{1}{2}}(0,(1,2)) >= \frac{\sqrt{3}}{2},\\
&< \chi^{\mathrm{p-Ps-He^+}}_{\frac{1}{2}\frac{1}{2}}((0,2),1)\,|\,\chi^{\mathrm{e^+-He}}_{\frac{1}{2}\frac{1}{2}}(0,(1,2)) >= \frac{1}{2},\\
&< \chi^{\mathrm{o-Ps-He^+}}_{\frac{1}{2}\frac{1}{2}}((0,2),1)\,|\,\chi^{\mathrm{e^+-He}}_{\frac{1}{2}\frac{1}{2}}(0,(1,2)) >= -\frac{\sqrt{3}}{2},
\end{aligned} \tag{B.11}$$

we obtain the spatial part of the total wave function

$$\begin{aligned}
\Phi(\boldsymbol{r}_0,\boldsymbol{r}_1,\boldsymbol{r}_2) \approx \sum_{\alpha}^{N_{\mathrm{He}}} F_\alpha(\boldsymbol{r}_0)\psi_\alpha(\boldsymbol{r}_1,\boldsymbol{r}_2) + \sum_{\mathrm{Ps}}^{N_\beta} \Big\{ &\psi_\beta(\boldsymbol{\rho}_1)\phi_{1s}(\boldsymbol{r}_2)\\
&\times \left[ -\frac{1}{2} G^{\mathrm{p-Ps-He^+}}_\beta(\boldsymbol{R}_1) + \frac{\sqrt{3}}{2} G^{\mathrm{o-Ps-He^+}}_\beta(\boldsymbol{R}_1) \right]\\
&- \psi_\beta(\boldsymbol{\rho}_2)\phi_{1s}(\boldsymbol{r}_1)\\
&\times \left[ \frac{1}{2} G^{\mathrm{p-Ps-He^+}}_\beta(\boldsymbol{R}_2) - \frac{\sqrt{3}}{2} G^{\mathrm{o-Ps-He^+}}_\beta(\boldsymbol{R}_2) \right] \Big\}.
\end{aligned} \tag{B.12}$$

The result is symmetric as we expected. Setting now

$$-\frac{1}{2}G_\beta^{\mathrm{p-Ps-He^+}}(\boldsymbol{R})+\frac{\sqrt{3}}{2}G_\beta^{\mathrm{o-Ps-He^+}}(\boldsymbol{R})\equiv G_\beta(\boldsymbol{R}), \tag{B.13}$$

we arrive at

$$\Psi(\boldsymbol{x}_0,\boldsymbol{x}_1,\boldsymbol{x}_2)=\Phi(\boldsymbol{r}_0,\boldsymbol{r}_1,\boldsymbol{r}_2)\chi_{\frac{1}{2}\frac{1}{2}}(0,(1,2)), \tag{B.14}$$

where

$$\Phi\approx\sum_\alpha^{N_{\mathrm{He}}}F_\alpha(\boldsymbol{r}_0)\psi_\alpha(\boldsymbol{r}_1,\boldsymbol{r}_2)+\sum_\beta^{N_{\mathrm{Ps}}}\{G_\beta(\boldsymbol{R}_1)\psi_\beta(\boldsymbol{\rho}_1)\phi_\beta(\boldsymbol{r}_2)+G_\beta(\boldsymbol{R}_2)\psi_\beta(\boldsymbol{\rho}_2)\phi_\beta(\boldsymbol{r}_1)\}, \tag{B.15}$$

is the final radial wave function used in the present work. We note that, provided

$$G_\beta^{\mathrm{o-Ps-He^+}}=\sqrt{3}G_\beta^{\mathrm{p-Ps-He^+}}, \tag{B.16}$$

we get $G_\beta(\boldsymbol{R})=G_\beta^{\mathrm{p-Ps-He^+}}$.

Let us finally consider the case when the incoming positron's spin is down. Then the corresponding channel spin function $\chi_{\frac{1}{2}-\frac{1}{2}}^{\mathrm{e^+-He}}(0,(1,2))$ would still be antisymmetric. However, the relevant overlap coefficients would be opposite in sign to those given in Eqs. (B.11). This would merely change the sign of the amplitude introduced in Eq. (B.13), something that would not affect the results of the present calculations.

Alternatively, using Eqs. (B.9) and (B.10) we could directly reduce the spin parts of the Ps-$He^+$ channels into that of the positron-He channel, i.e. the right-hand side of Eq. (B.4). However, this turns out to be only possible if we utilize the assumption (B.16). Though Eq. (B.16) is sometimes used in the literature, to our best knowledge its origin has remained unclear. The relation in Eq. (B.16) emerges naturally when we consider a general case given in Section 2.1.2.

# List of Figures

# List of Tables

# Bibliography


[1] H. S. W. Massey and C. B. O. Mohr, Proc. Phys. Soc. A **67**, 695 (1954).

[2] H. S. Massey and A. H. Moussa, Proc. Phys. Soc. (London) **77**, 811 (1961).

[3] J. Mitroy, Aust. J. Phys. **46**, 751 (1993).

[4] A. S. Kadyrov and I. Bray, Phys. Rev. A **66**, 012710 (2002).

[5] P. V. Reeth and J. W. Humberston, J. Phys. B **31**, L231 (1998).

[6] G. Laricchia and C. Wilkin, Phys. Rev. Lett. **79**, 2241 (1997).

[7] C. Kurz, R. G. Greaves, and C. M. Surko, Phys. Rev. Lett. **77**, 2929 (1996).

[8] I. F. Barna, Eur. Phys. J. D **30**, 5 (2004).

[9] M. Charlton and J. W. Humberston, *Positron Physics* (Cambridge University Press, Cambridge, 2001).

[10] C. M. Surko, G. F. Gribakin, and S. J. Buckman, Journal of Physics B: Atomic, Molecular and Optical Physics **38**, R57 (2005).

[11] P. Mandal, S. Guha, and N. C. Sil, Phys. Rev. A **22**, 2623 (1980).

[12] L. A. Parcell, R. P. McEachran, and A. D. Stauffer, J. Phys. B **16**, 4249 (1983).

[13] L. A. Parcell, R. P. McEachran, and A. D. Stauffer, J. Phys. B **20**, 2307 (1987).

[14] R. Campeanu, D. Fromme, G. Kruse, R. McEachran, L. Parcell, W. Raith, G. Sinapius, and A. Stauffer, J. Phys. B **20**, 3557 (1987).

[15] R. Campeanu, R. McEachran, and A. Stauffer, Can. J. Phys. **74**, 544 (1996).

[16] D. Fromme, G. Kruse, W. Raith, and G. Sinapius, Phys. Rev. Lett. **57**, 3031 (1986).

[17] H. Knudsen, L. Brun-Nielsen, M. Charlton, and M. R. Poulsen, J. Phys. B **23**, 3955 (1990).

[18] J. Moxom, P. Ashley, and G. Laricchia, Can. J. Phys. **74**, 367 (1999).

[19] M. K. Srivastava, M. Kumar, and A. N. Tripathi, J. Chem. Phys. **84**, 4715 (1986).

[20] S. Sen and P. Mandal, Phys. Rev. A **80**, 062714 (2009).

[21] A. L. Fetter and J. D. Walecka, *Quantum Theory of Many-Particle Systems* (McGraw-Hill, New York, 1971).

[22] M. Y. Amusia, N. A. Cherepkov, L. V. Chernysheva, and S. G. Shapiro, Journal of Physics B: Atomic and Molecular Physics **9**, L531 (1976).

[23] E. Jaduszliwer and D. A. Paul, Can. J. Phys. **51**, 1565 (1973).

[24] K. F. Canter, P. G. Coleman, T. C. Griffith, and G. R. Heyland, Journal of Physics B: Atomic and Molecular Physics **5**, L167 (1972).

[25] E. F. Varracchio, Journal of Physics B: Atomic, Molecular and Optical Physics **23**, L779 (1990).

[26] O. Sueoka, J. Phys. Soc. Japan **51**, 3757 (1982).

[27] P. G. Coleman and J. T. Hutton, Phys. Rev. Lett. **45**, 2017 (1980).

[28] G. F. Gribakin and W. A. King, Journal of Physics B: Atomic, Molecular and Optical Physics **27**, 2639 (1994).

[29] V. A. Dzuba, V. V. Flambaum, G. F. Gribakin, and W. A. King, Journal of Physics B: Atomic, Molecular and Optical Physics **29**, 3151 (1996).

[30] G. F. Gribakin and W. A. King, Can. J. Phys. **74**, 449 (1996).

[31] G. F. Gribakin and J. Ludlow, Phys. Rev. A **70**, 032720 (2004).

[32] W. Kohn, Phys. Rev. **74**, 1763 (1948).

[33] C. Schwartz, Phys. Rev. **124**, 1468 (1961).

[34] R. Campeanu and J. Humberston, J. Phys. B **8**, L244 (1975).

[35] R. Campeanu and J. Humberston, J. Phys. B **10**, L153 (1977).

[36] J. W. Humberston, J. Phys. B **6**, L305 (1973).

[37] P. V. Reeth and J. W. Humberston, J. Phys. B **28**, L511 (1995).

[38] E. A. G. Armour and J. W. Humberston, Physics Reports **204**, 165 (1991), ISSN 0370-1573.

[39] P. V. Reeth and J. W. Humberston, J. Phys. B **32**, L3651 (1999).

[40] T. Mizogawa, Y. Nakayama, T. Kawaratani, and M. Tosaki, Phys. Rev. A **31**, 2171 (1985).

[41] T. S. Stein, W. E. Kauppila, V. Pol, J. H. Smart, and G. Jesion, Phys. Rev. A **17**, 1600 (1978).

[42] I. McCarthy and A. T. Stelbovics, Phys. Rev. A **22**, 502 (1980).

[43] I. E. McCarthy and A. T. Stelbovics, Phys. Rev. A **28**, 2693 (1983).

[44] K. Ratnavelu, Aust. J. Phys. **44**, 265 (1991).

[45] Y. Zhou, K. Ratnavelu, and I. E. McCarthy, Phys. Rev. A **71**, 042703 (2005).

[46] Y. Cheng and Y. Zhou, Phys. Rev. A **76**, 012704 (2007).

[47] T. C. Griffith and G. R. Heyland, Phys. Rep. **44**, 169 (1978).

[48] R. P. McEachran, D. L. Morgan, A. G. Ryman, and A. D. Stauffer, J. Phys. B **10**, 663 (1977).

[49] A. R. Tancić, M. R. N. Tökési, I. F. Barna, and J. Burgdörfer, Facta Universitatis Series: Phys., Chem. and Thech. **2**, 183 (2002).

[50] F. A. Gianturco and R. Melissa, Nucl. Instr. and Meth. B **143**, 81 (1998).

[51] D. R. Schultz and R. Olson, Phys. Rev. A **38**, 1866 (1988).

[52] R. Abrines and I. C. Percival, Proc. Cambridge Philos. Soc. **88**, 861 (1966).

[53] R. E. Olson and A. Salop, Phys. Rev. A **16**, 531 (1977).

[54] K. Tökési, I. F. Barna, and J. Burgdörfer, Nucl. Instr. and Meth. B **233**, 307 (2005).

[55] P. Caradonna, A. Jones, C. Makochekanwa, D. S. Slaughter, J. P. Sullivan, S. J. Buckman, I. Bray, and D. V. Fursa, Phys. Rev. A **80**, 032710 (2009), ISSN 1050-2947.

[56] C. P. Campbell, M. T. McAlinden, A. A. Kernoghan, and H. R. J. Walters, Nucl. Instr. and Meth. B **143**, 41 (1998).

[57] W. E. Kauppila, T. S. Stein, J. H. Smart, M. S. Dababneh, Y. K. Ho, J. P. Downing, and V. Pol, Phys. Rev. A **24**, 725 (1981).

[58] L. S. Fornari, L. M. Diana, and P. G. Coleman, Phys. Rev. Lett. **51**, 2276 (1983).

[59] L. M. Diana, P. G. Coleman, D. L. Brooks, and P. K. Pendleton, Phys. Rev. A **34**, 2731 (1986).

[60] N. Overton, R. Mills, and P. Coleman, J. Phys. B **26**, 3951 (1993).

[61] N. R. Hewitt, C. J. Noble, and B. H. Bransden, J. Phys. B **23**, 4185 (1990).

[62] N. R. Hewitt, C. J. Noble, and B. H. Bransden, J. Phys. B **25**, 557 (1992).

[63] P. Chaudhuri and S. K. Adhikari, Phys. Rev. A **57**, 984 (1997).

[64] P. Chaudhuri and S. K. Adhikari, J. Phys. B **31**, 3057 (1998).

[65] P. Chaudhuri and S. K. Adhikari, J. Phys. B **32**, 129 (1999).

[66] A. Igarashi, N. Toshima, and T. Shirai, Phys. Rev. A **54**, 5004 (1996).

[67] I. Bray and A. T. Stelbovics, Phys. Rev. A **46**, 6995 (1992).

[68] D. V. Fursa and I. Bray, Phys. Rev. A **52**, 1279 (1995).

[69] I. Bray and A. T. Stelbovics, Phys. Rev. A **49**, R2224 (1994).

[70] H. Wu, Ph.D. thesis, Murdoch University, Australia (2004).

[71] H. Wu, I. Bray, D. V. Fursa, and A. T. Stelbovics, J. Phys. B **37**, L1 (2004).

[72] H. Wu, I. Bray, D. V. Fursa, and A. T. Stelbovics, J. Phys. B **37**, 1165 (2004).

[73] S. Zhou, H. Li, W. E. Kauppila, C. K. Kwan, and T. S. Stein, Phys. Rev. A **55**, 361 (1997).

[74] G. O. Jones, M. Charlton, J. Slevin, G. Laricchia, A. Kövér, M. R. Poulsen, and S. N. Chormaic, J. Phys. B **26**, L483 (1993).

[75] A. T. Stelbovics, I. Bray, D. V. Fursa, and K. Bartschat, Phys. Rev. A **71**, 052716(13) (2005).

[76] R. Utamuratov, A. S. Kadyrov, D. V. Fursa, I. Bray, and A. T. Stelbovics, J. Phys. B **43**, 125203 (2010).

[77] I. H. Sloan and E. J. Moore, J. Phys. B (Proc. Phys. Soc.) **1**, 414 (1968).

[78] A. S. Kadyrov, A. M. Mukhamedzhanov, A. T. Stelbovics, I. Bray, and F. Pirlepesov, Phys. Rev. A **68**, 022703 (2003).

[79] P. V. Reeth and J. W. Humberston, J. Phys. B **31**, L621 (1998).

[80] D. A. Varshalovich, A. N. Moskalev, and V. K. Khersonskii, *Quantum theory of angular momentum* (World Scientific Pub., Philadelphia, 1988), 1st ed.

[81] W. E. Kauppila, T. S. Stein, J. H. Smart, M. S. Dababneh, Y. K. Ho, J. P. Downing, and V. Pol, Phys. Rev. A **24**, 725 (1981).

[82] S. Mori and O. Sueoka, J. Phys. B **27**, 4349 (1994).

[83] F. M. Jacobsen, N. P. Frandsen, H. Knudsen, U. Mikkelsen, and D. M. Schrader, J. Phys. B **28**, 4691 (1995).

[84] D. J. Murtagh, M. Szluinska, J. Moxom, P. V. Reeth, and G. Laricchia, J. Phys. B **38**, 3857 (2005).

[85] D. J. Murtagh, D. A. Cooke, and G. Laricchia, Phys. Rev. Lett. **102**, 133202 (2009).

[86] G.P. Karwasz, Eur. Phys. J. D **35**, 267 (2005).

[87] G. P. Karwasz, R. S. Brusa, and D. Pliszka, J. Phys. Conference Series **199**, 012019 (2010).

[88] P. Caradonna, J. P. Sullivan, A. Jones, C. Makochekanwa, D. Slaughter, D. W. Mueller, and S. J. Buckman, Phys. Rev. A **80**, 060701 (2009).

[89] J. P. Sullivan, C. Makochekanwa, A. Jones, P. Caradonna, and S. J. Buckman, J. Phys. B **41**, 081001 (2008).

[90] J. P. Sullivan, C. Makochekanwa, A. Jones, P. Caradonna, and S. J. Buckman, J. Phys. Conference Series **133**, 012004 (2008).

[91] R. Utamuratov, A. S. Kadyrov, D. V. Fursa, and I. Bray, J. Phys. Conference Series **199**, 012021 (2010).

[92] R. Utamuratov, A. S. Kadyrov, D. V. Fursa, and I. Bray, J. Phys. B **43**, 031001 (2010).

[93] S. K. Adhikari and A. S. Ghosh, Chem. Phys. Lett. **262**, 460 (1996).

[94] P. Caradonna, A. Jones, C. Makochekanwa, J. Machacek, J. Sullivan, and S. J. Buckman, submitted to Phys. Rev. A (2010).

[95] R. P. McEachran, unpublished preliminary results (2010).

[96] P. V. Reeth, unpublished preliminary results (2010).

[97] I. Khurana, R. Srivastava, and A. N. Tripathi, Phys. Rev. A **37**, 3720 (1988).

[98] S. Verma and R. Srivastava, Chem. Phys. Lett. **74**, 521 (1996).

[99] S. Vucic, R. M. Potvliege, and C. J. Joachain, J. Phys. B **20**, 3157 (1987).

[100] J. Hanssen, P. A. Hervieux, O. A. Fojon, and D. Rivarola, Phys. Rev. A **63**, 012705 (2000).

[101] G. Ryzhikh and J. Mitroy, Journal of Physics B: Atomic, Molecular and Optical Physics **31**, 3465 (1998).

[102] L. J. Uhlmann, R. G. Dall, A. G. Truscott, M. D. Hoogerland, and S. J. Buckman, Phys. Rev. Lett. **94**, 173201 (2005).

[103] M. E. Lagus, J. B. Boffard, L. W. Anderson, and C. C. Lin, Phys. Rev. A **53**, 1505 (1996).

[104] G. A. Piech, J. E. Chilton, L. W. Anderson, and C. C. Lin, J. Phys. B **31**, 859 (1998).

[105] C. E. Moore, *Atomic Energy Levels as Derived from Analyses of Optical Spectra*, Circ. No. 467 Vol. 1 (Natl. Bur. Stand. (U.S.), U.S. GPO, Washington, DC, 1949).

[106] A. S. Kadyrov, I. Bray, and A. T. Stelbovics, Phys. Rev. Lett. **98**, 263202 (2007).